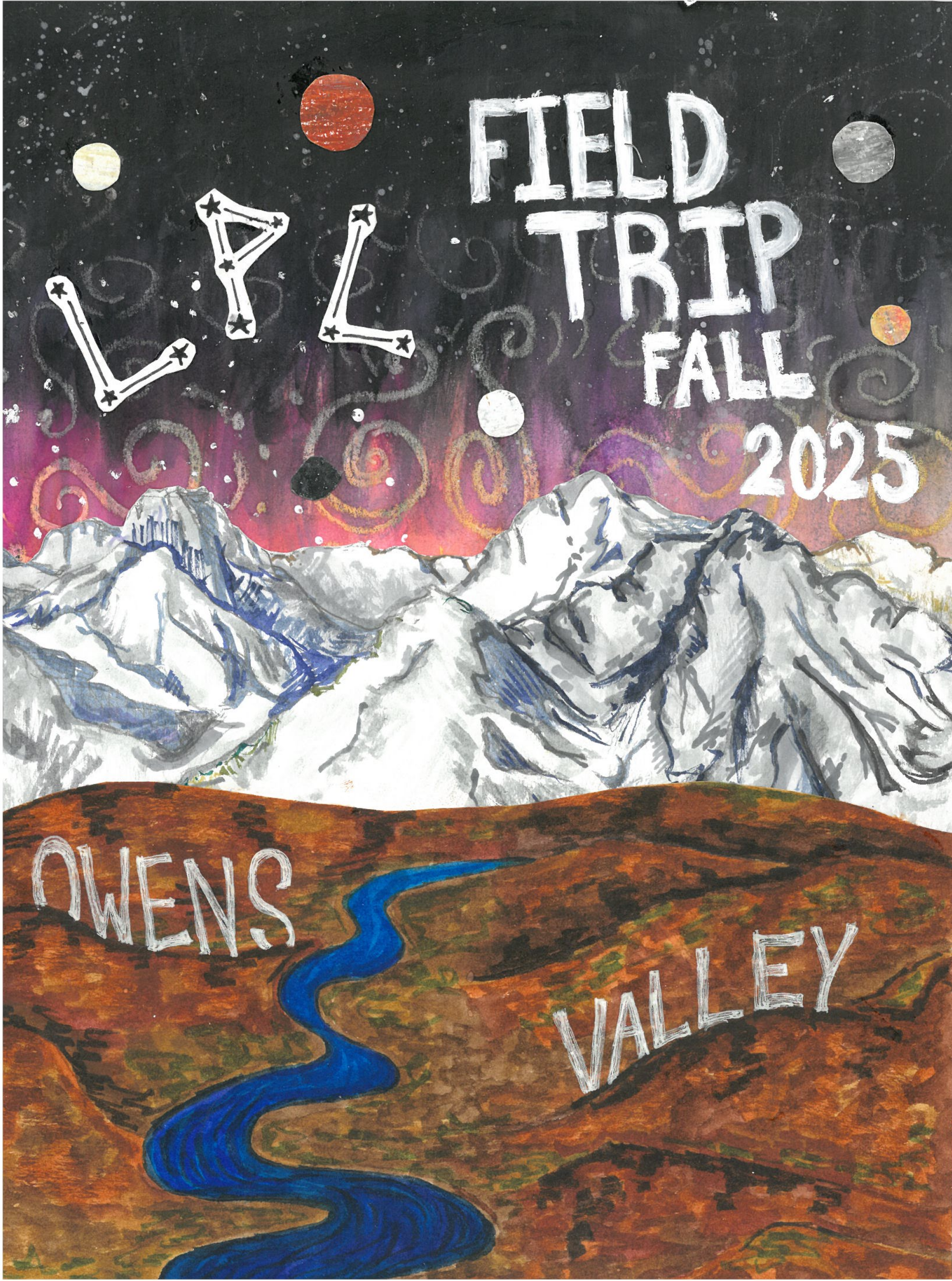
LPL
FIELD TRIP
FALL
2025
OWENS
VALLEY

# Table of Contents

**Note from the editor:** A huge thank you to the artists Thea, Ruby, Kiki, and Elana, who created the cover art for this field guide

Letter from the editor—

Owens Valley is a landscape shaped by extremes. Nestled between the towering Sierra Nevada to the west and the White–Inyo Range to the east, it lies within one of the deepest valleys in North America. Its striking topography is the product of active faulting and tectonic extension, with the valley floor dropping as the mountains rise. Layer onto that the history of glaciation, volcanism, and water diversion, and you have a place where the story of Earth is written in every outcrop and basin.

As someone who usually spends more time thinking about planets hundreds of light-years away, I love how field trips like this pull me back into the immediacy of Earth science. Walking across alluvial fans or standing at the edge of an ancient lakebed connects me to the processes I usually only read about—it's a reminder that the dynamics that shape distant exoplanets are alive and visible here, too.

I hope this guide gives you a sense of the complexity and beauty of Owens Valley, and I'm excited to learn more alongside you in the field. A special thank you to Thea, Ruby, Kiki, and Elana for their stunning cover art, which captures the spirit of this year's trip and sets the stage for the adventure ahead.

See you in the field,
Anna :)

**Land Acknowledgment**

We acknowledge that the land on which we will be gathering in Owens Valley is the traditional homeland of the Paiute and Shoshone peoples, including the Bishop Paiute Tribe, the Big Pine Paiute Tribe of the Owens Valley, the Fort Independence Indian Community, and the Lone Pine Paiute-Shoshone Tribe. These communities have lived in relationship with this land, water, and sky for thousands of years and continue to do so today.

We recognize the deep history of dispossession and displacement in this region, and we honor the resilience, knowledge, and ongoing stewardship of the Paiute and Shoshone peoples. As we learn and do science here, we commit to respecting this place and remembering that our work is carried out on Indigenous land.

- LPL Graduate Students

**Day 1.**
Meetup spot: Dairy Queen
25635 Crucero Rd
Ludlow, CA 92338

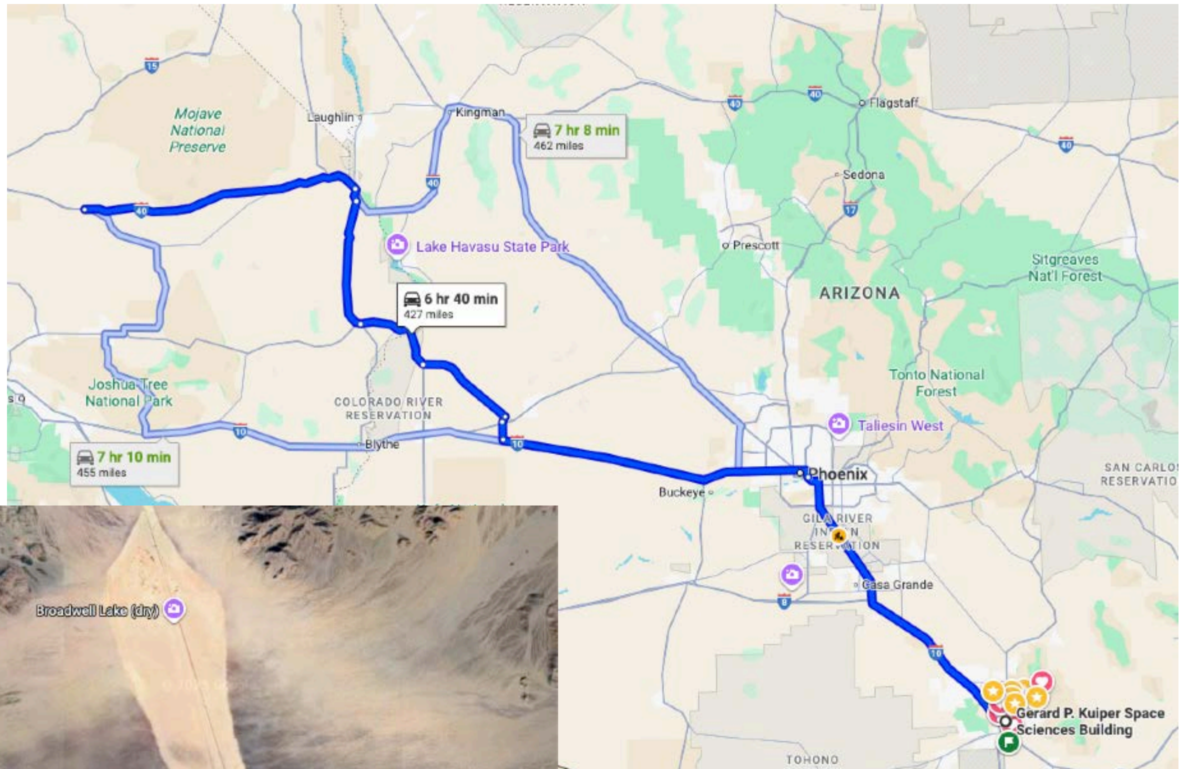



Campsite:
Approximately
34.815031 N,116.176967 W
(North on Crucero Rd from Ludlow)

**Day 2:** on to Fossil Falls, CA


At Fossil Falls, meet at small playa parking area (red dot)

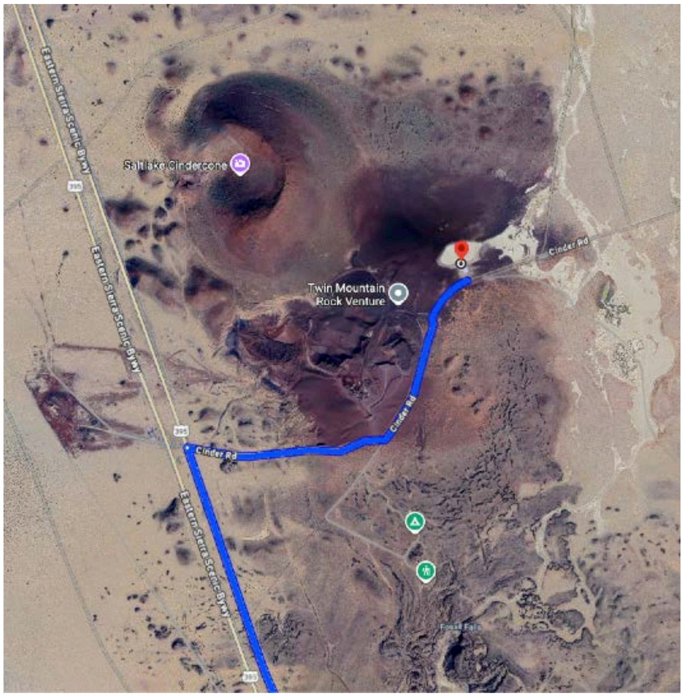

Onward to campground near Bishop, with several stops on the way (not all shown).  We will convoy for these.


**Days 3 and 4:**  We will be together or in groups, will share waypoints by WhatsApp and coordinate by radio en route as needed.

**Thursday** *achieve escape velocity*

8:00 Vehicle pickup, people meet at Kuiper loading dock
(one will go to Sonett to load radar gear)

9:00 Depart

5:30pm Meet at Dairy Queen: 25635 Crucero Rd, Ludlow, CA 92338
Last chance for Oreo Blizzard. And real bathrooms for the night.
Head to camp at dry lake, set up. (NOTE: SUNSET 6:30pm)

(evening) Chengyan - Pacific - North America plate interaction history
Anna - Joseph Rutherford Walker

**Friday** *enter the Valley*

0700 rise and shine
0800 depart camp, make dust

Robin - Ridgecrest Earthquake

11:00 arrive at Fossil Falls, meet up with UCLA folks

*Sarah Preston and Kenzie Day (UCLA) - discuss aeolian features*
Madison - lava flows and the falls
Radar activities - subgroup for full time

2:00pm 590 departs, some radaristas possibly stay longer

Sophie - LA County water/land grab
Gabe - Owens Lake
Kiki - Saline Valley salt tram
Joe (for Melissa) - 1872 Owens Valley Earthquake
Joanna - Big Pine volcanics
Arkadeep - mantle xenoliths (or move to Sat if not enough time)

6:00pm Arrive at campsite

**Saturday** *rock glacier extravaganza and south of Bishop*

0700 Rise and shine
0800 Depart camp for rock glacier

Jingyu - Glaciations of the Sierra Nevada
Euibin - rock glaciers overview
Ruby - rock glaciers internal structure

12:30pm 590 group departs for sites south:
Cole - OVRO
Chaucer - White-Inyo stratigraphy
Lily - Trilobites
Thea - Uplift of the Sierra Nevada

7:00pm Back at camp

(evening) Elana - Owens Valley meteorite

**Sunday** *North to volcanic mecca and salty inland lake of mystery*

0800 depart camp

Kylie - Pupfish
Carter - Bishop Tuff - Long Valley Caldera (two stops)
*Liz Warner (guest) - fossil fumaroles, geochemistry, etc.*
Kiki - Hot springs of the eastern Sierras
Christina - Glacial moraines
Mono Lake - radar extravaganza, *plus for non-radaristas: other stops around Mono Lake: Panum Crater, tufa towers, etc.*

**Monday** *return to real life*

butt-early depart camp, back to Tucson.

**Supplementary Maps and Figures**

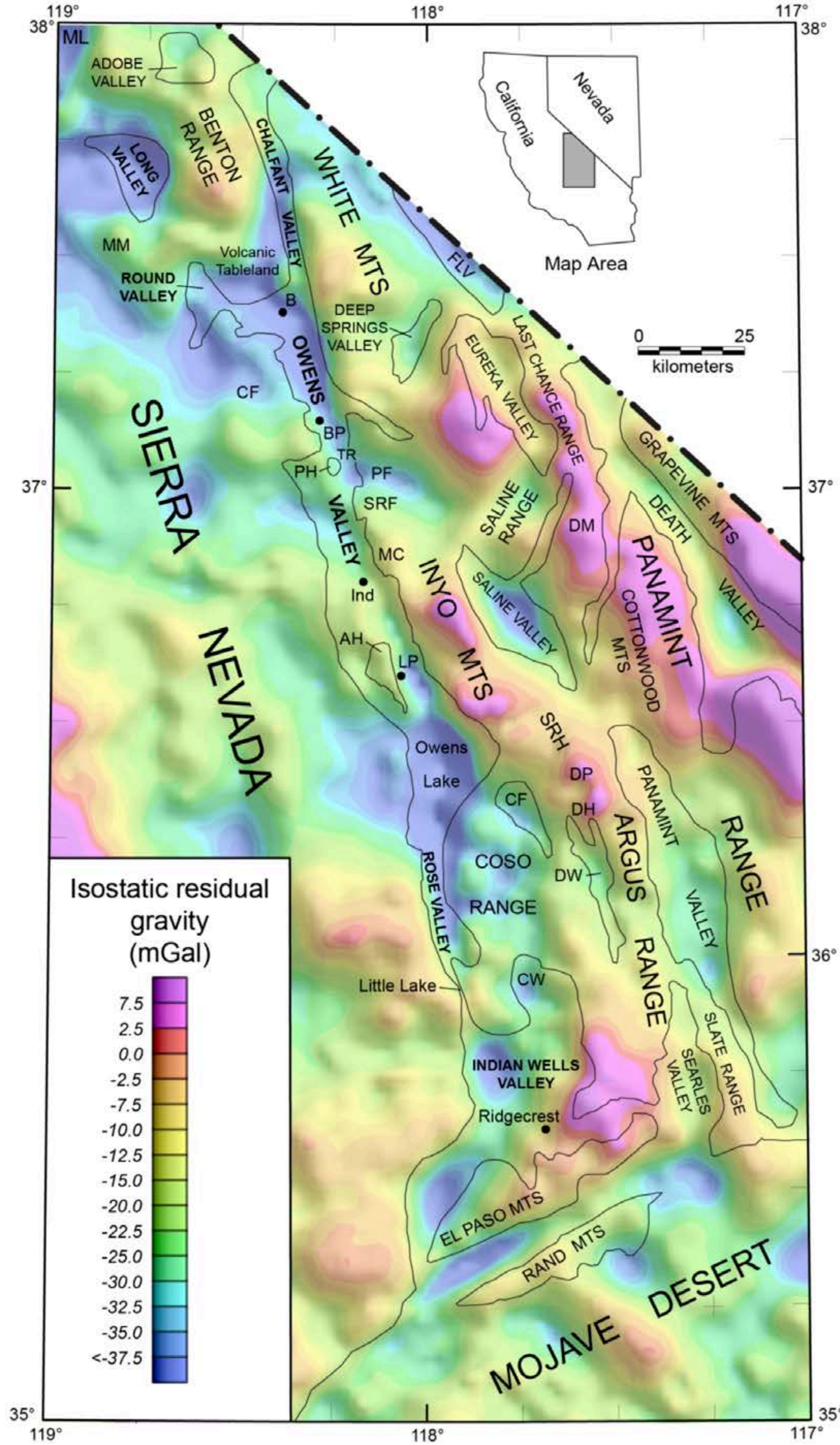

119°
118°
117°
38°
37°
36°
35°
ML
ADOBE VALLEY
LONG VALLEY
BENTON RANGE
CHALFANT VALLEY
WHITE MTS
California
Nevada
Map Area
MM
ROUND VALLEY
Volcanic Tableland
B
FLV
DEEP SPRINGS VALLEY
EUREKA VALLEY
LAST CHANCE RANGE
0 25
kilometers
OWENS
CF
SIERRA
BP
TR
PH
PF
SRF
VALLEY
MC
Ind
SALINE RANGE
DM
GRAPEVINE MTS
DEATH VALLEY
PANAMINT
INYO MTS
SALINE VALLEY
COTTONWOOD MTS
AH
LP
NEVADA
SRH
Owens Lake
DP
DH
CF
PANAMINT VALLEY
ARGUS RANGE
RANGE
COSO RANGE
DW
ROSE VALLEY
Isostatic residual gravity (mGal)
7.5
2.5
0.0
-2.5
-7.5
-10.0
-12.5
-15.0
-20.0
-22.5
-25.0
-30.0
-32.5
-35.0
<-37.5
Little Lake
CW
INDIAN WELLS VALLEY
Ridgecrest
SEARLES VALLEY
SLATE RANGE
EL PASO MTS
RAND MTS
MOJAVE DESERT


Mono Lake
Grant Lake
Owens River
Lake Crowley
NEVADA
CALIFORNIA
Tinemaha Reservoir
Owens (Dry) Lake
Haiwee Reservoir
L.A. Aqueduct
Los Angeles-Long Beach-
-Santa Ana Metro. Area

## Emergency Information

U of A Travel Emergency: 520-307-9576

U of A Travel Incident: 800-243-6124

U of A Risk Management: 520-621-1790

Jack Holt's cell phone: 512-299-5316

Jack's Garmin InReach: jack.w.holt@inreach.garmin.com

Joe Schools' cell phone: 714-308-2592

# Pacific - North America plate interaction

Chengyan Xie

## 1. Introduction

The theory of plate tectonics provides the framework for understanding the large-scale motions of Earth's lithosphere. Tectonic plates, massive slabs of Earth's crust and upper mantle, interact at their boundaries, leading to the creation of mountains, volcanoes, and earthquakes. The Pacific Plate, the largest tectonic plate on Earth, and the North American Plate, the second largest, share a complex and evolving boundary [1]. I will explain the key tectonic processes and then focus on the significant changes that have occurred in the last 10 million years (10 Myr), which have directly shaped the modern landscape of western North America [2].

## 2. Geological Background: From Subduction to Transform Motion

For much of the Mesozoic and early Cenozoic eras, the dominant mode of interaction along the western edge of North America was **subduction**. The Farallon Plate (and its remnants, the Juan de Fuca and Cocos plates) was diving eastward beneath the North American Plate [1]. This convergent boundary was responsible for the massive volcanic activity that formed the Sierra Nevada batholith and later the Cascade Range.

A major shift began approximately 30 million years ago as the spreading center between the Pacific and Farallon plates, the East Pacific Rise, started to collide with the North American trench. This initiated the transition from a convergent boundary to a **transform boundary**, where the Pacific Plate began sliding horizontally past the North American Plate [2][3]. This change set the stage for the geologic events of the last 10 million years.

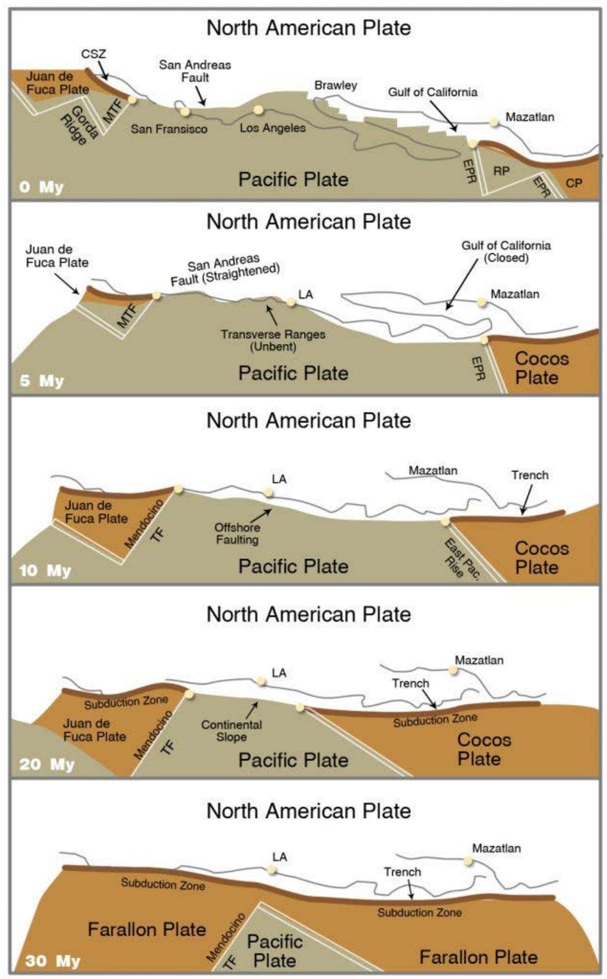


Fig. 1 Sketch of the Plate interaction from 30Myr ago [3]

### 3. Major Tectonic Events of the Last 10 Million Years

The last 10 million years have been a period of intense and consequential tectonic activity along the Pacific-North America boundary. The two most important processes during this time are the development of the San Andreas transform system and the rifting in the Gulf of California.

#### 3.1 The San Andreas Fault System

The San Andreas Fault is the definitive feature of this transform boundary. For the past 10 million years, the Pacific Plate has been grinding horizontally past the North American Plate at an average rate of about 5 cm/year [3]. This motion is not smooth but occurs in sudden, catastrophic jumps that generate major earthquakes. The cumulative effect of this movement over millions of years has been the displacement of geological features by hundreds of kilometers. This fault system is a primary reason for the high seismic hazard in California [4].

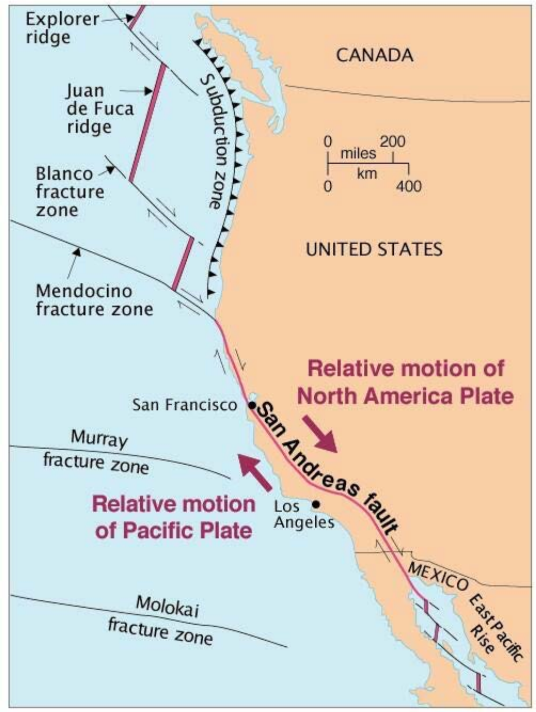


Fig. 2 Sketch of the plate motion that shapes the San Andreas fault [2]

#### 3.2 The Eastern California Shear Zone and Distributed Deformation

It is important to understand that the movement between the plates is not taken up only by the San Andreas Fault. A significant portion, perhaps 15-25%, is accommodated by a network of faults to the east, known as the **Eastern California Shear Zone (ECSZ)**. This zone is a wide belt of right-lateral strike-slip faults, including the famous Owens Valley, Panamint Valley, and Death Valley fault systems [7]. The activity in the ECSZ shows that the plate boundary is not a single line but a broad, complex zone of deformation. Major earthquakes, such as the 1872 Owens Valley earthquake, demonstrate that this zone is seismically active and important for understanding the total tectonic picture. Some scientists suggest that over time, the ECSZ may become the new primary plate boundary, replacing the current San Andreas Fault in Southern California.

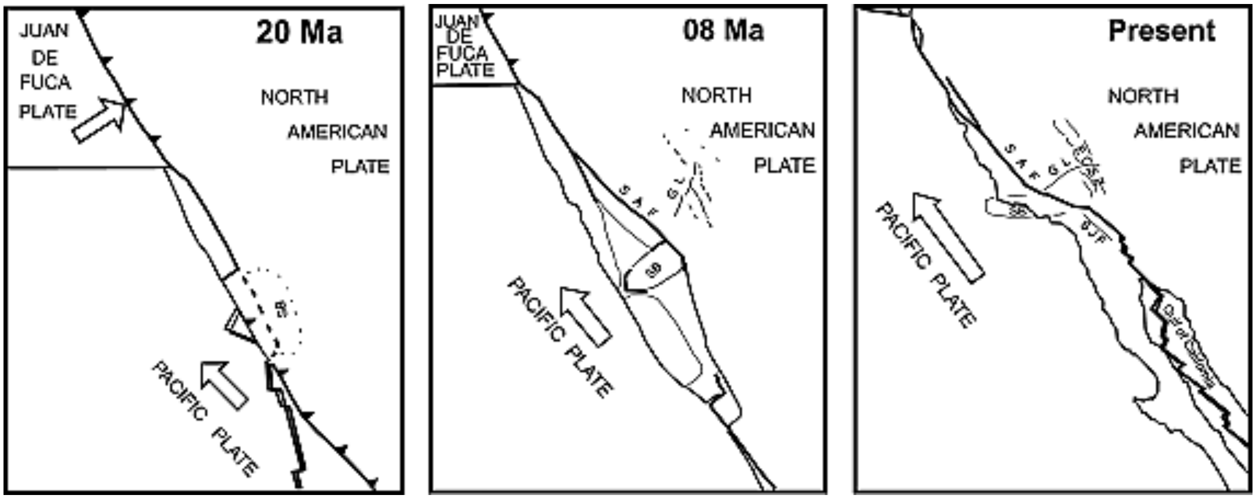


Fig. 3 Sketch of the Eastern California Shear Zone [7]

### 3.3 Basin and Range Extension

To the east of the Sierra Nevada, a very different tectonic phenomenon occurs: the Basin and Range Province. This vast area is characterized by parallel mountain ranges separated by flat, sediment-filled valleys, forming a distinctive pattern. This topography is the result of crustal extension, where the Earth's crust is being pulled apart in an east-west direction. While this extension began earlier, it has continued actively throughout the last 10 million years. The driving forces for this extension are complex and debated. One major theory connects it to the subduction of the Farallon Plate. As the plate sank into the mantle, it may have created a flow that stretched the overlying continent. Another factor is the westward movement of the North American Plate relative to the San Andreas system, which may also contribute to pulling the region apart. The combination of the transform boundary to the west and this ongoing extension to the east creates a unique and dynamic tectonic environment.

Table 1: Key Tectonic Features along the Pacific-North America Boundary

| Tectonic Feature | Type of Boundary/Deformation | Geological Result | Recent Activity (Last 10 Myr) |
|---|---|---|---|
| **San Andreas Fault** | Transform (Primary) | Horizontal displacement of terrain | Primary site of earthquake activity in California . |

| | | | |
|---|---|---|---|
| **Eastern California Shear Zone (ECSZ)** | Transform (Distributed) | Network of fault zones east of Sierra Nevada | Accommodates ~15-25% of plate motion; significant seismic hazard . |
| **Basin and Range Province** | Extensional (Divergent) | Parallel mountain ranges and valleys (horsts and grabens) | Ongoing crustal stretching, thinning the continental crust . |

**4. Implications for Seismic and Volcanic Hazards**
The tectonic processes described above have direct implications for the millions of people living in western North America. The **San Andreas Fault system** poses a persistent and major earthquake threat. However, the recognition of the **Eastern California Shear Zone** means that the seismic hazard is spread over a wider area, affecting regions east of the main fault. The **Basin and Range Province** also experiences earthquakes due to the ongoing extensional faulting. Understanding the history and current state of these plate interactions is essential for risk assessment and preparedness.

**5. Comparison to other planets**

On Earth, the complex plate interaction—combining strike-slip motion, subduction, and mountain-building—is driven by the planet's vigorous internal heat engine, which fuels mantle convection and plate motion. This serves as a key point of comparison. Venus, for instance, lacks Earth-style plate tectonics, yet its surface shows evidence of vast, recent tectonic and volcanic activity, suggesting a different mode of releasing internal heat—perhaps through episodic global resurfacing. The distributed deformation and volcanism of the western North American margin provide a possible analog for understanding how strain is accommodated on a planet without rigid, moving plates.

Furthermore, the evolution of this boundary over tens of millions of years, from a dominant subduction zone to a primarily transform system, models how planetary surfaces can be radically reconfigured over geologic time. This history of tectonic switching provides a framework for interpreting cryptic surface features on other bodies. For example, the complex fault systems and potential ancient tectonic belts on Mars suggest it may have experienced a transitional phase of plate-like activity before its interior cooled sufficiently to shut down large-scale horizontal motion.

**6. Conclusion**
The interaction between the Pacific and North American plates has evolved significantly over time. The last 10 million years, in particular, have been a period of dramatic change

that has defined the present-day geology of the region. The establishment of the San Andreas Fault as a mature transform boundary and the opening of the Gulf of California are the key developments of this period. These processes continue today, meaning that the tectonic evolution of western North America is an ongoing story. The plates continue to move, storing energy for future earthquakes and gradually reshaping the continent. Continued study of this dynamic boundary is crucial for both scientific understanding and public safety.

**Reference**:


[1] Website page, https://www.worldatlas.com/geography/7-major-tectonic-plates.html

[2] USGS page, https://pubs.usgs.gov/gip/dynamic/understanding.html

[3] Robert S. Yeats (2018), Living With Earthquakes In The Pacific Northwest https://open.oregonstate.education/earthquakes/

[4] National geographic textbook, https://education.nationalgeographic.org/resource/plate-tectonics-ring-fire/

[5] Wikipedia page, https://en.m.wikipedia.org/wiki/List_of_tectonic_plate_interactions

[6] Website page, https://www.mbari.org/news/the-geologic-setting-of-the-gulf-of-california/

[7] Mian Liu et al. (2010), Inception of the eastern California shear zone and evolution of the Pacific-North American plate boundary: From kinematics to geodynamics, https://doi.org/10.1029/2009JB007055

# Glaciations of the Sierra Nevada

Jingyu Wang

## Introduction of Sierra Nevada

Nestled in eastern California, the Sierra Nevada is a massive, fault-block mountain range stretching approximately 400 miles (640 km) north-to-south. Geologically, it is defined by its dramatic asymmetry: a gentle, sloping western side that descends toward the Central Valley, and a steep, rugged eastern escarpment that rises sharply from the Basin and Range Province.

The terrain is dominated by the exposed granite of the Sierra Nevada batholith, a vast body of igneous rock formed deep underground during the Mesozoic Era. This granitic core has been uplifted and tilted, then sculpted by erosion into a dramatic landscape of high, rolling ridges and profoundly deep, river-cut canyons. The most striking features, however—including sheer cliffs, jagged peaks, and U-shaped valleys—are the direct result of extensive glaciation during the Ice Ages. This combination of tectonic history and glacial erosion has created the range's characteristically rugged and rocky topography.

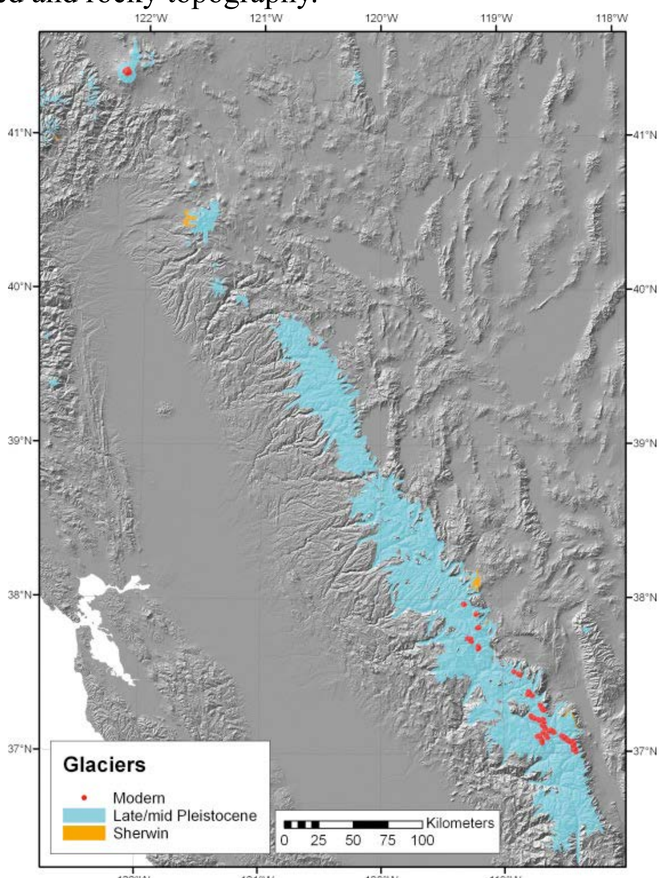


Figure 1. Extent of Quaternary glaciers in the Sierra Nevada. Late Pleistocene (Tioga) and older glacial deposits are, in general, so similar in extent that they are difficult to distinguish at this scale (Gillespie&Clark, 2011).

## Introduction of glaciation mechanism

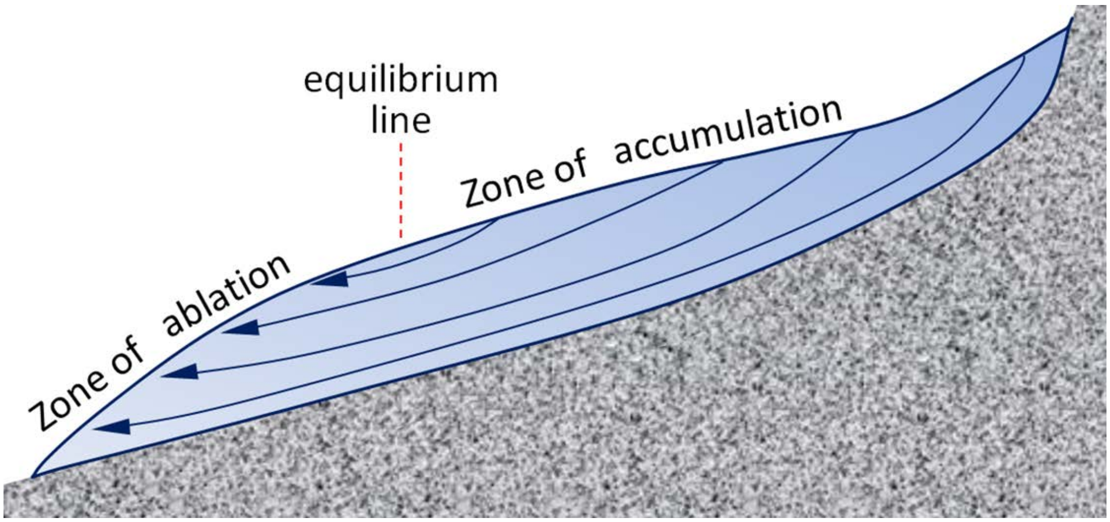


Figure 2. Schematic ice-flow diagram for an alpine glacier (Harris & Huff, 2020).

Glaciation is the process involving the formation, movement, and erosive power of glaciers. It begins with the accumulation of snow that, over time, is compressed into dense, granular firn and then recrystallized into solid glacial ice. When this ice mass becomes sufficiently thick (typically over 30-50 meters), it begins to flow under the pressure of its own weight (Harris & Huff, 2020).

Glaciers move via two primary mechanisms: internal deformation, where ice crystals slide past one another, and basal sliding, where the entire glacier slides over its bedrock base, often lubricated by meltwater (Harris & Huff, 2020). This movement makes glaciers powerful agents of erosion. They sculpt the landscape primarily through two processes:

1. Abrasion: The debris-rich base of the glacier acts like sandpaper, grinding the underlying bedrock and creating striations (scratches) and polished surfaces.
2. Plucking: The glacier freezes onto and fractures bedrock. As it moves, it pulls or "plucks" loose these rock fragments, which are then incorporated into the ice.

Through these mechanisms, glaciers carve distinctive landforms such as U-shaped valleys, cirques, and arêtes, fundamentally reshaping the topography.

## Major Glacial Episodes

The glacial history of the Sierra Nevada is a complex record of multiple advances and retreats throughout the Quaternary Period, driven by global climate cycles and modulated by the region's unique topography. The chronology has been refined through mapping, relative dating techniques (like soil development), and, increasingly, numerical dating methods such as cosmogenic nuclide exposure dating (e.g., $^{36}Cl$, $^{10}Be$).

The major glaciations are summarized from oldest to youngest as follows:

**1. Pliocene and Early Pleistocene Glaciations (> ~820 ka)**

The evidence for the earliest glaciations is sparse and fragmentary due to erosion by later ice sheets. The oldest identified till is the McGee Till, found atop McGee Mountain. Its age is constrained by the fact that it overlies a 2.7-million-year-old basalt flow, and the deep incision of McGee Creek since the boulders were deposited suggests a very old age, likely around 1.5 million years. These early deposits consist of deeply weathered erratic boulders on highland surfaces, indicating that the landscape was significantly different and that numerous unnamed glaciations likely occurred during this period.

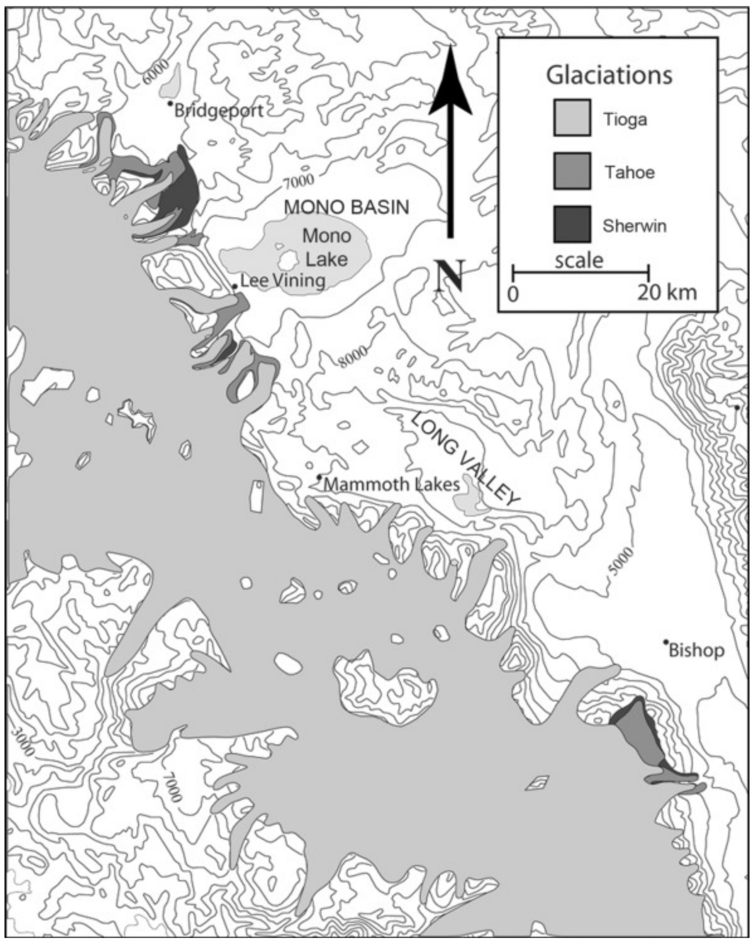


Figure 3. Extent of the ~ 820 ka Sherwin drift relative to ~ 20 ka Tioga drift in the central Sierra Nevada. Contour intervals are 305 m (Gillespie&Clark, 2011).

**2. Sherwin Glaciation (~820 ka)**
The Sherwin Till is a key marker, as it is found beneath the Bishop Tuff, a volcanic deposit dated precisely to 759 ± 2 ka. Weathering characteristics and cosmogenic nuclide dating suggest the Sherwin glaciation itself occurred around 820 ka. Sherwin glaciers were more extensive than their successors in many areas, spreading further onto the low-gradient floors of basins like Bridgeport. This greater extent, however, may be due to the gentle topography, requiring only a modest additional depression of the Equilibrium-Line Altitude (ELA) compared to later glaciations.

**3. Middle Pleistocene Glaciations (MIS 22-6: ~830–186 ka)**
This long interval contains evidence for several glaciations, but the record is incomplete. Deposits correlated with the Rockland Ash (~550 ka) suggest glaciation around that time. Other tills, such as the "pre-Tahoe" deposits in Bloody Canyon and the Casa Diablo Till near Mammoth Lakes, are tentatively placed within the Marine Isotope Stage (MIS) 8-6 interval (roughly 300-130 ka). However, numerical age control for this period remains problematic, with often contradictory results from different dating techniques.

**4. MIS 6 Glaciations (e.g., Mono Basin and Tahoe I: ~186–128 ka)**
The glacial record becomes clearer with MIS 6. This period includes the Mono Basin and Tahoe I glaciations. Moraines from this era are broad-crested and deeply eroded. Cosmogenic exposure ages for Mono Basin moraines were initially around ~103 ka but were later revised downward to ~80–60 ka, highlighting challenges in dating older surfaces subject to erosion. The Tahoe glaciation, originally defined by Blackwelder, was later shown to be composite at type localities like Bloody Canyon, consisting of at least two advances (Tahoe I and Tahoe II). ELAs during MIS 6 were depressed about 100–200 m below those of the last glacial maximum.

**5. Late Pleistocene Glaciations (MIS 5-2: ~128–14 ka)**
This period saw the most detailed sequence of advances, including the Tenaya and Tioga glaciations. Lake sediment cores indicate numerous short-lived advances, but only the most significant left preserved moraines.

- Tenaya Glaciation: Occurring around 31-28 ka, this was a significant advance prior to the last glacial maximum.
- Tioga Glaciation: This was the most extensive advance of the last glacial cycle, with multiple stades (Tioga 1-4) between ~25 and 15 ka. The maximum extent was reached around 21–20 ka, with ELAs depressed about 820 meters relative to modern glaciers. Retreat from the maximum positions was rapid, likely taking only 1,000-2,000 years, with the Sierra crest nearly ice-free by ~15.2 ka.

**6. Post-Tioga (Holocene) Advances**
Following the Tioga retreat, there were minor re-advances during the Holocene:

- Recess Peak Advance: Previously thought to be a Neoglacial event (last few thousand years), rigorous dating of lake sediments showed this advance was much older, occurring between ~14.2 and 13.1 ka. This places it before the global Younger Dryas cold period, for which there is no evidence of significant glaciation in the Sierra Nevada.
- Neoglaciation and Matthes (Little Ice Age) Advance: Glaciers re-formed during the late Holocene, with the most recent significant advance, the Matthes glaciation, reaching its maximum after a volcanic eruption ~180 cal years BP, during the last few centuries (circa 1600-1850 AD).

## Planetary analogy

The Sierra's glaciers, which persist today only in sheltered cirques well below the regional snowline due to wind-blown accumulation and shade, mirror the behavior of ice on Mars (Head & Marchant, 2014). Martian glaciers, particularly in mid-latitudes, are thought to survive in similarly protected niches where local topography creates favorable conditions despite a generally inhospitable climate. Furthermore, the concept of an equilibrium-line altitude (ELA)—a specific elevation where ice accumulation equals ablation—is a transferable principle. On a moon like Titan, which has a methane-based hydrologic cycle, one could theorize about a "methane-ice ELA," an altitude or latitude where conditions are just right for the stability of solid hydrocarbons.

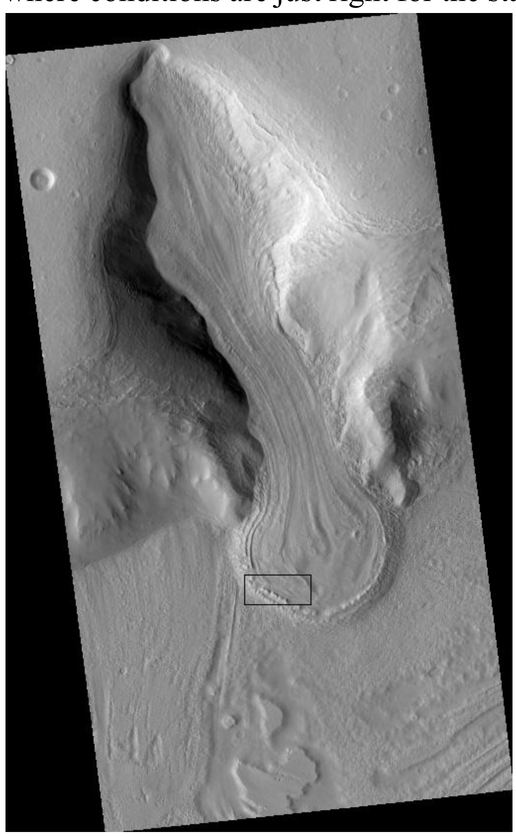

Figure 4. Martian glacier as seen by HiRISE.

# References:

Harris, R., & Huff, L. C. (Eds.). (2020). Physical geology (2nd Canadian ed.). BCcampus. https://opentextbc.ca/physicalgeology2ed/

Head, J. W., & Marchant, D. R. (2014). The climate history of early Mars: Insights from the Antarctic McMurdo Dry Valleys hydrologic system. Antarctic Science, 26(6), 774–800. https://doi.org/10.1017/S0954102014000686

Gillespie, A. R., & Clark, D. H. (2011). Glaciations of the Sierra Nevada, California, USA. In J. Ehlers, P. L. Gibbard, & P. D. Hughes (Eds.), Developments in Quaternary Science: Vol. 15. Quaternary glaciations-extent and chronology (pp. 447–462). Elsevier. https://doi.org/10.1016/B978-0-444-53447-7.00034-9

# <u>2019 Ridgecrest Earthquake</u>

Robin B. Van Auken

<u>Overview:</u>

- Thursday, July 4th (10:33 a.m. PDT): A magnitude 6.4 foreshock occurred 11 miles E-NE of Ridgecrest, along a SW-NE striking fault (*indicated by the orange circle in Figure 1*).

- Friday, July 5th (8:20 p.m. PDT): A magnitude 7.1 mainshock struck northwest of the previous earthquake, rupturing in a primarily NW-SE direction (*indicated by the red circle in Figure 1*)

- These two ruptures are examples of a conjugate fault pair, where faults occur at an angle related to the orientation of the principal stresses $\sigma_1$ and $\sigma_2$.

- These earthquakes occurred in the Eastern California Shear Zone (ECSZ), the southern extension of Walker Lane. This area accommodates 25% of the motion of the San Andreas fault and over large time scales (millions of years) both Walker Lane and the ECSZ may evolve to take over more of the Pacific-North American plate boundary strain (Cochran et al., 2020).

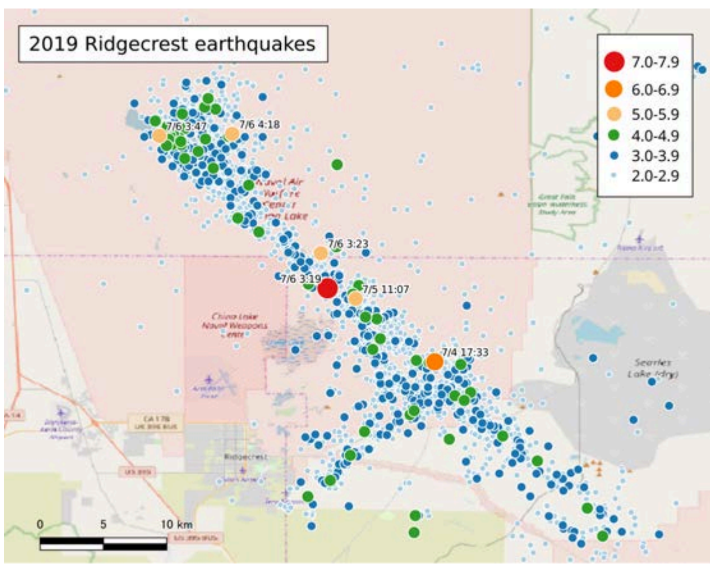


*Figure 1. Map of the 2019 earthquakes, showing their magnitudes and locations. The orange circle indicates the 6.4 foreshock and the red circle indicates the 7.1 main earthquake. (Phoenix7777, 2019)*

<u>Principal Stresses and Faulting</u>

When rocks are subjected to stress, that stress can be broken down into three principal stresses, which are mutually perpendicular to each other:

- $\sigma_1$ = maximum compressive stress
- $\sigma_2$ = intermediate stress
- $\sigma_3$ = minimum compressive stress

Faults and fractures tend to form in predictable orientations relative to these stresses:

- $\sigma_1$ vertical -> normal faulting occurs
- $\sigma_2$ vertical -> strike-slip faulting occurs
- $\sigma_3$ vertical -> thrust/transverse faulting occurs

Along the western seaboard, strike-slip faulting dominates as the Pacific Plate moves north relative to the North American Plate moving to the south. In this environment $\sigma_2$ is vertical, $\sigma_1$ has a N-S orientation, and $\sigma_3$ has an E-W orientation. Faults in this configuration form at a ~30° angle from the maximum compressive stress ($\sigma_1$), creating two possible shear orientations. These paired faults are known as conjugate faults and slip can occur along either orientation. Notice that the Ridgecrest conjugate faults are oriented closer to ~45° from $\sigma_1$, likely reflecting rupture along pre-existing regional fracture orientations.

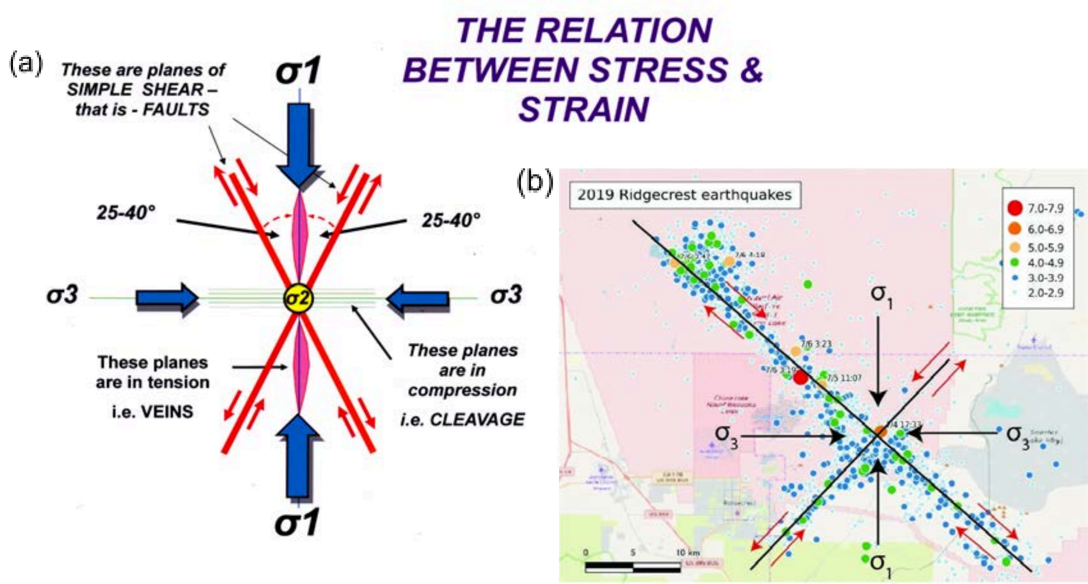


*Figure 2. (a) Relation between $\sigma_1$ and $\sigma_3$ and conjugate faults. (b) $\sigma_1$ and $\sigma_3$ in relation to the 2019 Ridgecrest earthquakes.*

An unusual thing about the Ridgecrest earthquake sequence is that slip occurred along both conjugate fault planes. Typically one of the conjugate faults is more likely to fail based on pre-existing weaknesses that localize strain. Slip occurs on one set and usually relieves stress on the conjugate set, reducing the likelihood of subsequent rupture. Why didn't that happen?

- Seismic studies show that both the NE-SW and NW-SE planes had accumulated significant strain (Ross et al., 2019; DuRoss et al., 2020).

- The foreshock didn't fully release the regional stress. Instead, because many faults in the area are linked at shallow depth, the foreshock ruptured only a short segment and actually brought the adjacent NW-SE system closer to the Coulomb failure envelope (Nanjo, 2020).

Aftermath:

- The epicenter was about 200 km north of Los Angeles, but shaking was felt throughout the city, with noticeable swaying of tall buildings in downtown L.A. Buildings have a natural period of vibration, the time it takes them to sway back and forth, and long-period seismic waves (surface waves, i.e. Love and Rayleigh) from the Ridgecrest earthquake resonated with these periods.

- The Los Angeles early warning alert system did not trigger during the earthquakes, which drew criticism from the public. In response, the threshold for issuing alerts was lowered to ensure future notifications are sent even for moderate shaking that could impact urban areas.

*Figure 3. Road damage resulting from 3 to 5 feet of right-lateral motion (USGS, 2019).*

*Figure 4. Crack in my LA apartment (Van Auken, 2019).*

Planetary Analog: Conjugate Faults on Mars

Conjugate faults have been observed in Mars' Tharsis region (Andrews-Hanna et al., 2008).Volcanic loading from the Tharsis volcanic rise flexed and stressed the lithosphere. This created large horizontal stresses radiating away from Tharsis. ($\sigma_1$). As Mars cooled, the whole planet shrank, and this was responsible for the lowest compressive stress, which was also horizontal ($\sigma_3$). The overburden acts as $\sigma_2$, which creates a strike slip regime and allows for conjugate strike-slip faulting.

Based on Figure 5 of these conjugate faults, what direction are $\sigma_1$ and $\sigma_3$ in the picture?

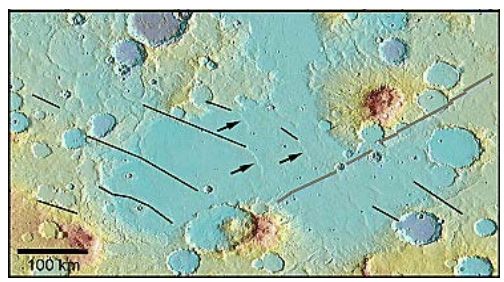


*Figure 5. Potential strike-slip faults (black lines) are conjugate faults (Andrews-Hanna et al., 2008).*

References:

Andrews-Hanna, J. C., Zuber, M. T., & Hauck, S. A. (2008). Strike-slip faults on Mars: Observations and implications for global tectonics and geodynamics. *Journal of Geophysical Research: Planets, 113*(E8).

Cochran, W. J., Spotila, J. A., & Prince, P. S. (2020). Incipient evolution of the Eastern California shear zone through the transpressional zone of the San Bernardino Mountains and San Gorgonio Pass, California. *Geosphere, 16*(4), 919–935.

DuRoss, C. B., Gold, R. D., Dawson, T. E., Scharer, K. M., Kendrick, K. J., Akciz, S. O., ... & Zinke, R. (2020). Surface displacement distributions for the July 2019 Ridgecrest, California, earthquake ruptures. Bulletin of the Seismological Society of America, 110(4), 1400-1418.

Nanjo, K. Z. (2020). Were changes in stress state responsible for the 2019 Ridgecrest, California, earthquakes?. Nature communications, 11(1), 3082.

Phoenix7777. (2019, July 6). Map of 2019 Ridgecrest earthquakes [SVG]. *Wikimedia Commons*. https://commons.wikimedia.org/wiki/File:Map_of_2019_Ridgecrest_earthquakes.svg

Ross, Z. E., Idini, B., Jia, Z., Stephenson, O. L., Zhong, M., Wang, X., ... & Jung, J. (2019). Hierarchical interlocked orthogonal faulting in the 2019 Ridgecrest earthquake sequence. Science, 366(6463), 346-351.

USGS. (2019, October 15). The ups and downs of groundwater levels after the July 2019 Ridgecrest earthquakes [Photograph]. *U.S. Geological Survey*. https://www.usgs.gov/news/groundwater-news/ups-and-downs-groundwater-levels-after-july-2019-ridgecrest-earthquakes

# FOSSIL FALLS LAVA FLOWS

Madison Tuohy[1, 2]
[1]Department of Geosciences, 1040 E 4th St, Tucson, AZ 85719
[2]Lunar and Planetary Laboratory, 1629 E University Blvd, Tucson, AZ 85721

## I. The Coso Volcanic Field

The Coso Volcanic Field, located along the western edge of the Basin and Range Province, covers ~400 km² and has been active from ~3.5 Ma to as recently as 40 ka (Duffield & Bacon, 1981; Hildreth, 2007). It records a diverse history of volcanism, producing both basaltic lava flows and cinder cones as well as high-silica rhyolitic domes and flows**.**

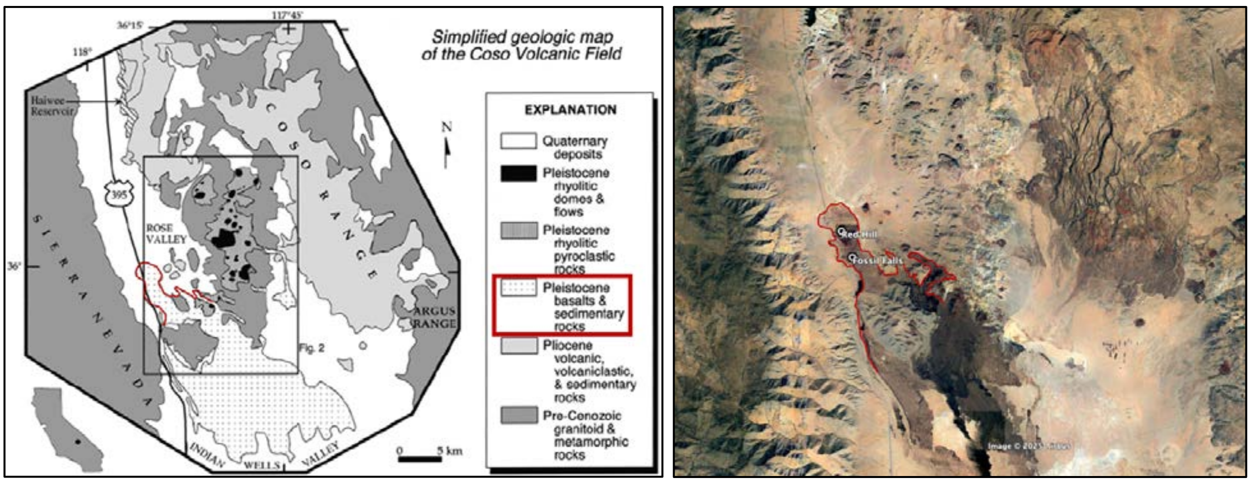


*Figure 1. Left: Simplified geologic map of the Coso Volcanic Field, showing the Fossil Falls lava flows outlined in red (modified from Duffield & Bacon, 1981). Right: Google Earth satellite image highlighting the same lava flows in red for comparison, with Fossil Falls and Red Hill marked.*

The Coso field is best known for its Pleistocene rhyolite (*NOTE*: the Pleistocene Epoch lasted from ~2.6 million to ~11,700 years ago, which is *very* recent on the geologic time scale). Thirty-eight rhyolite domes and flows form an elongate array atop a north-trending 8 × 20 km horst of Mesozoic bedrock. Nearby uneroded constructional forms are exhibited by most domes. Many are nested within tuff ring craters, and some filled and overrode their craters to feed flows one to two kilometers long (Duffield, Bacon, & Dalrymple, 1980). Obsidian is exposed locally on most extrusions, and geochemical analyses show that the rhyolite is high-silica (~77% $SiO_2$). Trace-element variations define at least seven compositional age groups (Hildreth, 2007).

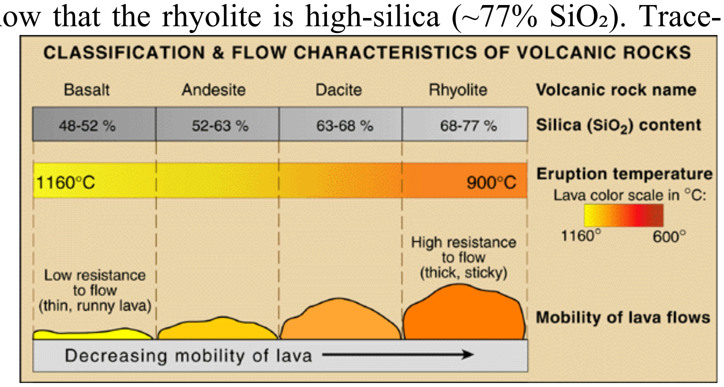


*Figure 2. Classification and flow characteristics of volcanic rocks, including basalt, andesite, dacite, and rhyolite. Note the increasing SiO content and the decreasing temperature as rocks transition to more silicic rocks.* (Sigurdsson et al. 2015)

The coexistence of rhyolite and basalt reflects the bimodal character of volcanism in the Coso Volcanic Field. According to Bacon (1982), the timing and volume of these eruptions are closely tied to Basin and Range extension. Dikes were injected into the crust as extensional strain accumulated; each dike-forming event relieved a portion of this strain, and the volume of erupted material reflected the amount of strain released. In this way, volcanism at Coso directly records the tectonic forces driving extension across the Basin and Range Province. Basaltic eruptions, especially from the Red Hill cinder cone (~10 ka), produced extensive lava flows that filled valleys and redirected the Owens River, setting the stage for the formation of Fossil Falls (Getman, UCLA).

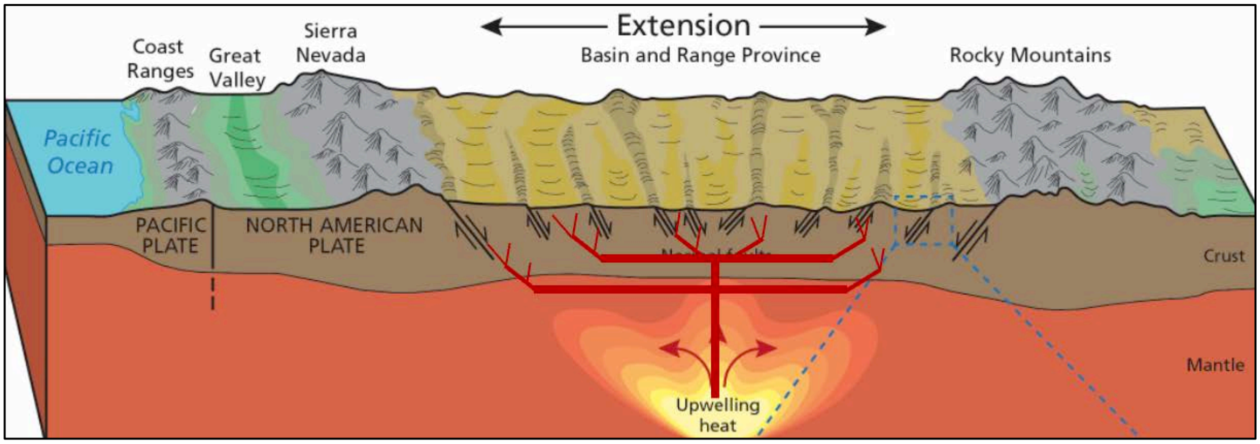


***Figure 3.*** *Schematic cross-section of the Basin and Range Province showing crustal extension, normal faulting, and associated feeder dike intrusion. Extension has stretched the crust to nearly twice its original width, producing alternating horsts (uplifted blocks) and grabens (downdropped basins). At Coso, this tectonic extension provided fractures and pathways for basaltic and rhyolitic magma to reach the surface, driving eruptions that formed features such as the Fossil Falls lava flows. Red lines indicate generalized examples of extensional dike intrusions and are not drawn to scale, orientation, or exact location.*

## II. Fossil Fall Lithology and Volcanics

The rock at Fossil Falls consists of basaltic lava flows erupted between ~440 ka and ~10 ka (Duffield, Bacon & Dalrymple, 1980). These lavas are typically dark gray to black in color, with abundant gas bubbles (vesicles) that formed during eruption. In several exposures, features such as columnar jointing and flow banding are visible, providing evidence of cooling and emplacement dynamics (Hildreth, 2007). The observed basaltic unit at Fossil Falls is interpreted as volcanic outflow from Red Hill, a nearby cinder cone that last erupted approximately 10,000 years ago (Duffield & Bacon, 1981; Hildreth, 2007; Day, UCLA).

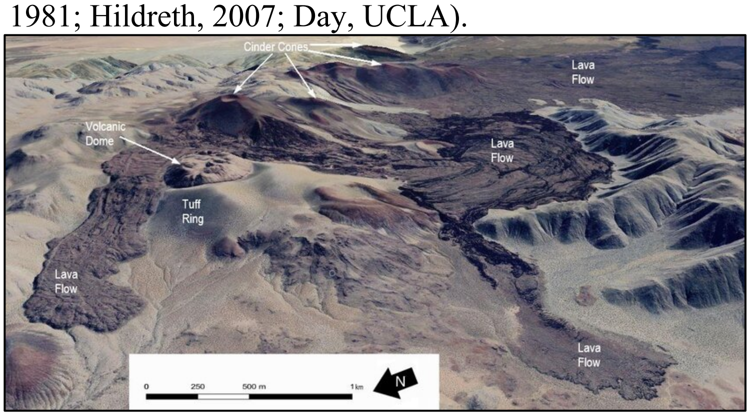


*Figure 4. Satellite image of the Coso Volcanic Field showing Red Hill cinder cone and associated lava flows (modified from Google Earth, 2024).*

Red Hill is a cinder cone volcano that rises ~630 feet and is composed primarily of pumice and scoria. Scoria consists of irregularly shaped, highly vesicular fragments of basaltic lava that cool and solidify before landing on the surface. This pyroclastic material is typically produced during moderately explosive eruptions of gas-rich basalt, a common feature of Strombolian activity that builds cinder cones (Lockwood & Hazlett, 2010).

While Red Hill erupted explosively to produce scoria and ash, the same vent also fed effusive basaltic lava flows that extended into surrounding valleys (Duffield, Bacon & Dalrymple, 1980). These flows now form the bedrock of Fossil Falls. The combination of pyroclastic cone-building activity and lava outpouring is typical of Strombolian eruptions, where both explosive and effusive products are generated from the same vent (Macdonald, 1972; Lockwood & Hazlett, 2010).

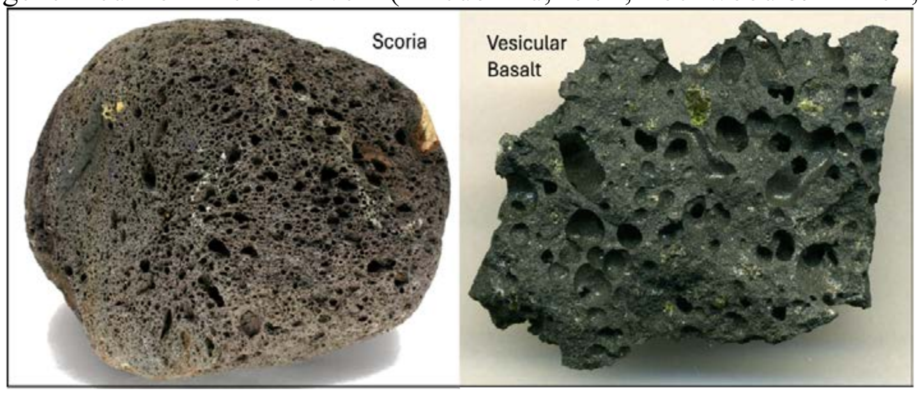


*Figure 5. Scoria compared to basalt. Image depicts rock types from the Cascades.*

## III. Geomorphology of Fossil Falls

The landforms at Fossil Falls formed when the Owens River cut across basalt flows during the Pleistocene (Duffield, Bacon & Dalrymple, 1980). The river incised into the resistant rock, leaving behind eroded basalt surfaces, potholes, plunge pools, and cliffs that mark ancient waterfalls (Day, UCLA). Channels and grooves trace the paths of concentrated flow, but with the river now diverted, these features remain "fossilized" in the landscape.

At the main falls, the canyon drops 70–80 feet, a demonstration of the power of the paleoriver. Erosion was enhanced by plunge pool processes, where falling water scoured the base of the falls, gradually causing it to retreat upstream (Hildreth, 2007). Elsewhere, smooth, rounded potholes formed as pebbles swirled in vortex currents, grinding into the basalt like natural drills. These range from small bowls to cavities large enough to climb inside, offering clear evidence of the river's erosive force (Macdonald, 1972). For those who attended the Channeled Scablands fieldtrip, these should look familiar! ☺

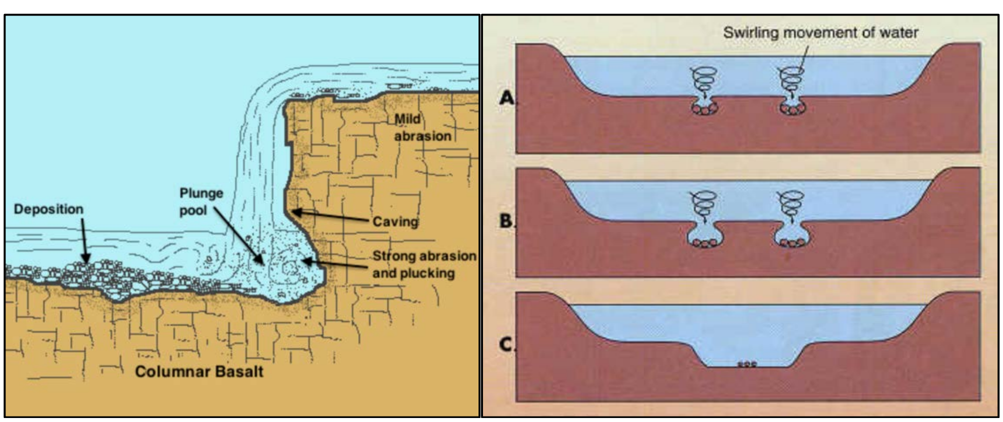


*Figure 6. Left: Diagram illustrating plunge pool erosion at the base of a waterfall, where abrasion and plucking drive upstream retreat. Right: Sequence showing pothole formation through the swirling action of sediment-laden water.*

## IV. Planetary analog

Fossil Falls provides an excellent terrestrial analog for interpreting volcanic and fluvial interactions on other planetary bodies. Comparable processes are inferred on Mars, particularly in regions such as Athabasca Valles within Elysium Planitia, where basaltic flood lavas interacted with large volumes of water during the Amazonian period (Jaeger et al., 2007; Burr et al., 2002). Orbital imagery reveals streamlined islands, scoured bedrock, and channels that suggest catastrophic floods incised into basaltic surfaces. Like Fossil Falls, these Martian terrains preserve evidence of water eroding volcanic rock, although on a much larger scale.

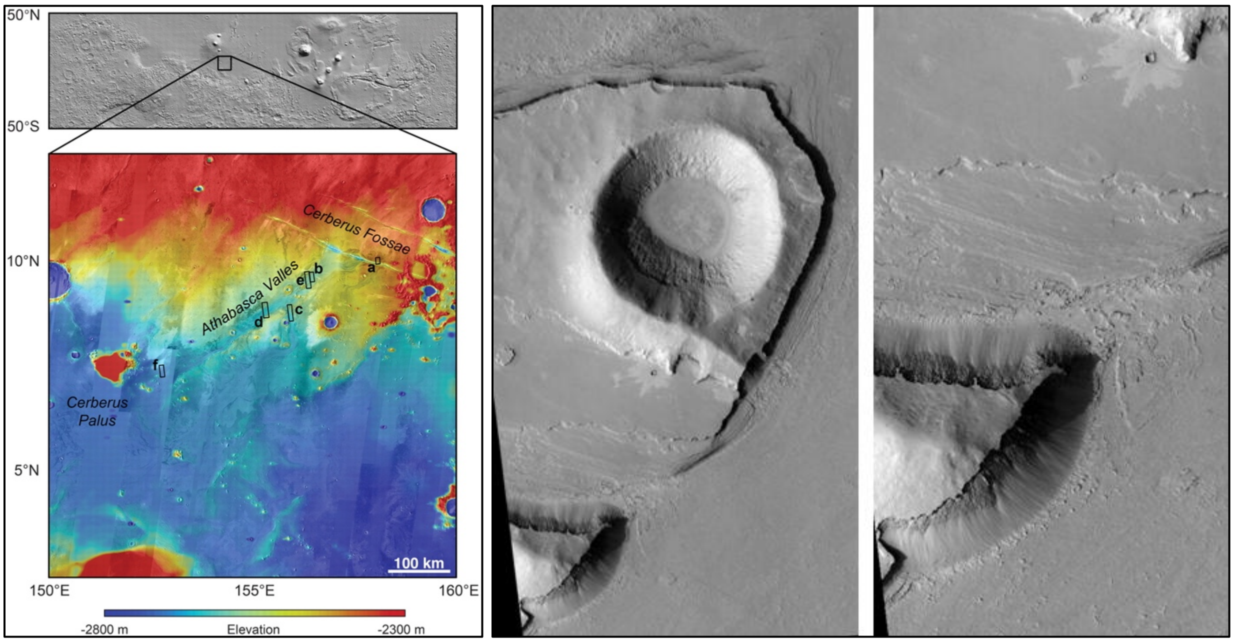


*Figure 7. Orbital imagery of Athabasca Valles in Elysium Planitia, Mars. Left: Regional topographic map with Athabasca Valles outlined, sourced from Cerberus Fossae. Right: High-resolution images showing streamlined islands and scoured bedrock formed by catastrophic flooding and lava–water interactions. These features provide a planetary-scale analog to the fluvial erosion of basaltic lava flows observed at Fossil Falls, California (after Jaeger et al., 2007; Burr et al., 2002).*

## V. References


1. Bacon CR (1982) Time-predictable bimodal volcanism in the Coso Range, California. *Geology* 10(2):65–69
2. Burr DM, Grier JA, McEwen AS, Keszthelyi LP (2002) Repeated aqueous flooding from the Cerberus Fossae: Evidence for very recently extant, deep groundwater on Mars. *Icarus* 159(1):53–73
3. Day M Fossil Falls geology. Department of Earth, Planetary, and Space Sciences, UCLA. Available at: https://faculty.epss.ucla.edu/~mday/index.php/fossil-falls/
4. Duffield WA, Bacon CR (1981) Geologic map of the Coso volcanic field and adjacent areas, Inyo County, California. *US Geological Survey Miscellaneous Investigations Series Map I–1200*
5. Duffield WA, Bacon CR, Dalrymple GB (1980) Late Cenozoic volcanism, geochronology, and structure of the Coso Range, Inyo County, California. *J Geophys Res Solid Earth* 85(B5):2381–2404
6. Hildreth W (2007) *Coso Volcanic Field*. US Geological Survey Professional Paper 1740
7. Jaeger WL, Keszthelyi LP, Skinner JA, Milazzo MP, McEwen AS, Titus TN, Rosiek MR (2007) Athabasca Valles, Mars: A lava-draped channel system. *Science* 317(5845):1709–1711
8. Lockwood JP, Hazlett RW (2010) *Volcanoes: Global Perspectives*. Wiley-Blackwell, Oxford, 539 pp
9. Macdonald GA (1972) *Volcanoes*. Prentice-Hall, Englewood Cliffs, NJ, 510 pp
10. Sigurdsson H, Houghton B, McNutt S, Rymer H, Stix J (2015) *The Encyclopedia of Volcanoes* (2nd ed.). Academic Press, San Diego, 1456 pp

Name: Anna Taylor
Student ID: 23835951

**Joseph Rutherford Walker**

PTYS 590 - Planetary Geology Field Study - Final Report

## Introduction

Joseph Rutherford Walker (1798–1876) was one of the most influential but often overlooked figures of the American West. As a mountain man, fur trapper, guide, and explorer, Walker charted pathways across the Sierra Nevada and into California that shaped migration and settlement patterns for decades to come. His 1833 expedition through the Sierra Nevada, which introduced non-Indigenous travelers to the Yosemite Valley and crossed into Owens Valley, was among the earliest recorded journeys through these regions. Owens Valley itself is a dramatic geological and cultural landscape: a long fault-bounded basin between the Sierra Nevada and the White Mountains, home to the Paiute people for thousands of years. Walker's exploration intersected with the valley's Indigenous inhabitants and permanently altered its trajectory, as his reports brought settlers, surveyors, and eventually conflicts to the region. This paper explores Walker's life and travels with special focus on his connection to Owens Valley, situating his story within both the broader narrative of western exploration and the specific geology and history of this remarkable valley.

Figure 1: Portrait of Joseph Rutherford Walker (1798–1876). Courtesy of public domain collections.

## Early Life and Career as a Mountain Man

Joseph Walker was born in Tennessee in 1798 and grew up during a period of rapid American expansion into frontier lands. Like many young men of his era, he was drawn westward by opportunities in the fur trade. By the 1820s he had joined trapping expeditions that took him into the Rocky Mountains, honing his skills as a hunter, scout, and leader. Walker's reputation grew as he became known for his physical endurance, calm leadership, and ability to navigate difficult terrain. He joined General William Ashley's fur trading enterprise, which helped open up the Rocky Mountains to American trappers. These formative years shaped Walker's abilities as a trailblazer, preparing him for the journeys that would later bring him into California and Owens Valley.

Figure 2: Artists' depiction of fur trappers in the Rocky Mountains during the 1820s–30s, when Walker gained experience.

## The 1833 Expedition and Entry into Owens Valley

In 1833, Walker was chosen by Benjamin Bonneville to lead a party westward from the Green River in present-day Wyoming into California. This expedition became legendary for being one of the first American groups to cross the Sierra Nevada. Walker guided his men through what is now Yosemite Valley, making them the first non-Indigenous Americans to record its grandeur. From there, they descended into the eastern Sierra and reached Owens Valley. Owens Valley, stretching over 100 miles between towering ranges, must have struck Walker's party with its stark beauty and aridity. The fertile floodplains along the Owens River contrasted with the barren alluvial fans and salt flats. Crucially, the Paiute people had long cultivated these floodplains with irrigation networks that supported crops such as native grasses and tubers. Walker's journals noted the valley's water resources and habitability, observations that later attracted settlers and surveyors.


Figure 3: Map of Owens Valley showing the Sierra Nevada to the west and White/Inyo Mountains to the east. Walker's 1833 route likely followed a northern entry through the Sierra.

## Interactions with Indigenous Peoples

Like many explorers of his era, Joseph Walker's expeditions brought him into frequent contact with the Indigenous peoples of the regions he traversed. His early career as a trapper in the Rocky Mountains involved trading and seasonal cooperation with Shoshone, Bannock, and Ute groups. Walker earned a reputation among contemporaries for maintaining relatively peaceful relations, preferring diplomacy and mutual exchange over open conflict. This pragmatism distinguished him from some other mountain men, who often resorted to violence when tensions rose. In Owens Valley, Walker encountered the Paiute people, whose sophisticated irrigation systems sustained dense settlements along the Owens River. While the Walker Party in 1833 recorded the valley's resources and habitability, they did not initiate large-scale conflict with the Paiute. Instead, Walker's reports indirectly shaped the future of the valley: by describing the Paiute's irrigation practices and the valley's fertile potential, he attracted the attention of later settlers and surveyors. These newcomers were far less accommodating. By the 1860s, the influx of ranchers and the U.S. military had led to violent clashes known as the Owens Valley Indian Wars, which culminated in the forced relocation of many Paiute people. Walker himself did not lead campaigns against Indigenous communities, but his explorations formed part of the process by which Indigenous homelands were mapped, described, and eventually claimed by outsiders. His legacy in Owens Valley therefore illustrates the dual role of exploration: on one hand advancing geographic knowledge, and on the other hand opening the door to displacement and cultural upheaval for the peoples who had thrived there for centuries.

## Environmental Observations

Walker's journals and secondhand accounts from his companions provide some of the earliest Euro-American descriptions of Owens Valley's environment. He remarked on the contrast between the arid alluvial fans stretching from the Sierra Nevada foothills and the fertile ribbon of land nourished by the Owens River. Snowmelt-fed streams descending from the Sierra created verdant floodplains, which stood in stark relief against the desert expanses of sagebrush and saltbush. The Walker Party took particular note of the abundance of water relative to the surrounding desert basins. The Owens River, perennial and steady, appeared as a rare resource in the Great Basin landscape. Walker's men also observed the valley's salt flats and alkaline soils, which limited cultivation in some areas but suggested mineral wealth to later surveyors. Wildlife—such as waterfowl and fish in the river—added to the impression that the valley could sustain permanent settlement. What Walker recorded aligned with what Indigenous Paiute communities had long known: Owens Valley was uniquely habitable within a larger desert environment. His recognition of the valley's agricultural and hydrologic potential helped spark later interest from emigrants, miners, and settlers. In retrospect, these seemingly simple environmental observations played a pivotal role in transforming Owens Valley from an isolated homeland to a focal point of California's colonial expansion.

## Later Years and Legacy in California

After the 1833 expedition, Walker remained an important figure in western exploration. He guided emigrant parties, worked with John C. Frémont during his surveys, and was instrumental in opening routes into California. Although he did not settle permanently in Owens Valley, his reports ensured that the valley would not remain unknown to Euro-Americans. Walker lived out his final years in Contra Costa County, California, where he died in 1876. His name is commemorated across the West: Walker Pass (a Sierra crossing south of Owens Valley), Walker River and Lake in Nevada, and numerous other landmarks. These names highlight the widespread impact of his travels, including the routes that intersected Owens Valley.


Figure 4: Walker Pass, named after Joseph Walker, later became a key emigrant route into California, closely tied to Owens Valley.

## Owens Valley After Walker

The valley that Walker introduced to wider attention would undergo immense changes. By the late 19th century, settlers had displaced most Paiute communities. In the 20th century, the Los Angeles Department of Water and Power diverted the Owens River into the Los Angeles Aqueduct, draining Owens Lake and transforming the valley's ecology. These legacies of colonization, resource extraction, and displacement trace back to the earliest explorations, including Walker's.

## Conclusion

Joseph Rutherford Walker exemplifies the paradox of American western exploration: a man of great endurance and skill who revealed extraordinary landscapes like Owens Valley to the world, but whose journeys paved the way for profound cultural and ecological upheavals. His 1833 descent into Owens Valley linked Indigenous homelands, fault-scarped geology, and the march of westward expansion. Owens Valley thus stands as both a geologic wonder and a historical crossroads, forever tied to Walker's name and legacy.

## References

[1] Brooks, G. R. *Joseph Walker and the Opening of the West.* University of Oklahoma Press, 1989.
[2] Farmer, J. D. *Owens Valley History.* Eastern California Museum Publications, 2005.
[3] Hundley, N. *The Great Thirst: Californians and Water.* University of California Press, 2001.
[4] Eastern California Museum. "Owens Valley Paiute Irrigation Systems." Accessed 2025.
[5] National Park Service. "Joseph R. Walker: Mountain Man and Pathfinder." Accessed 2025.

# Glacial Moraines of the Eastern Sierras

PTYS 590 Fall 2025 Owens Valley LPL Field Trip

Christina Singh

<u>What is a moraine?</u>

Moraines are distinct ridges or mounds of unconsolidated debris deposited directly by glaciers or pushed up along their margins. The term moraine is used to describe a wide variety of landforms created by the **dumping**, **pushing**, and **squeezing** of loose rock material, as well as the melting of glacial ice. Moraines serve as clear markers of former ice margins and allow researchers to reconstruct the size and extent of past glaciers, track glacial movement, and gain insights into paleoclimate.

**Ground-penetrating radar (GPR)** can be used to investigate the internal structure and depositional processes associated with moraines. GPR surveys can reveal features like buried ice, layered deposits, and buried moraine ridges by detecting differences in **dielectric properties** between different media. This provides detailed subsurface information that can support surface observations. Combining GPR with other remote sensing data, geophysical methods, or drone-based surveys in challenging terrain, can provide a more comprehensive understanding of moraine dynamics and formation.

Several types of moraines exist. **Lateral moraines** form along the sides of glaciers from debris that is plucked from valley walls and deposited along the edges of glaciers; **medial moraines** run down the center of glacial valley floors when two glaciers meet and their lateral moraines merge. **Terminal moraines** are found at the terminus of glaciers and record the furthest advance of glaciers before they retreat. As a glacier retreats and temporarily stops, ridges called **recessional moraines** are formed.

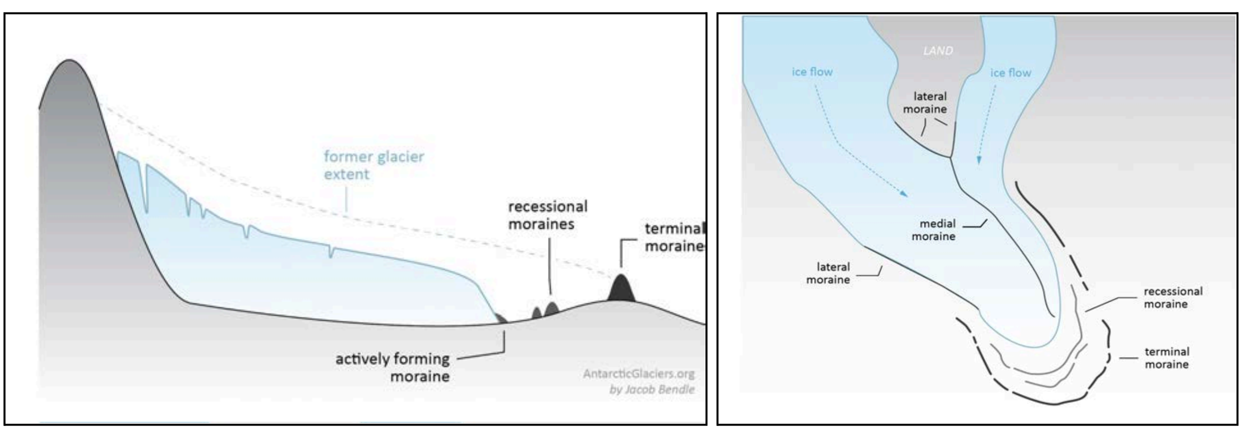


*Fig. 1. Diagram of different types of glacial moraines.*

# PTYS 590 Fall 2025 Owens Valley LPL Field Trip

Christina Singh

Relevance to Owens Valley and the Eastern Sierras:

Owens Valley has experienced multiple glaciations during the Pleistocene. These glaciations are recorded by moraines created during glacial **advances** and **retreats** [2]. The Bloody Canyon and Sawmill moraines are prime examples of these prevalent features scattered around Owens Valley. These canyons contain **nested moraines** that occur in sets; radiometric dating of moraine clasts allow for constraining the ages of these features with the youngest of them being several thousands of years old and the oldest being hundreds of thousands years old. A study conducted by *Sampson and Smith (2006)* analyzed the surface clast size distributions of these moraines and found that older deposits have finer clasts distributions (see Fig. 3.) than younger moraines [3]. This relative age relationship was consistent with $^{36}Cl$ radiometric dating results, strengthening confidence in both approaches.

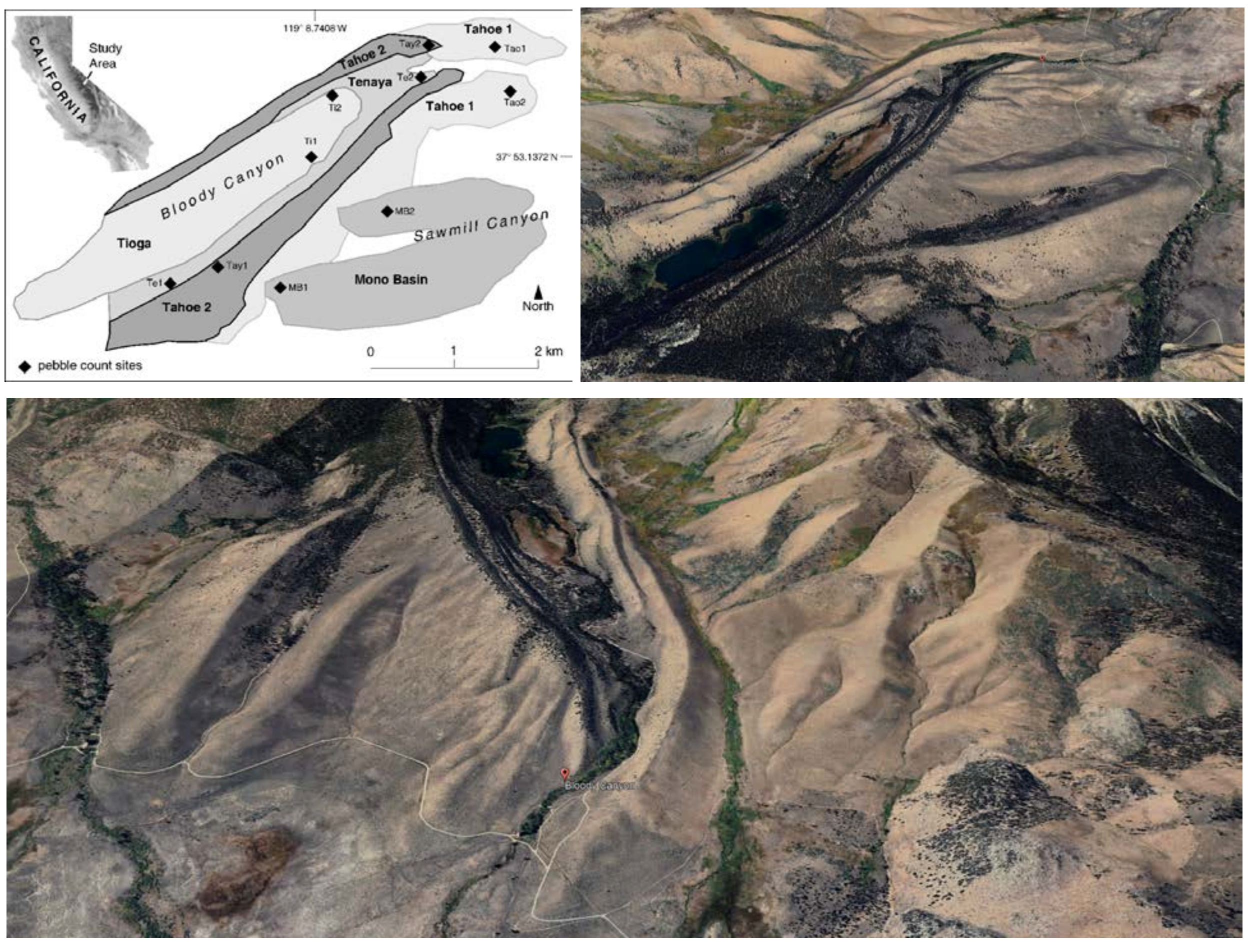


*Fig. 2. Moraine deposits of Bloody Canyon and Sawmill Canyon mapped by Sampson and Smith (2006) and some Google Earth images showing the deposits.*

# PTYS 590 Fall 2025 Owens Valley LPL Field Trip

Christina Singh

| | Glaciation Event | Radiometric Age | Morphometric Classification |
|---|---|---|---|
| **Youngest** | Tioga | > 20,400-23,100 | High surface elevations, steep slopes, large and less weathered boulders |
| | Tenaya | > 23,300-25,500 | Very sharp, high crests, slightly weathered large boulders |
| | Tahoe 2 | 55,900-65,800 | Broken and weathered boulders, gullied flanks, eroded termini |
| | Tahoe 1 | > 133,000-218,000 | Highly weathered, few boulders, greater soil development. gentle slopes |
| **Oldest** | Mono Basin | > 92,000-119,000 | Similar to Tahoe 1, finer clasts |

*Table. 1. Radiometric ages and geomorphic characteristics of the moraine deposits of Bloody Canyon and Sawmill Canyon.*

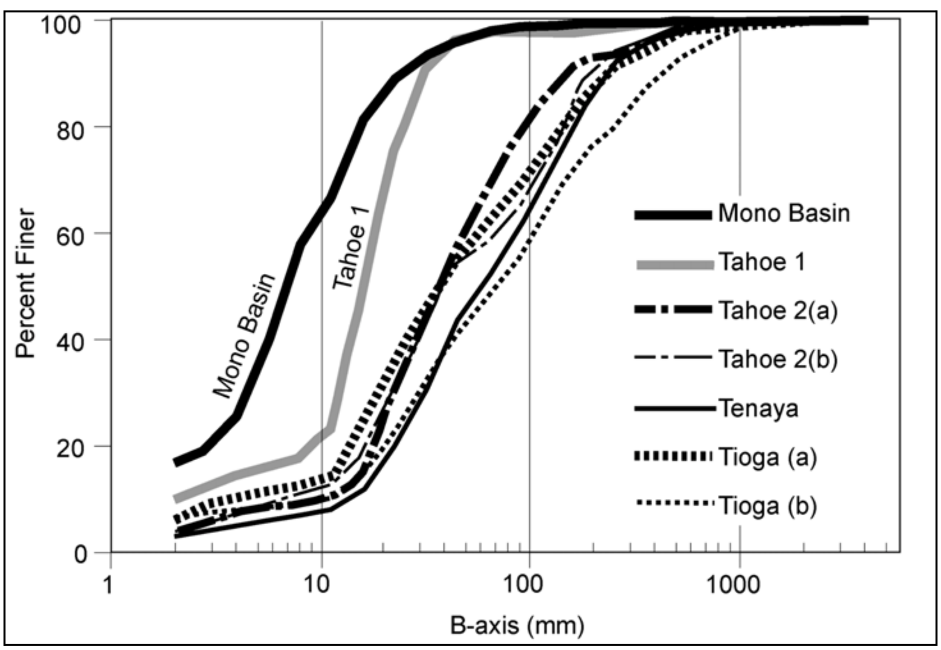


*Fig. 3.Cumulative clast size distributions for the moraine deposits of Bloody Canyon and Sawmill Canyon. The oldest deposits (Mono Basin and Tahoe 1) have distinct finer clast size distributions compared to the younger moraines.*

# PTYS 590 Fall 2025 Owens Valley LPL Field Trip

Christina Singh

Planetary Connection:

Moraines serve as planetary analogs for moraine-like features on Mars. These pronounced ridges appear texturally distinct, ‘arcuate’, devoid of many impact craters, and in the forefield of glacial-like features (GLFs) [4]. Detailed mapping and analysis of these ridges can be used to reconstruct past glacier limits, volumes, and thermal conditions on Mars. GLFs are important archives of recent (late Amazonian) Martian climate change. A global analysis of 1293 GLFs showed strong signs that 436 of the GLFs (~ ⅓ of the survey population) were receding [4]. This is indicative of global climatic changes late in the planet’s history.

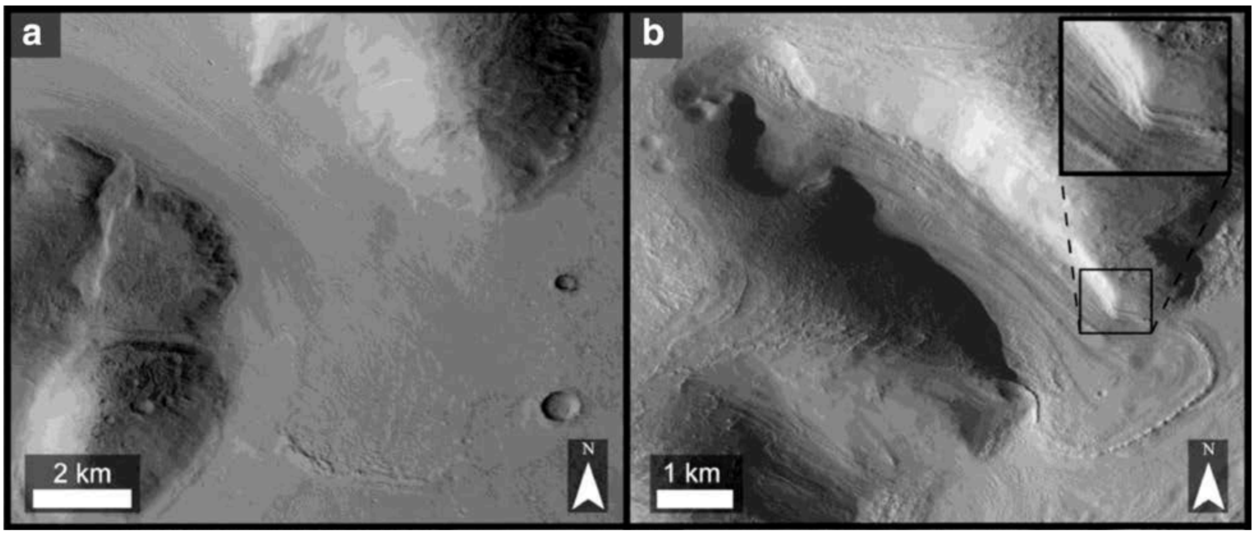


*Fig. 4. CTX imagery of: (a) a well-developed arcuate moraines that appear to record the furthest extent of glacial advance and periods of glacial recession in Phlegra Montes, Mars and (b) a lateral moraines of a GLF in Protonilus Mensae, Mars.*

**References:**

**[1]** Alan R. Gillespie, Paul H. Zehfuss, Glaciations of the Sierra Nevada, California, USA, Editor(s): J. Ehlers, P.L. Gibbard, Developments in Quaternary Sciences, Elsevier, Volume 2, Part B, 2004, Pages 51-62, ISSN 1571-0866, ISBN 9780444515926, https://doi.org/10.1016/S1571-0866(04)80185-4.

**[2]** Kelson, K.I., Hitchcock, C.S., Zeeb, R.B., and Lettis, W.R., 1995, Displacement of late Pleistocene glacial moraines by the Almanor fault, Plumas County, California in Page, W., trip leader, Quaternary geology along the boundary between the Modoc Plateau, Southern Cascade Mountains, and Northern Sierra Nevada: Friends of the Pleistocene, 1995 Pacific Cell Field Trip, Appendix 2-6, 19

**[3]** Sampson, K. M., & Smith, L. C. (2006). Relative Ages of Pleistocene Moraines Discerned from Pebble Counts: Eastern Sierra Nevada, California. Physical Geography, 27(3), 223–235. https://doi.org/10.2747/0272-3646.27.3.223

**[4]** Stephen Brough, Bryn Hubbard, Alun Hubbard, Former extent of glacier-like forms on Mars, Icarus, Volume 274, 2016, Pages 37-49, ISSN 0019-1035, https://doi.org/10.1016/j.icarus.2016.03.006.

**Trilobites**
**Lily Robinthal**
**PTYS590, Fall 2025**

## Introduction

Over the more than 3.5 billion year history of life on Earth, many a strange and wonderful creature has walked, scuttled, and swam over land and sea. A large number of these are no longer with us; however, in many cases their fossilized remains allow us a glimpse into a long-gone ecosystem.

Such is the case of the trilobite. These hardy and hearty marine arthropods are one of the most recognizable varieties of preserved extinct life. Existing for nearly 300 million years from the early Cambrian to the late Permian [1], nearly 20,000 trilobite species have been identified [2], ranging in size from under a millimeter [3] to over two feet [4]. Their prevalence in the fossil record is due in part to the fact that they were the first arthropods to have a calcite exoskeleton, which preserves well [5].


*Figure 1: Small trilobite, quarter for scale (above, Groden Bell via National Park Service); life-size model of large trilobite, despondent-looking man for scale (right, Prehistoric Planet Store).*

The name ‘trilobite’ refers to the creatures’ distinctive length-wise three-fold midsection; they are the only arthropod to demonstrate this feature [2]. The width-wise sections allowed the trilobite to roll up like a modern-day pillbug [1]. Additionally, they are one of the first animals in the fossil record to show evidence of having had eyes [2].

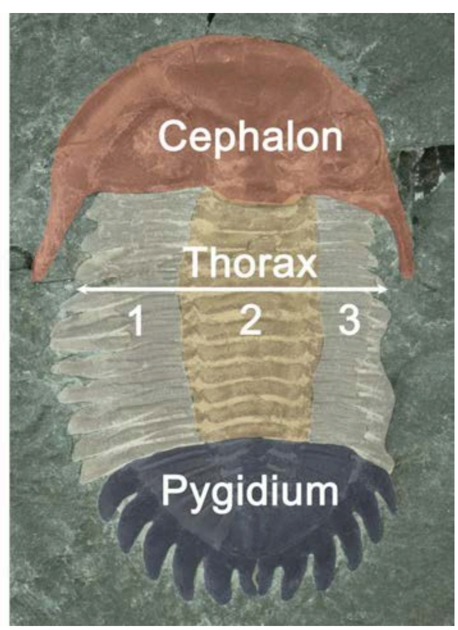


*Figure 2 (right): Diagram showing the anatomy of a trilobite, including their three-fold thorax (Museum of the Earth).*

## Lifestyle and Evolution

Given the tremendous variety of species, it follows that different types and eras of trilobites would live diverse lives. They existed essentially everywhere there was saltwater, from the briny depths of the ocean to the shallow water near the shore [5]. While many, primarily the smallest, were particle feeders, it is thought that some of the larger varieties were predators and scavengers, and others plankton feeders [5].

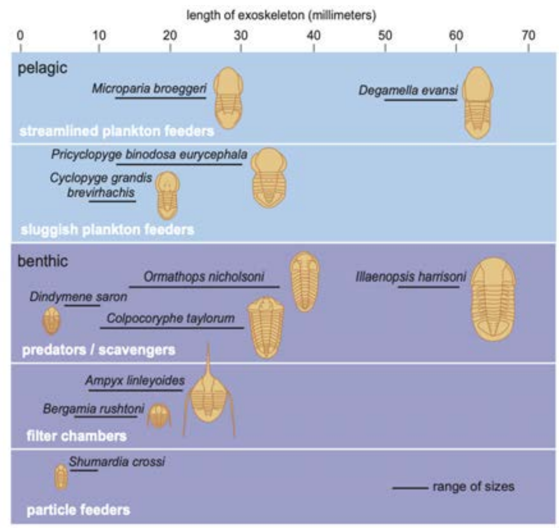


*Figure 3 (right): A diagram showing the diversity in diets of trilobites from the same era and site. From [5].*

Trilobites first appeared in fossil records from the early Cambrian, and their heyday of maximum diversity began in the late Cambrian [6]. They experienced their first major extinction event at the end of the Ordovician during the Late Ordovician Mass Extinction, at which point they lost about half of their diversity; this marked the beginning of their slow but steady decline [7]. They persisted through the Silurian and Devonian, took a massive hit during the Late Devonian Mass Extinction, and the only remaining order staggered wearily into the Carboniferous [6]. The trilobite's reign finally came to an end with the Permian Mass Extinction Event [8].

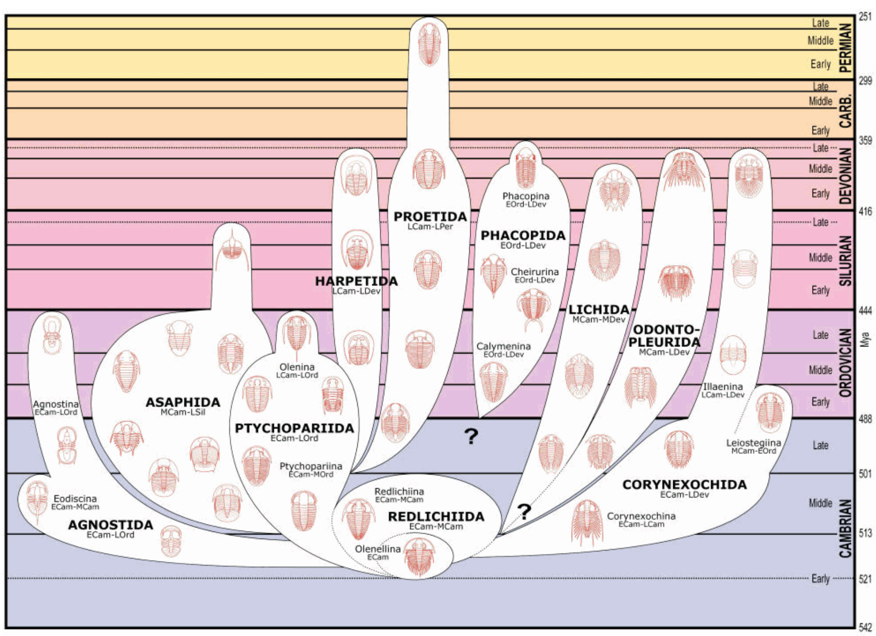


*Figure 4: Chart showing the decline of trilobite orders over geologic time (S.M. Gon via trilobite.info).*

## Trilobite Paleontology

Trilobites have inspired fascination in humans since the early days of our comparatively young species. There are very early petroglyph depictions of the creatures, and the first written record describing them dates to the 4th century BCE [9]. They began to take on scientific interest in the late 1600s, when the Welsh reverend Edward Lhwyd created the first published illustration of a trilobite; he referred to it as a ‘flatfish’ [10].

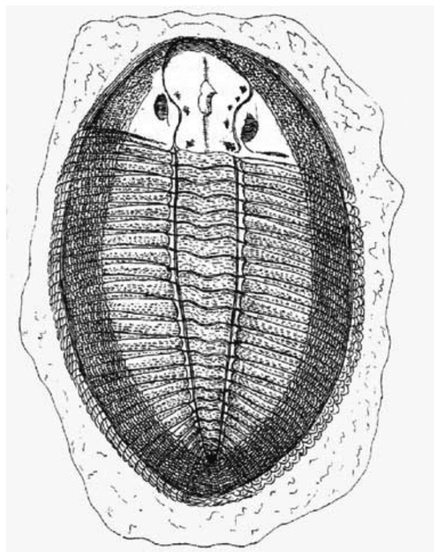

*Figure 5: Lhwyd’s trilobite drawing (left) and the subject (right) (From Fortey 2000).*

Lhwyd did not fully accept that his ‘flatfish’ was of a biological nature, however. The fact that trilobites were animals was not established until the 18th century, when natural philosopher Johann Walch determined that they were likely arthropods and coined the name “trilobite” [9]. This marked the beginning of the field of trilobite paleontology, which continues to reveal new secrets to this day.

## California Trilobites (They’re Unforgettable)

Nearly 30 trilobite species have been found in the White-Inyo Mountains of California. Most are from the Cambrian and early Ordovician [11]. Below are a few that I deemed particularly cute.


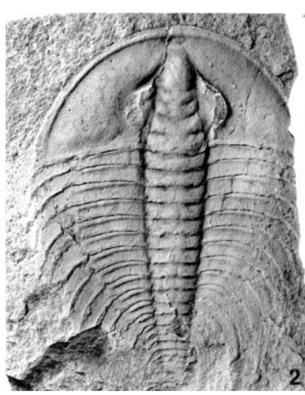



*Figure 5 (from left to right): Fallotaspis longa, Nevadia weeksi, Olenellus gilberti, Perrisopyge triangulata. West coast represent indeed!*

## References


1. *What were trilobites?* (n.d.). Oxford University Museum of Natural History. https://oumnh.ox.ac.uk/learn-what-were-trilobites
2. Paleontological Research Institute. (2022). Trilobites. Museum of the Earth. Retrieved September 24, 2025, from https://www.museumoftheearth.org/ny-rocks/devonian-sea-life/taxon/trilobites
3. Whittington, H. B. (1997), "Morphology of the Exoskeleton", in Kaesler, R. L. (ed.), *Treatise on Invertebrate Paleontology, Part O, Arthropoda 1, Trilobita, revised. Volume 1: Introduction, Order Agnostida, Order Redlichiida*, Boulder, CO & Lawrence, KA: The Geological Society of America, Inc. & The University of Kansas, pp. 1–85, ISBN 978-0-8137-3115-5
4. Rudkin, D.A.; Young, G. A.; Elias, R. J.; Dobrzanske, E. P. (2003), "The world's biggest trilobite: Isotelus rex new species from the Upper Ordovician of northern Manitoba, Canada", *Journal of Paleontology*, 70 (1): 99–112
5. Fortey, R. A. (2004). Lifestyles of the trilobites. *American scientist*, *92*(5), 446-453.
6. Bault, V., Balseiro, D., Monnet, C., & Crônier, C. (2022). Post-Ordovician trilobite diversity and evolutionary faunas. *Earth-Science Reviews*, *230*, 104035.
7. Adrain, J. M., Fortey, R. A., & Westrop, S. R. (1998). Post-Cambrian trilobite diversity and evolutionary faunas. *Science*, *280*(5371), 1922-1925.
8. Lerosey-Aubril, R., & Feist, R. (2012). Quantitative approach to diversity and decline in late Palaeozoic trilobites. In *Earth and life: global biodiversity, extinction intervals and biogeographic perturbations through time* (pp. 535-555). Dordrecht: Springer Netherlands.
9. LANDING, E. FABULOUS FOSSILS—300 YEARS OF WORLDWIDE RESEARCH ON TRILOBITES: INTRODUCTION. *FABULOUS FOSSILS—300 YEARS OF WORLDWIDE RESEARCH ON TRILOBITES*, 1.
10. Rábano, I., Gozalo, R., & García-Bellido, D. (2008). Cryptopalaeontology: magical descriptions of trilobites about two thousand years before scientific references. *Advances in trilobite research*, 237.
11. *Fallotaspis etc. Biozones*. (n.d.). https://www.westerntrilobites.com/Formations/White-Inyo.htm

Carter Mucha
**Long Valley Caldera and the Bishop Tuff**

| **Key Terms:** |
| --- |
| **Caldera** - A large, basin-shaped volcanic depression significantly larger than volcanic vents within it [4]. **Tephra** - Rock expelled from a volcanic eruption which took an airborne path prior to emplacement [4]. **Ignimbrite** - Rock formed by the compaction and welding of pyroclastic flows [4]. |

The Long Valley Caldera is an elliptical topographic depression on the Eastern front of the Californian Sierra Nevada range (50 km NW of Bishop and 30 km S of Mono Lake), measuring 17 by 32 km [1]. The Caldera was formed through a supereruption event, defined by *Chamberlain et al. (2015)* as an eruption involving $>10^{15}$ kg or ~450 $km^3$ of magma [2]. It is generally agreed upon that the Long Valley Caldera eruption, which occurred 0.76 million years ago, resulted in the emplacement of two major categories of volcanic products: plinian fall deposits and ignimbrites [3]. Evacuation of the subsurface magma chamber resulted in a partially-emptied space, which subsided to form the topographic depression of the caldera [1]. During a 600,000 year postcaldera interval of quiescence, the depression was infilled by the Pleistocene Long Valley Lake, likely fed by glacial icemelt associated with heating generated by volcanism. The lake left behind calcareous sediments, tufa deposits, and >700 m of lacustrine sediments, which layer the flat surface on the Eastern caldera floor [1, 4]. Lake drainage was initiated by overflow, and completed during the last 0.1 million years [1]. The original caldera boundary has been expanded due to erosional processes such as landslides, glaciation, and rapid erosion since the original eruptive event [4]. Basement rocks underlying the Long Valley Caldera include Jurassic and Cretaceous granodiorites, granites of the Sierra Nevada batholith, and metamorphic units of paleozoic and mesozoic age, overlain by late Tertiary volcanics (basalt, andesite, and rhyodacite) [1].

Long Valley Caldera, as imaged by Erik Olsen for *California Curated*, 2025.

***More Recent Activity***

Following this major event, several intracaldera volcanic eruptions have occurred, including heightened activity at ~0.65, 0.5, 0.3, 0., and 0.05 million years ago, with residual magma in the main caldera chamber persisting until ~450 years ago [1]. In addition to these eruptive events, heightened activity has been recorded within the Long Valley Caldera in the form of seismic and tectonic events, including periods of enhanced deformation in 1980, 1983, 1989-1990, and 1997-1998. A resurgent dome is present within the caldera, which is fed by a shallow (7-10 km) source of silicic magma and hydrothermal fluid and a deeper (15 km) source. It is estimated that the cumulative volume increase within the caldera since the late 1970s is roughly equivalent to the 1980 Mount St. Helens eruptive volume. The resurgent dome is continuously uplifting at variable rates, indicating an active intrusion of magma into the crust from a source in the southern Long Valley region [5].

***The Bishop Tuff***

Carter Mucha

**Long Valley Caldera and the Bishop Tuff**

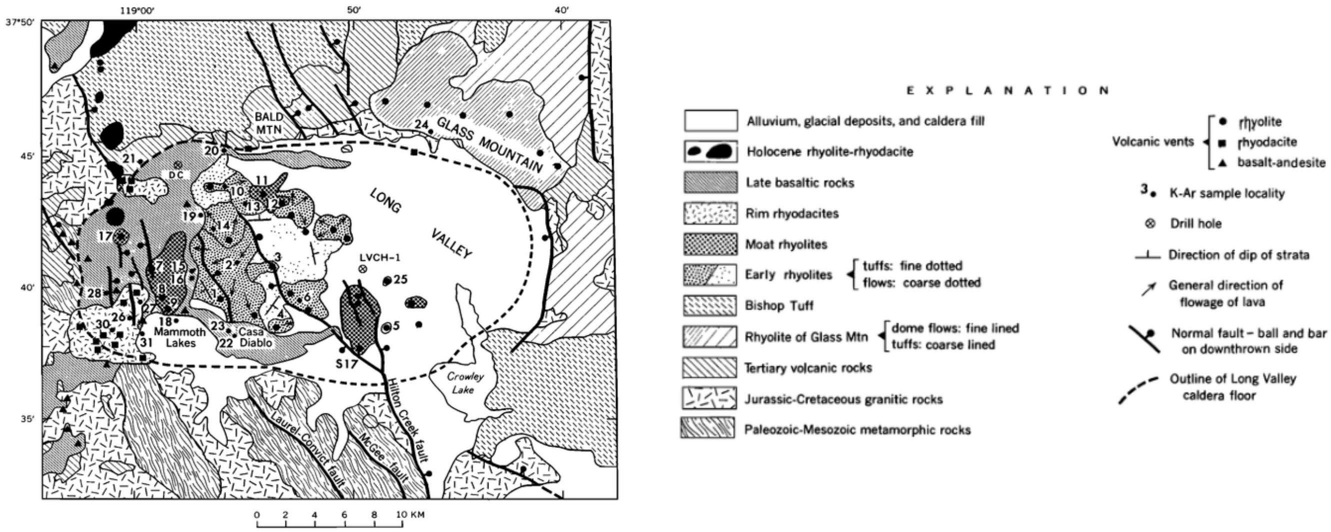


A geologic map of the Long Valley Caldera, with the Bishop Tuff units visible above and below the main caldera depression (from Bailey, Dalrymple and Lanphere, 1976).

Accounting for 80% of the erupted magma within Long Valley in the last 2.1 million years is the Bishop Tuff, a voluminous partly welded ignimbrite, which was emplaced during the caldera-forming eruption 0.76 million years ago [3]. The Bishop Tuff consists of a widespread plinian fall deposit (tephra dispersed as ashfall), intercalated with compositionally zoned ignimbrite deposits of varying pyroxene contents and degrees of welding [3, 2, 6]. Compositionally, the bishop Tuff is a crystal-rich rhyolite with 76% silica, containing up to 30% quartz, sanidine, plagioclase, biotite, and Fe-Ti oxide phenocrysts. The deposit covers an area of 1040 - 1150 km, amounting to a volume of ~500 km when the volumes within and outside of the caldera are considered. During emplacement, ash flows extended radially from vents now buried beneath the caldera, into the area occupied now by Owens River, northwards into adobe valley, northwestwards into Mono basin, and westwards into the San Joaquin River Valley [1].

***References***

[1] Bailey, R. A., G. B. Dalrymple, and M. A. Lanphere (1976), Volcanism, structure, and geochronology of Long Valley Caldera, Mono County, California, J. Geophys. Res., 81(5), 725–744, doi:10.1029/JB081i005p00725.

[2] K. J. Chamberlain, C. J. N. Wilson, P. J. Wallace, M.-A. Millet, Micro-analytical Perspectives on the Bishop Tuff and its Magma Chamber, Journal of Petrology, Volume 56, Issue 3, March 2015, Pages 605–640, https://doi.org/10.1093/petrology/egv012

[3] Wilson, C. J. N., & Hildreth, W. (1997). The Bishop Tuff: New Insights From Eruptive Stratigraphy. The Journal of Geology, 105(4), 407–440. https://doi.org/10.1086/515937

[4] “Features of the Long Valley Caldera.” USGS, www.usgs.gov/volcanoes/long-valley-caldera/science/features-long-valley-caldera. Accessed 22 Sept. 2025.

[5] Sorey, M. L., McConnell, V. S., & Roeloffs, E. (2003). Summary of recent research in Long Valley Caldera, California. Journal of Volcanology and Geothermal Research, 127(3–4), 165–173. https://doi.org/10.1016/s0377-0273(03)00168-9

[6] “Bishop Tuff in Long Valley Caldera, California.” USGS, www.usgs.gov/volcanoes/long-valley-caldera/science/bishop-tuff-long-valley-caldera-california. Accessed 22 Sept. 2025.

**OWENS VALLEY RADIO OBSERVATORY** Cole Meyer; Lunar and Planetary Laboratory, University of Arizona

**Introduction:** The Owens Valley Radio Observatory (OVRO) is located in eastern California's Owens Valley, a high desert basin bounded by the Sierra Nevada to the west and the White Mountains to the east (see Figure 1). This unique geographic setting provides an exceptionally dry climate, stable atmosphere, and relative isolation from major sources of radio interference, making it ideal for radio astronomy. Since its founding in 1956, OVRO has been central to astrophysical research, contributing to studies of the cosmic microwave background, quasars, solar flares, and fast radio bursts. The observatory has also long been part of the cultural and educational fabric of nearby communities, serving as both a scientific resource and a point of local pride. Its appearances in popular films have given it a visibility beyond astronomy, making it a familiar landmark even to those outside the scientific community.

**Facilities & Capabilities:** Over its history, OVRO has developed a range of powerful instruments. The 40-meter telescope (see Figure 2), operating since the late 1960s, remains one of the most productive single-dish radio facilities, currently serving as a key instrument for long-term blazar monitoring in coordination with NASA's Fermi mission [1]. The Expanded Owens Valley Solar Array (EOVSA) is dedicated to broadband microwave imaging of the Sun, producing dynamic maps of coronal magnetic fields and flare energetics [e.g., 2, 3]. The Deep Synoptic Array (DSA), now being expanded, is designed to detect and localize fast radio bursts, allowing astronomers to probe the distribution of baryonic matter across intergalactic space [4]. Earlier interferometers at OVRO pioneered techniques in aperture synthesis and long-baseline radio astronomy [e.g., 5, 6], laying groundwork that fed into the development of larger national and international facilities. Collectively, these instruments offer broad frequency coverage, high temporal resolution, and sustained monitoring capabilities that complement observations across the electromagnetic spectrum.


Figure 1: Map of the upper Owens Valley region with the red rectangle indicating the location of the Owens Valley Radio Observatory.

**Key Scientific Contributions:** OVRO has made key contributions across multiple areas of astrophysics. In the mid-1960s, its early measurements of the cosmic microwave background helped refine the blackbody spectrum of relic radiation and solidify the Big Bang paradigm [e.g., 7, 8]. In the same era, OVRO radio surveys were instrumental in the identification of quasars, work that revealed their extragalactic nature and established them as among the most energetic phenomena in the universe, powered by accretion onto supermassive black holes [e.g., 9, 10]. In recent years, EOVSA

Figure 2: Owens Valley Radio Observatory 40-m dish.

has produced unprecedented images of solar flares, such as during the powerful X-class events of 2017, which demonstrated how coronal magnetic fields reconfigure and accelerate particles [e.g., 2]. These findings carry direct implications for space weather, with relevance to both Earth's atmosphere and the environments of other planets. Most recently, the DSA prototype known as DSA-10 successfully localized a fast radio burst to its host galaxy in 2019 [11], opening a new era in transient radio astronomy. The current expansion of the array will enable systematic localization of fast radio bursts, transforming them into powerful cosmological probes of matter distribution and intergalactic plasma [12].

**Environment & Local Community:** The observatory is embedded in the geology and environment of Owens Valley, a graben formed between major fault systems of the Sierra Nevada and White Mountains. The region's stable ground, high elevation, and arid climate provide excellent transparency for radio observations. Seasonal variations in wind and dryness can occasionally affect operations, but overall the local environment has proven highly advantageous for precision radio measurements. OVRO maintains ties with surrounding communities including Bishop, Big Pine, and Lone Pine, offering open houses, school partnerships, and public observing nights that connect residents and visitors with ongoing research. These programs make OVRO both a world-class facility and a regional resource for education and outreach, while also serving as a training ground for Caltech students in astronomy, planetary science, and instrumentation.

**Pop Culture & Visibility:** OVRO has also entered the public imagination through its appearances in major films. The observatory played a central role in *The Arrival* (1996), with multiple scenes filmed on site and even a climactic sequence staged on the 40-meter dish itself. In *Contact* (1997), OVRO is referenced as the place where the protagonist completed her thesis research, highlighting its academic pedigree even though the visual sequences were filmed at the Very Large Array, New Mexico. More recently, *Man of Steel* (2013) used the solar array complex for exterior shots during its closing military drone scene, introducing OVRO to broader audiences. These portrayals are responsible, in part, for the observatory's symbolic role as a place where humanity listens for signals from beyond Earth.

**Conclusion:** OVRO is one of the longest-running radio observatories in the world, with a history that spans from the early days of radio astronomy to modern transient sky science. Its role in measuring the cosmic microwave background, identifying quasars, imaging solar flares, and localizing fast radio bursts has left a lasting mark on modern astrophysics. At the same time, its setting in Owens Valley ties the observatory to a distinctive geologic landscape and to nearby communities that have grown alongside it. Taken together, these make OVRO a key site for astronomy and an important part of the scientific landscape of the western United States.

**References:** **[1]** Joseph L. Richards et al. "Blazars in the Fermi Era: The OVRO 40 m Telescope Monitoring Program". en. In: *The Astrophysical Journal Supplement Series* 194.2 (May 2011). Publisher: The American Astronomical Society, p. 29. DOI: 10.1088/0067-0049/194/2/29. **[2]** Dale E. Gary et al. "Microwave and Hard X-Ray Observations of the 2017 September 10 Solar Limb Flare". en. In: *The Astrophysical Journal* 863.1 (Aug. 2018), p. 83. DOI: 10.3847/1538-4357/aad0ef. **[3]** Zhitao Wang et al. "Coronal Magnetography of a Simulated Solar Active Region from Microwave Imaging Spectropolarimetry". en. In: *The Astrophysical Journal* 805.2 (June 2015), p. 93. DOI: 10.1088/0004-637X/805/2/93. **[4]** Casey J. Law et al. "Deep Synoptic Array Science: First FRB and Host Galaxy Catalog". en. In: *The Astrophysical Journal* 967.1 (May 2024). Publisher: IOP Publishing, p. 29. DOI: 10.3847/1538-4357/ad3736. **[5]** Geoffrey A. Blake et al. "A lambda = 1.3 millimeter Aperture Synthesis Molecular Line Survey of Orion Kleinmann-Low". en. In: *The Astrophysical Journal* 472 (Nov. 1996), p. L49. DOI: 10.1086/310347. **[6]** D. J. Wilner, Paul T. P. Ho, and Q. Zhang. "Searching for Infall: Aperture Synthesis HCO +(1–0) and SiO(2–1) Observations of the G45.47+0.05 Region". en. In: *Astrophysical Journal v.462, p.339* 462 (May 1996), p. 339. DOI: 10.1086/177155. **[7]** A. C. S. Readhead et al. "A Limit on the Anisotropy of the Microwave Background Radiation on Arcminute Scales". en. In: *Astrophysical Journal v.346, p.566* 346 (Nov. 1989), p. 566. DOI: 10.1086/168039. **[8]** E. M. Leitch et al. "A Measurement of Anisotropy in the Cosmic Microwave Background on 7'-22' Scales". en. In: *The Astrophysical Journal, Volume 532, Issue 1, pp. 37-56.* 532.1 (Mar. 2000), p. 37. DOI: 10.1086/308529. **[9]** Thomas A. Matthews and Allan R. Sandage. "Optical Identification of 3C 48, 3C 196, and 3C 286 with Stellar Objects." en. In: *The Astrophysical Journal* 138 (July 1963), p. 30. DOI: 10.1086/147615. **[10]** E. B. Fomalont et al. "A Measurement of Excess Antenna Temperature at 4080 Mc/s." en. In: *The Astrophysical Journal* 142 (July 1965), pp. 419–421. DOI: 10.1086/148307. **[11]** V. Ravi et al. "A fast radio burst localized to a massive galaxy". en. In: *Nature* 572.7769 (Aug. 2019), pp. 352–354. DOI: 10.1038/s41586-019-1389-7. **[12]** J. Kocz et al. "A fast radio burst localized to a massive galaxy". en. In: *Nature* 572.7769 (Aug. 2019), pp. 352–354. DOI: 10.1038/s41586-019-1389-7.

# Uplift of the Sierra Nevadas

Thea McKenna

**Overview and Formation**

The Sierra Nevadas originally formed when the Farallon Plate, an ancient tectonic plate off the western coast of North America, began subducting underneath the North American plate. As the plate began to melt underneath, magma upwelled and erupted, creating a magmatic arc of volcanoes. This magma cooled and became granitic plutons, forming the Sierra Nevada batholith. This initial formation and uplift occurred in the late Cretaceous period, or about 70 million years ago [1]. It is believed that there was a second period of slower, more gradual uplift starting in the late Cenozoic period, 5–10 million years ago, and continuing into the present day [1]. This is due to the complex tectonics in the area. Climate also has a hand in present-day uplift seasonal variation.

**Geologic/Tectonic Uplift Today**

The Sierra Nevadas and the Great Valley form a semi-rigid microplate wedged between the North American Plate and the Pacific Plate [2]. They are bounded by the Owen's Valley fault on the east, the Garlock fault in the south, the San Andreas fault to the west, and the Northern California Shear Zone to the north (Fig 1). Late Cenozoic to present day uplift is believed to come from normal faulting on the east in Owen's Valley that has caused westward tilting of the whole block [1, 2]. It uplifts about 2 mm/yr according to GPS measurements (Fig 3) [3].

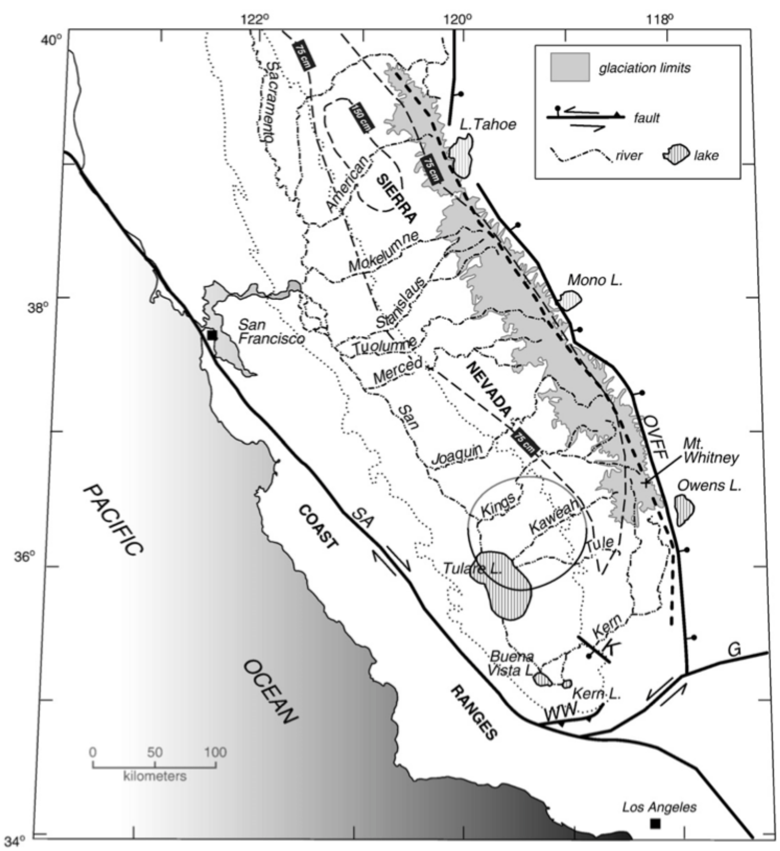


**Figure 1.** Regional tectonic context map from Figueroa and Knott 2010. Long dashed line is the Sierra Nevada crest location. Major faults are labeled as San Andreas (SA), Garlock (G), Owen's Valley frontal fault (OVFF), White Wolf (WW), and Kern River Gorge (K).

# Uplift of the Sierra Nevadas

Thea McKenna

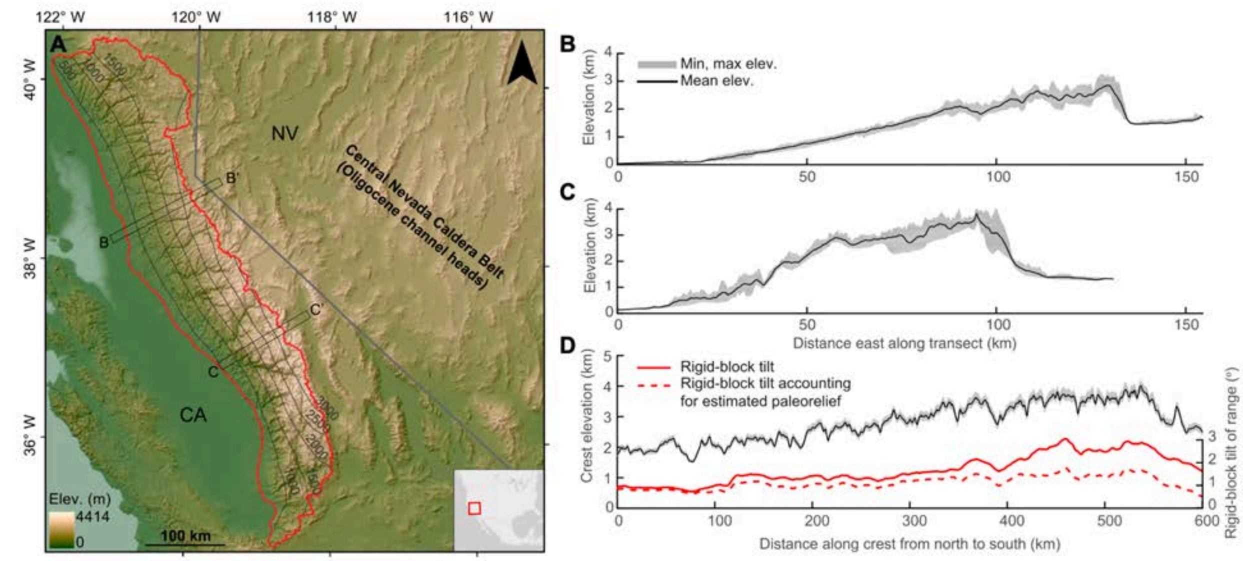


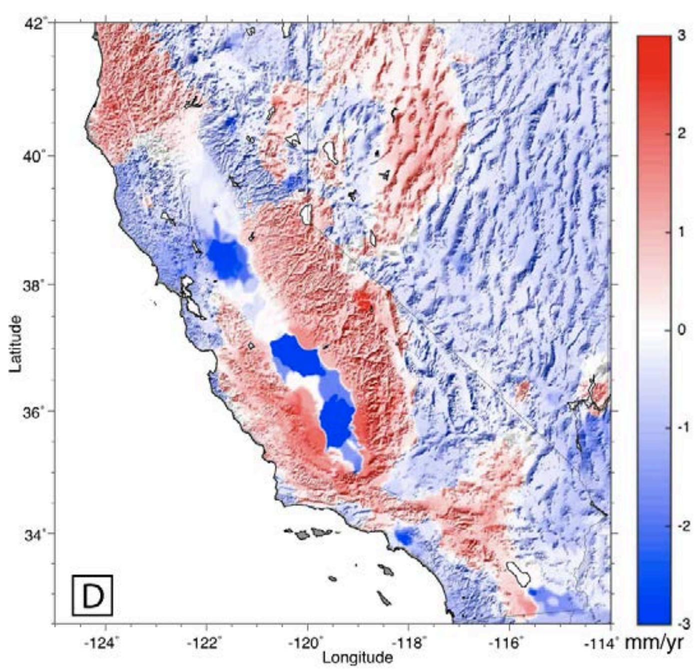


**Figure 2 (above).** From Beeson and McCoy 2022. A) Digital elevation model of the Sierra Nevadas outlined in red with elevation profile transects labeled. B) and C) elevation profiles corresponding to transects in A). D) N-S elevation profile in black, uplift due to western tilt in red.

**Figure 3 (left).** Tectonic uplift of the Sierra Nevadas using GPS measurements from Hammond et al. 2016. The color scale is in mm/yr with red positive upward and blue negative downward motion.

**Other Contributing Factors**

The Sierra Nevadas were heavily glaciated in the last glacial maximum and then deglaciated about 15,000 years ago [4]. This reduction in top load would have caused a period of post-glacial rebound where the mountain range uplifted. This is not still in effect in the present day, but does have an impact on the height of the range as we observe it today.

Precipitation is an important seasonal factor. The California drought from 2011-2015 had a huge impact on Sierra Nevada uplift, as water weight was unloaded from the mountain range. Argus et al. 2017 used GPS measurements over this time period to measure a total of 24 mm of uplift. Of this, 17 mm is the Earth's elastic response to water loss [5]. Additionally, years with heavy precipitation can cause subsidence, such as the 2009-2011 heavy precipitation that caused ~15 mm of subsidence [5].

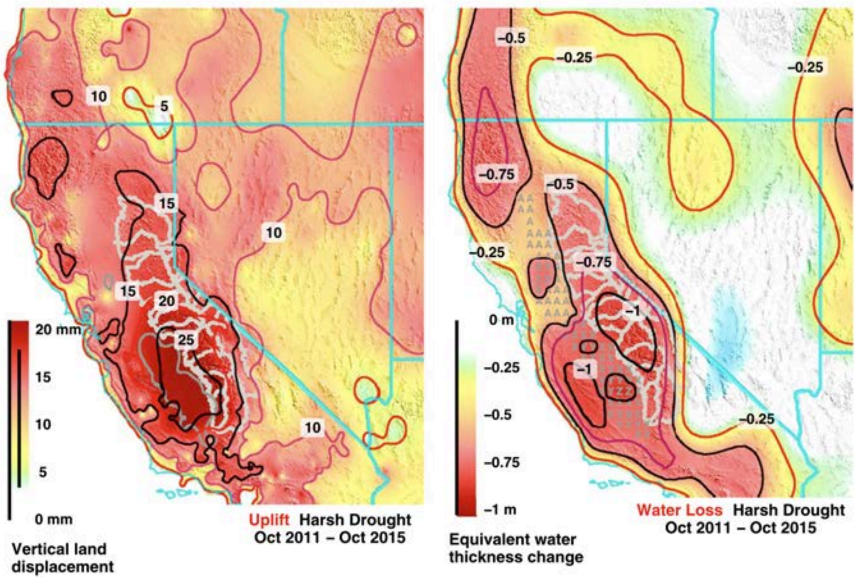


**Figure 3.** GPS measurements from Argus et al. 2017 showing the water loss from the 2011-2015 drought and subsequent mountain range uplift.

**References**

[1] Andrea M. Figueroa, Jeffrey R. Knott, Tectonic geomorphology of the southern Sierra Nevada Mountains (California): Evidence for uplift and basin formation, Geomorphology, Volume 123, Issues 1–2, 2010, Pages 34-45, ISSN 0169-555X, https://doi.org/10.1016/j.geomorph.2010.06.009.

[2] Helen W. Beeson, Scott W. McCoy; Disequilibrium river networks dissecting the western slope of the Sierra Nevada, California, USA, record significant late Cenozoic tilting and associated surface uplift. *GSA Bulletin* 2022;; 134 (11-12): 2809–2853. doi: https://doi.org/10.1130/B35463.1

[3] Hammond, W. C., G. Blewitt, and C. Kreemer (2016), GPS Imaging of vertical land motion in California and Nevada: Implications for Sierra Nevada uplift, *J. Geophys. Res. Solid Earth*, 121, 7681–7703, doi:10.1002/2016JB013458.

[4] Granger, D. E., and G. M. Stock (2004), Using cave deposits as geologic tiltmeters: Application to postglacial rebound of the Sierra Nevada, California, *Geophys. Res. Lett.*, 31, L22501, doi:10.1029/2004GL021403.

[5] Argus, D. F., Landerer, F. W., Wiese, D. N., Martens, H. R., Fu, Y., Famiglietti, J. S., … Watkins, M. M.(2017). Sustained water loss in California's mountain ranges during severe drought from 2012 to 2015 inferred from GPS. *Journal of Geophysical Research: Solid Earth*, 122, 10,559–10,585. https://doi.org/10.1002/2017JB014424

# 1872 Owens Valley Earthquake

Melissa Kontogiannis

**Introduction**

Owens Valley lies between the Sierra Nevada mountains to the west and the White-Inyo Mountains to the east, and the dramatic relief from the nearly 14,000-foot peaks in the surrounding mountain ranges to the 4,000-foot elevation of the valley floor make it the deepest valley in the United States (Smith and Putnam, 1976). The valley floor is dominated by sandy clay material and lake sediments, with scattered volcanic features, including basaltic cinder cones and lava flows (Bacon, 2003). Perhaps the most notable geologic feature of Owens Valley is the fault zone that extends approximately 100km along the valley floor, from the town of Big Pine to Owens Lake (Beanland and Clark, 1994). This complex fault zone is part of the Pacific-North American Plate boundary, which also contains the San Andreas fault. The Owens Valley fault zone is a normal oblique right-lateral fault, meaning the movement along the fault is both vertical, with the hanging wall block moving downwards, and horizontal, with the two sides of the fault sliding past each other so that the block on the opposite side appears to have moved to the right to a viewer looking across the fault (Fig. 1) (Bacon et al., 2003). This geologic and tectonic setting creates a prime location for a major earthquake to occur, which is exactly what happened at approximately 2:30 am on March 26, 1872.

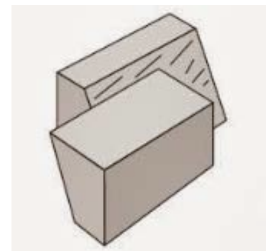

*Figure 1: The relative movement of two plates along a normal oblique right-lateral fault.*

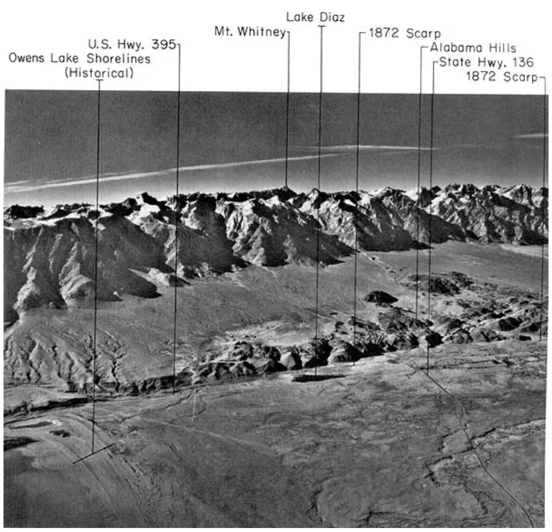


*Figure 2: The geographic context of the Owens Valley fault zone and features created by the 1872 earthquake.*

**Earthquake**

During the 1872 earthquake, surface ruptures occurred in multiple segments of the fault along the entire extent of the Owens Valley fault zone- approximately 100km- with an average right-lateral offset of 6m and a vertical displacement of about 1m (Beanland and Clark, 1994). However, the maximum right lateral offset, which was observed in the town of Lone Pine, was about 10m, and the maximum vertical displacement was about 4.4m (Beanland and Clark, 1994). Though modern seismic instruments were not yet available to record the earthquake, estimates based on the displacement and surface rupture place the moment magnitude of the earthquake between 7.4 and 7.9 and the modified Mercalli intensity at least at VIII, but possibly reaching IX-X in regions closest to the fault, meaning the 1872 Owens Valley Earthquake is among the three largest earthquakes in California's history (Beanland and Clark, 1994; Hough and Hutton 2008). Despite the fact that the surface rupture was less than a third of the length of that observed during the well-known 1906 San Francisco earthquake along the San Andreas fault, the magnitude and the maximum fault displacement associated with the two earthquakes are similar, and shaking due to the Owens Valley earthquake was actually felt at greater distances than the San Francisco earthquake (Hough and Hutton, 2008). This may be due to the highly efficient transmission of energy through the Sierra Nevada region, or could indicate that the 1872 Owens Valley earthquake was a high stress-drop rupture- an earthquake that released a significant amount of high-frequency energy, creating a significant change in the stress on the fault and causing more intense shaking (Hough and Hutton, 2008). The massive earthquake was felt across the entire state of California and into parts of Arizona, Nevada, Oregon, and Utah (Beanland and Clark, 1994). Well-known naturalist John Muir was in Yosemite National Park at the time of the earthquake and provided several written accounts of the event, including his observations of a rockslide in Yosemite and a description of "walking as if on the deck of a ship among the waves," (Muir, 1873; Muir, 1901). The intense and far-reaching effects of the 1872 Owens Valley earthquake emphasize the event's geologic and historical significance, even though it was not as destructive as other major earthquakes.

**Aftermath**

The epicenter of the earthquake was near Lone Pine, a mining supply town with a population of 250-300 at the time of the earthquake. The sparse population of the immediate region limited the damage to human life and property caused by the intense earthquake, especially relative to the devastation caused by the 1906 San Francisco earthquake, though the effects were still significant (Figs. 3 and 4). About 27 people in Lone Pine- approximately 10% of the total population- are believed to have lost their lives during the earthquake, and 56 additional people were injured, though the exact numbers are disputed, (Whitney, 1872a). Many of the earthquake victims were buried in a mass grave on the north side of Lone Pine, near the fault that caused the earthquake. Only 20 of the 80 buildings in Lone Pine remained standing, and 52 of the destroyed structures were houses. Many of the buildings in Lone Pine were constructed using adobe and brick, so the collapse of these heavy structures was the cause of most casualties. Several accounts of the earthquake mention that wood-frame structures were largely undamaged, which has helped more recent studies to constrain the intensity of the earthquake (Hough and Hutton, 2008).


HORRORS!!
Appalling Times!
EARTHQUAKES
Awful Loss of Life!
25 Persons Killed!
Earth Opens!
HOUSES PROSTRATED
LONE PINE!
ITS TERRIBLE CONDITION
MOST HEART-RENDING SCENES!
Miraculous Escapes!
Individual Heroism!
A Demoralized Printing Office.

*Figure 4: A newspaper headline describing the devastation caused by the earthquake.*

*Figure 3: A collapsed adobe structure between two undamaged wood-frame structures.*

In addition to the havoc it caused in the developed communities of Owens Valley, the earthquake changed the natural landscape as well. The vertical displacement of the ground created both graben, which are low-lying depressions in the surface, and scarps, which are steep, step-like features where one side of the fault is higher than the other. One graben region created by the earthquake filled with water and formed Diaz Lake, while scarps formed along approximately 70km of the ruptured fault (Beanland and Clark, 1994). Scarps can be seen northeast of Manzanar, west of Lone Pine and north of Whitney Portal Road, or north of Lone Pine, in a region east of the main fault and just west of Highway 395.

*Figure 5: A scarp formed by the 1872 Owens Valley earthquake. This scarp is located west of Lone Pine and north of Whitney Portal Road.*

The Owens Valley fault zone remains an active fault system, though the 1872 earthquake was the most recent major event in the region and the recurrence interval is 3300-5000 years (so probably nothing to worry about during the field trip) (Bacon et al, 2003). The scale and geographic reach of the 1872 Owens Valley earthquake illustrate the region's intense seismic activity and the potential for earthquakes to shape both human and natural geography.

**References**

Bacon, S. N., Pezzopane, S. K., and Burke, R. M. (2003). Paleoseismology on the Owens Valley Fault and latest Quaternary stratigraphy in Owens Valley near Lone Pine, eastern California, USGS Final Technical Report, Grant 01HQGR0013.

Beanland, S. and Clark, M. M. (1994). The Owens Valley fault zone, eastern California, and surface rupture associated with the 1872 earthquake, U.S. Geological Survey Bulletin 1982.

Hough, S. E. and Hutton, K. (2008). Revisiting the 1872 Owens Valley, California, earthquake, Bulletin of the Seismological Society of America 98, 931–949, doi: 10.1785/0120070186.

Muir, J. (1873). On the effects of the earthquake of March 1872 in the Yosemite Valley, John Muir: A Reading Bibliography by Kimes (1986), John Muir articles 1866–1986, No. 20, https://scholarlycommons.pacific.edu/jmb/20.

Muir, J. (1901). The Earthquake, Sierra Club, John Muir Exhibit – Writings, https://vault.sierraclub.org/john_muir_exhibit/writings/the_earthquake.aspx.

Smith, G. and Putnam, J. (1976). Deepest Valley: A Guide to Owens Valley, Its Roadsides and Mountain Trails, 2nd edition, Genny Smith Books.

Whitney, J. D. (1872a). The Owens Valley earthquake, part I, Overland Monthly 9, 130–140.

# Mars/Earth Overview of Debris-Covered and Rock Glaciers

**Euibin Kim**

## 1. Existing Glacier Classification Systems (Janke, 2015)

Rock Glaciers are often interpreted as debris-covered glaciers despite having different inertial ice structures and varying ice contents and in some cases, they are grouped together in a single class.

A three-tier classification is commonly used in literature:

- **Uncovered (white) glacier:**
  - Ice is clearly visible and contains very little internal/external impurities or debris
- **Debris-covered glacier:**
  - Surface is mantled with supraglacial debris that varies in coverage and thickness (~50% of the ablation zone covered by debris),
    - Supraglacial debris delivered by avalanching, rockfall, or other relatively fast mass movements
  - Thickness of debris ranges between 0.5 - 2.0 m.
- **Rock glacier:**
  - Thicker surface rock layer compared to debris-covered glaciers
    - Top debris layer covers the entire ablation and accumulation zones.
  - Mixture of ice and rock underneath the surface surface debris

| | Debris covered glaciers | | | Rock glaciers | | |
|---|---|---|---|---|---|---|
| | Class 1 | Class 2 | Class 3 | Class 4 | Class 5 | Class 6 |
| Common name | Semi | Fully | Buried | Proper | Transitional | *Glacier* of rock |
| Debris coverage | ~25% | ~95% | 100% | Fully covered | Fully covered | Fully covered |
| Debris thickness | <50 cm | 0.5 m to 3 m | >3 m | Thickly covered | Thickly covered | Thickly covered |
| Ice content | >85% | 65–85% | 45–65% | 25–45% | 10–25% | <10% |
| Ice form | Glacial | Glacial | Glacial<br>Interstitial ice<br>Segregated ice | Glacial<br>Interstitial ice<br>Segregated ice | Interstitial ice<br>Segregated ice | Pore ice |
| Visual characteristics | Debris accumulates in the ablation zone. Thicker debris is found near the toe. | The head of the glacier is often disconnected from the uncovered part. | Thermokarst is present. | Transverse ridges and furrows are pronounced arches. The front slope is steep differentiated by color and texture. | Transverse ridges and furrows are linear to flow and less pronounced. The front slope is less steep and elongated. | Surface topography is subdued, rounded, and weathered away. |

**Table 1.** Characteristics of debris-covered glaciers and rock glaciers (Janke, 2013).

## 2. Examples of Terrestrial Debris-Covered/Rock Glaciers

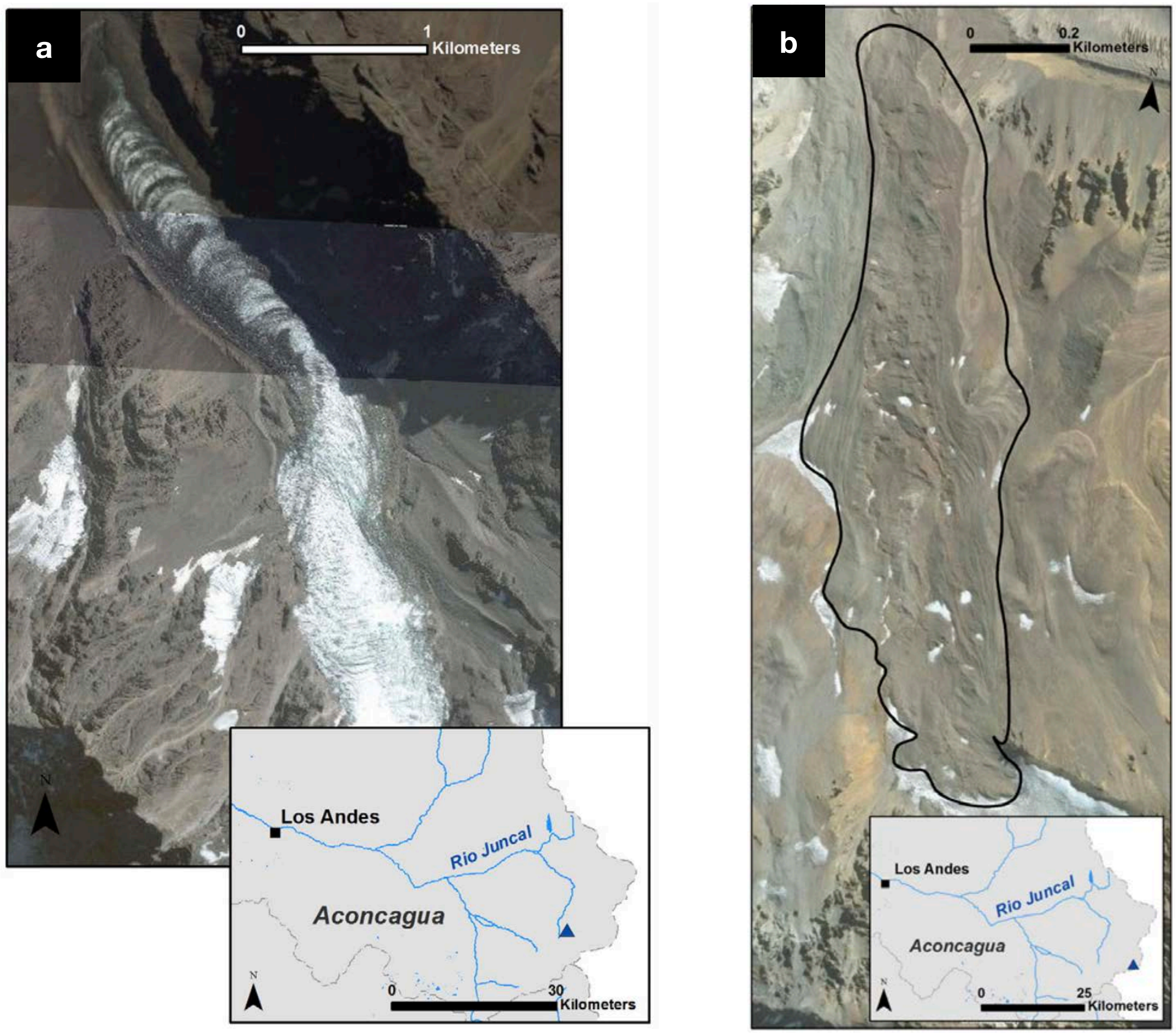


**Figure 1. Two end members of debris-covered glaciers. (a)** The semicovered Juncal Norte glacier. The glacier has experienced constant retreat since 1955. Between 1989 and 2010, the Juncal Norte glacier has receded at a rate of 14 m/yr, at a much slower rate than the uncovered South Juncal glacier which has receded at a rate of 79 m/yr. **(b)** An example of a class 3 (buried) glacier in Chile. Although the surface is entirely covered by debris, englacial material is exposed in collapse features (thermokarst) as the debris is relatively thin.

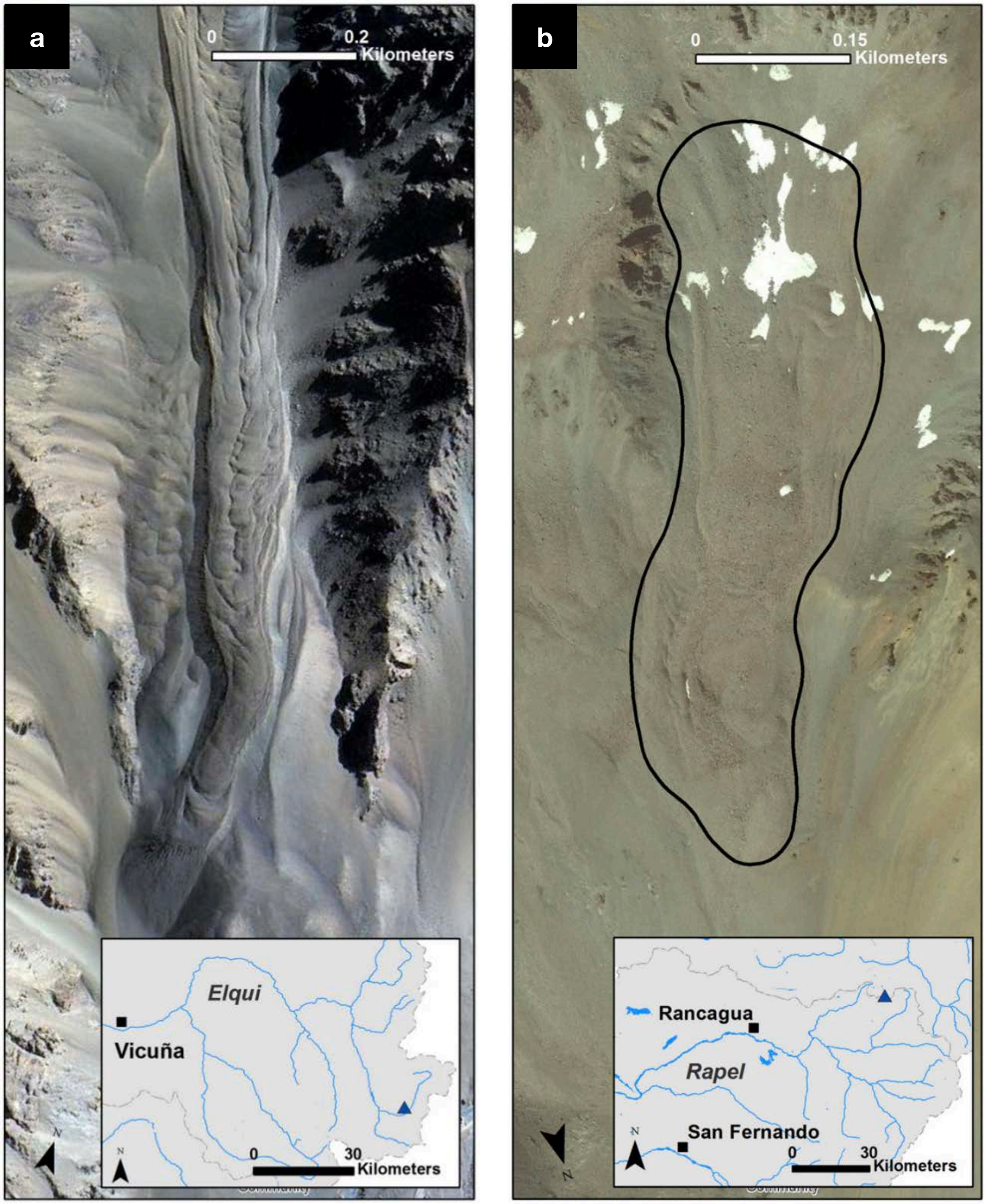


**Figure 2. Two end members of rock glaciers. (a)** An example of a class 4 rock glacier. Note the formation of transverse ridges extending down the center of the rock glacier. **(b)** An example of a class 6 rock glacier. The surface topography has been weathered and snow accumulates in depressions created by the melting of internal ice near the head of the rock glacier.

### 3. Debris-Covered Ice Features on Mars

- Extensive glacial activity during the late Amazonian period is evidenced by debris-covered ice landforms in Martian mid-latitudes. (Baker and Carter, 2019, Driver 2024).
- Mid-latitude debris-covered features have viscous flow morphologies analogous to terrestrial glaciers and **radar observations confirmed** that the largest of these features are **composed of nearly pure water ice beneath a thin debris layer** (Holt et al., 2008, Plaut et al., 2009).

- Glacial records on Mars are expected to provide key evidence for the planet's climatic history and how volatile reservoirs have evolved over the past billion years.
- Mean GLF flow speed ~ 7.5 mm/yr => Can this be detected in repeated HiRISE observations with > 10 yr gap?

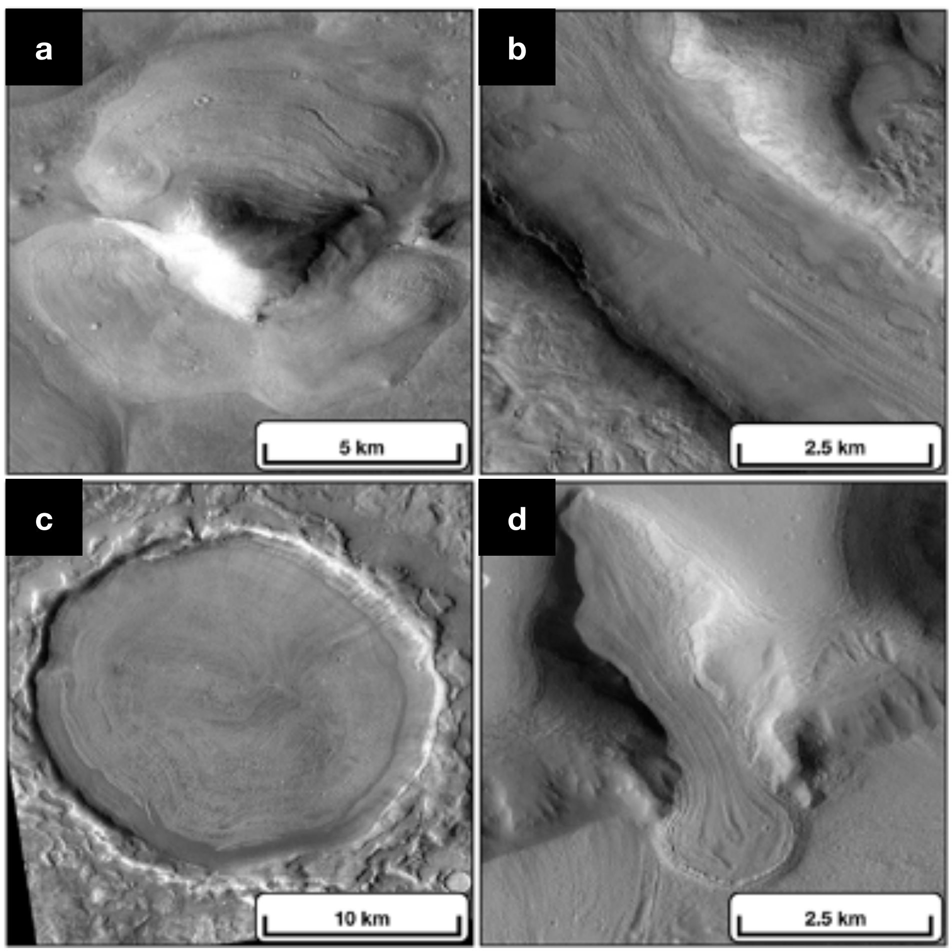


**Figure 3. Context Camera (CTX) examples of Martian mid-latitude debris-covered ice features. (a) Lobate Debris Apron (LDA):** CTX ID: D16_033363_2226 _XN_42N341W. **(b) Lineated Valley Fill (LVF):** CTX ID: B17_106287_2222_XI_42N344 W. **(c) Concentric Crater Fill (CCF):** CTX ID: U19_078358_2172_XI_37N337W. **(d) Glacier-Like Form (GLF):** CTX ID: P22_009653_2224_XN_42N309W.

References

**[1]** Janke et al., Classification of debris-covered glaciers and rock glaciers in the Andes of central Chile. Geomorphology, 2015. 241: p. 98-121
**[2]** Janke et al., Rock glaciers. In: Shroder. J. (Ed.), Treatise in Geomorphology. Elsevier, 2013, p. 238-273.
**[3]** Baker, D.M. and L.M. Carter, Probing supraglacial debris on Mars 1: Sources, thickness, and stratigraphy. Icarus, 2019. 319: p. 745-769.
**[4]** Driver, G., et al., Large glacier-like forms on Mars: Insights from crater morphologies and crater retention ages. Journal of Geophysical Research: Planets, 2024. 129(8): p. e2023JE008207.
**[5]** Holt, J.W., et al., Radar sounding evidence for buried glaciers in the southern mid-latitudes of Mars. Science, 2008. 322(5905): p. 1235-1238.
**[6]** Plaut, J.J., et al., Radar evidence for ice in lobate debris aprons in the mid-northern latitudes of Mars. Geophysical research letters, 2009. 36(2).
**[7]** Hubbard, B., Souness, C., and Brough, S. Glacier-like forms on Mars. The Cryosphere, 2014, 8, 2047–2061

# Owens Valley Pupfish

Kylie Hall

October 2025

## 1 Meet the Owens Valley Pupfish

Named for their "frolicsome, playful behavior" [6], pupfish are a group of fish species of the genus *Cyprinodontidae* living in and near Death Valley [1]. They are typically a few inches in length with arched backs [7]. The females are an olive green color with dark vertical bars along their sides, and the males are blue with orange-edged tail fins [7, 8]. They have upturned mouths used to catch food on the surface of the water, and their usual diet consists of immature insects and algae [7, 6]. The females and non-breeding males travel in small schools, while the breeding males are highly territorial [7].

The Owens Valley pupfish, *Cyprinodon radiosus*, is currently confined to only five populations in the Owens Valley region [2]. They can be distinguished from other pupfish species by their length, the anterior placement of their dorsal fin, and their excess of fin rays, among other details (see Figure 1 for an image of the Owens Valley pupfish and Figure 2 for a comparison of the desert pupfish species) [8].

The breeding season of the Owens Valley pupfish is in April through October. During this time, breeding males turn a brighter blue color and become highly aggressive. Females lay only one egg per spawning, but may spawn multiple times per season [7]. Pupfish

Figure 1: The Owens Valley pupfish. Figure from [2].

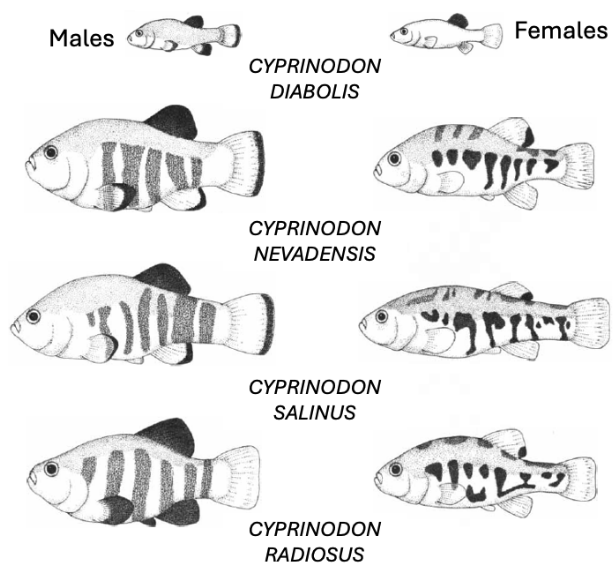


Figure 2: A comparison of the appearances of different species of desert pupfish. The Owens Valley pupfish, *Cyprinodon radiosus*, is in the bottom row. Figure from [1], modified to improve text readability.

young grow to maturity within 3-4 months [8].

## 2 Where Do the Owens Valley Pupfish Live?


Figure 3: Range of the Owens Valley pupfish. Figure from [8].

Pupfish were once abundant in warm, shallow sloughs, spring pools, irrigation ditches, and marshes along the Owens River (see Figure 3) [8, 5]. They are now mostly confined to deep pools artificially created for conservation purposes, although they still exist in some naturally-occurring locations such as Fish Slough and BLM Spring [2, 4]. Pupfish need high quality water, aquatic vegetation, and sand- or silt-covered floors to survive and reproduce [5].

Because the Death Valley region drainage areas where pupfish live are geographically isolated, their evolutionary pathways are similarly isolated, much like the finches discovered by Darwin in the Galapagos Islands [6]. They survive in environments that would be considered extreme by other species: water temperatures average 100 degrees Fahrenheit in the summer and can reach as high as 116 degrees, and in the winter pupfish can survive in water temperatures as cold as 32 degrees. They can also survive a water salinity of 4 times higher than the ocean's and in water with very little oxygen [7]. Their hardiness makes them intriguing subjects of study on the topics of kidney function, temperature adaptation, and more [6].

## 3 The Past and the Present of the Owens Valley Pupfish

The Owens Valley pupfish is considered an endangered species due to its limited geographical range, its limited number of populations, and its susceptibility to population declines without frequent management [5]. The threats that brought it to the brink of extinction include the introduction of game fish into and the diversion of water from its habitat [5].

When the species was first scientifically described in 1948, it was thought to have already gone extinct. However, in 1964, a population was discovered near Bishop and attempts were made to rehabilitate the species. Despite these efforts, population levels continued to drop, and they reached a particularly critical level in 1969 when they were believed to exist only in a pond in Fish Slough that began to inexplicably deplete. A team of biologists, including Edwin Philip Pister, were alerted to the issue and traveled to the area to rescue the pupfish in the pond. They began by moving the $\sim$ 800 individuals in the pond to a different stream of water nearby in baskets, with the intention of returning later to move them to safer locations. However, when Pister went back to check on the pupfish, he discovered that many of the fish had begun to die off, likely due to the stress caused by the change in environment. He then single-handedly transferred the remaining fish into two buckets he had in his truck to move them to a better location. He remarked in a reflection on the event later: "I

Figure 4: Edwin Pister in 2003, re-enacting his rescue of the Owens Valley pupfish species.

had walked perhaps fifty yards when I realized that I literally held within my hands the existence of an entire vertebrate species." Luckily, he did not drop either bucket, and thanks to his efforts the Owens Valley pupfish continue to exist today [6].

Unfortunately, the threats faced by the Owens Valley pupfish in the past are still present today, and they face additional challenges with the onset of climate change. Careful population management and protection is needed to preserve this species [3].

## References


[1] James H. Brown. The Desert Pupfish. *Scientific American*, 225(5):104–110, November 1971.

[2] California Department of Fish and Wildlife. Owens pupfish (*Cyprinodon radiosus*). https://wildlife.ca.gov/Regions/6/Desert-Fishes/Owens-pupfish, n.d. Accessed: 2025-09-22.

[3] Daniel Cox. 5-Year Review: Owens pupfish (Cyprinodon radiosus). Technical report, Reno Fish and Wildlife Office, September 2022.

[4] Floyd E Hayes. FINDING AND PHOTOGRAPHING THE FABLED FIVE PUPFISHES OF THE MOJAVE AND COLORADO DESERTS IN CALIFORNIA AND NEVADA. *American Currents*, May 2024.

[5] IUCN. Species profile: *Owens Pupfish* (iucn red list). https://www.iucnredlist.org/species/6164/15363754, n.d. Accessed: 2025-09-22.

[6] Edwin Philip Pister. Species in a bucket. *American Currents*, 40:15–20, 2015.

[7] U.S. Bureau of Land Management, California. Wildlife details – blm california (serial number 2803). https://web.archive.org/web/20090121103816/http:/www.blm.gov/ca/forms/wildlife/details.php?metode=serial_number&search=2803, 2009. Accessed: 2025-09-22; archived version from 2009-01-21.

[8] U.S. Fish and Wildlife Service. Species profile: *Owens Pupfish* (u.s. fish & wildlife service). https://ecos.fws.gov/ecp/species/4982, n.d. Accessed: 2025-09-22.

**History and Shorelines of Owens Lake, California**

Gabe Gowman
PTYS 590 FA25

## Introduction

Owens Valley is a graben lying east of the Sierra Nevada range in eastern California. It forms a large drainage area (~8450 $km^2$ [1]) that fills the Owens Lake playa during rainfall. In the past, a rainier climate and tectonic shifts (along with a lack of human activity) allowed for a much larger lake to exist in this valley (Fig. 1). Today, the lake has dried up to become a playa and only has water following rainfall, but in the past it was filled year-round.

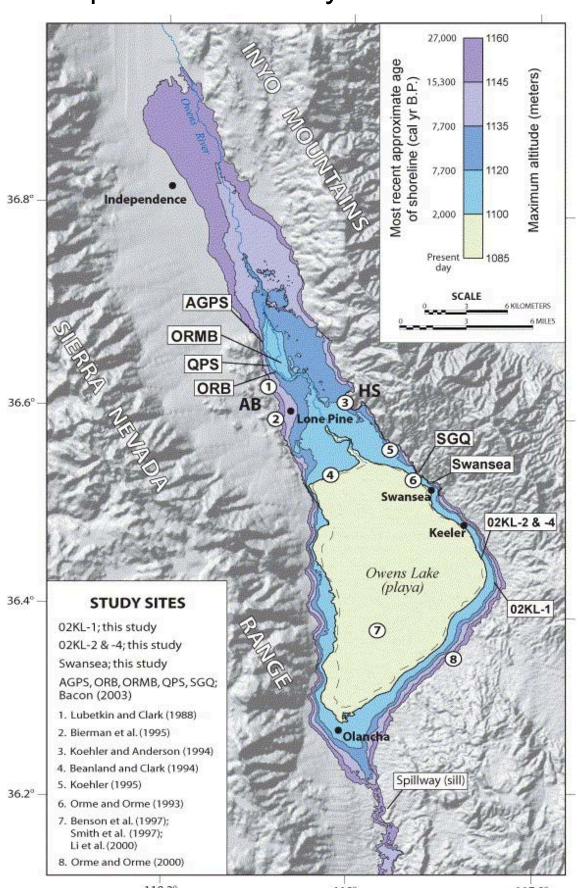


**Fig. 1**: Historical lake extents, from [1]. Times are in “calibrated years before present.”

## Lake Levels and Paleo-Shorelines

Mapping historical shorelines is a challenging task anywhere, but it is particularly difficult in the tectonically active basin and range region of the southwestern U.S. [1]. The Owens Lake shoreline has been shifted by earthquakes, including the major quake in 1872, complicating observations. Historical shorelines (Fig. 1) have been determined from remnant morphologies including beach ridges and notches incised into cliffs [1]. Animal fossils and dung have also contributed to lake level estimates in some locations, which can be $^{14}C$-dated to give relatively confident constraints on timing. Weaker constraints can be determined from sediment cores in the surrounding region. Certain periods in the lake’s history have been highly variable in lake level, including some very dry periods (Fig. 2). On average, however, the trend has generally been a decrease in lake level (and therefore size) over time [1].

## Evaporation and Environmental Effects

With development of agriculture in the nearby region starting in the 1860s and the construction of the Los Angeles Aqueduct in 1913, the Owens River was diverted and used in other locations. This reduced the amount of water available to fill the lake and, ultimately, the lake which had been gradually reducing in size for millennia became a dry playa by the mid-to-late 1920s [2]. As at the Salton Sea, as the lake dried up, what little water remained became increasingly saline. Even today, surface and groundwater continue to evaporate as they are refreshed by rainfall, preserving a very small brine pool in a mostly dry lakebed [2]. The salts that are deposited onto the lakebed cannot resist the strong winds that blow through Owens Valley, leading to enormous quantities of dust emitted into the surrounding region [2]. Efforts in the last 20 years have attempted to revive the lake somewhat, bringing additional water and plant and animal life to the region [3].

**Dust Mitigation and Management**

With the drying of Owens Lake into a dessicated playa over the last century, dust has become a major environmental hazard. This is true on both local and national scales, with an estimated 6% of airborne dust in the continental U.S. as of 1993 coming from Owens Lake [2]. As such, the Los Angeles Department of Water and Power is leading efforts to limit dust while preserving existing habitats and infrastructure, claiming to have reduced dust emission by 99.4% [3]. Part of the challenge is that most methods take a very large amount of water, and a lack of water is the source of all the problems in the first place. As such, conservation and reuse of water is key [3].

There are a few methods used to reduce dust, either by blocking the wind or by strengthening soil cohesion [3]. First is shallow flooding, just covering the playa with water to reduce dust generation and trap any dust that may blow in from elsewhere. Naturally, this is fairly water-intensive, but can use a shallow layer to reduce the required load. To avoid water usage, an alternative method is gravel coverage. This is a simple approach of just reducing the wind that reaches the dust level by spreading gravel over the surface. Channels and drainage are built to reduce the possibility and extent of flooding during rainfall. Finally, vegetation can be used to both reduce wind and hold the soil in place. This has the additional benefit of supporting native plant ecosystems through managed planting and maintenance.

Today, Owens Valley is an important stop for migrating birds, which use what is left of Owens Lake as a resting point [3].

**References:**

[1] Bacon, Steven N., et al. *Quaternary Science Reviews*, vol. 25, nos. 11–12, Jun. 2006, pp. 1264–82. [2] Tyler, Scott W., et al. *Journal of Hydrology*, vol. 200, nos. 1–4, Dec. 1997, pp. 110–35. [3] Los Angeles Department of Water and Power, https://ladwpeasternsierra.com/owenslake.

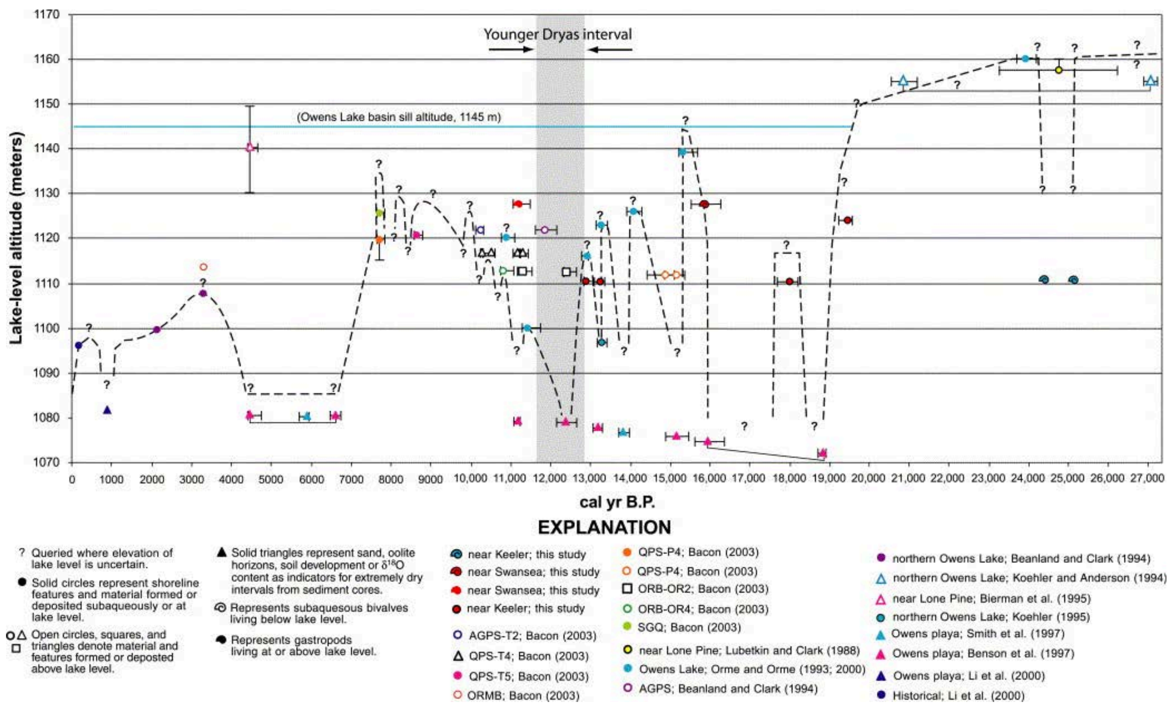


**Fig. 2**: Lake-level curve for Owens Lake over the last 27,000 years (to 1950), combining stratigraphic, geomorphic, and sediment core data. Figure taken from [1].

# Hot Springs of the Eastern Sierra Region

Kiki Gonglewski

Figure 1: Travertine Hot Springs near Bridgeport, California

## Introduction

Hot springs are surface expressions of geothermal circulation: meteoric water percolates downward, heats in the crust, and re-emerges through faults carrying dissolved minerals and gases (see Fig. 2). In the Eastern Sierra Nevada of California, these features are linked to the tectonic and volcanic history of the Long Valley Caldera, one of the largest Quaternary volcanic systems in the U.S. This report highlights the geologic context, representative sites, hydrothermal dynamics, and the relevance of these systems to microbiology and planetary science [1, 2, 3].

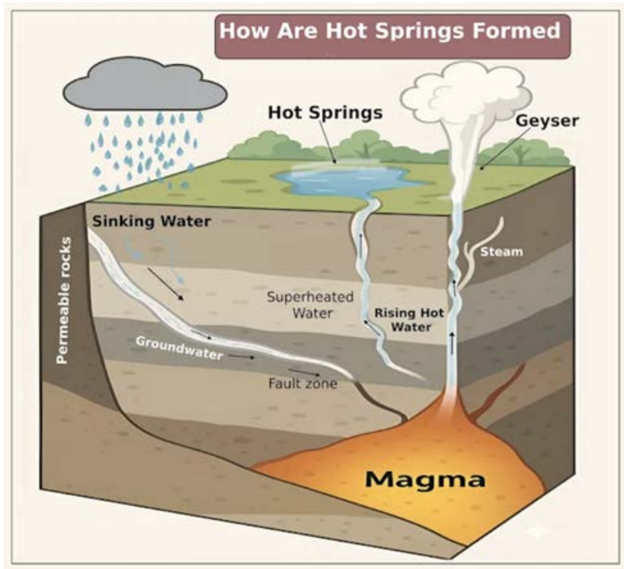


Figure 2: A representative diagram of the processes behind hot spring formation

## Geologic and Hydrothermal Context

The Long Valley Caldera is a ∼450 km$^2$ depression formed after the 0.76 Ma Bishop Tuff eruption. Residual magmatic heat sustains a vigorous hydrothermal system, with aquifer temperatures estimated at 180–280°C [1]. Flow paths shift as fractures seal with mineral precipitates or reopen during seismic activity, explaining the transient nature of spring discharge and vent location [4]. Ongoing deformation of the resurgent dome and active faulting provide fluid pathways, and USGS monitors discharge, gas flux, and seismicity to assess hazards and system evolution [3].

## Representative Springs

Taken together, the hot springs of the Eastern Sierra region illustrate a wide spectrum of human interactions (see Fig. 4): from pools left in their natural state or informal soaking pools bordered by local stonework, to sites closed because of hazards, developed spas, and even geothermal power plants.

**Hot Creek**, near Mammoth Lakes, is the most visible outlet of the system. Water temperatures can reach boiling, and sudden shifts in flow or geysering have led to closures [2, 5] (see also Fig. 5a).

**Casa Diablo**, east of Mammoth Lakes, hosts a geothermal power facility that taps the hydrothermal system for electricity [3, 6]

**Travertine Hot Springs**, near Bridgeport, features terraced carbonate deposits formed

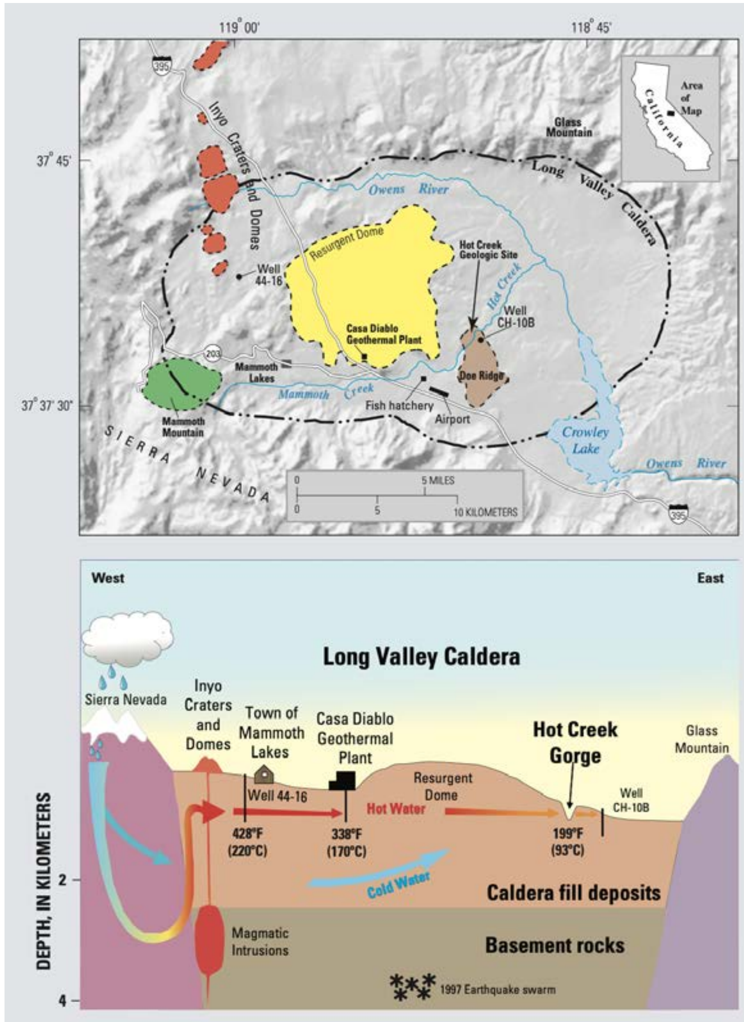


Figure 3: Map and cross section of Long Valley Caldera showing snowmelt-heated groundwater emerging as hot springs at Hot Creek.

Figure 4: The two hot springs of Keough, contrasting different states of development. Keough Hot Ditch (left) has some local stonework, whereas Keough's Hot Springs (right) has been fully developed as a spa.

as $CO_2$-rich waters cool and degas [7].

**Informal/Local Springs** elsewhere in the Long Valley basin, like "Wild Willy's," "Shepard's Tub," or "Crab Cooker," remain largely undeveloped, often modified only by visitor-built stone pools, reflecting a more informal interaction with the geothermal landscape [6].

## Chemistry and Travertine Formation

Thermal waters carry silica, calcium, carbonate, and sulfate. Cooling and degassing of $CO_2$ drive precipitation of calcite, aragonite, and silica sinter [7]. Travertine facies—vent, apron, and pond—show distinct textures shaped by microenvironments [8]. These deposits record both abiotic processes and microbial influences.

## Microbial Ecosystems

Studies in the Long Valley hydrothermal system confirm diverse microbial communities. At Little Hot Creek, microbial mats—including Aquificae, Thermodesulfobacteria, and novel archaeal lineages—modify carbonate precipitation and isotopic signatures [9, 10]. These findings demonstrate that California hot springs, like those at Yellowstone, support thermophiles that thrive on chemical gradients in extreme environments (see also Fig. 5b).

## Planetary Relevance

Hydrothermal systems are prime analogs for astrobiology. Silica-rich sinters on Mars resemble terrestrial hot spring deposits, suggesting similar preservation of biosignatures [11]. On icy moons such as Enceladus, plume chemistry reveals ongoing hydrothermal activity that could sustain life [12]. By studying Eastern Sierra springs, scientists can refine models for habitability in extraterrestrial hydrothermal environments.

## References

[1] M. L. Sorey, R. E. Lewis, and F. H. Olmsted. The hydrothermal system of long valley caldera, california. Technical Report 1044-A, U.S. Geological Survey, 1978. URL https://pubs.usgs.gov/publication/pp1044A.

(a) Cooked fish at Hot Creek.



(b) Keough's warning sign (Naegleria fowleri).

Figure 5: Hydrothermal hazards in the Eastern Sierra: (a) sudden temperature changes; (b) biological hazards.


[2] Christopher D. Farrar, William C. Evans, Dina Y. Venezky, Shaul Hurwitz, and Lynn K. Oliver. Boiling water at hot creek—the dangerous and dynamic thermal springs in california's long valley caldera. Technical Report Fact Sheet 2007-3045, U.S. Geological Survey, 2007. URL https://pubs.usgs.gov/fs/2007/3045/.

[3] U.S. Geological Survey. Hydrothermal monitoring at long valley caldera. USGS Volcanoes page, 2023. URL https://www.usgs.gov/volcanoes/long-valley-caldera/science/hydrothermal-monitoring-long-valley-caldera.

[4] U.S. Geological Survey. Bubble trouble? tracking changing hydrothermal features in long valley's hot creek. USGS California Volcano Observatory news, 2023. URL https://www.usgs.gov/observatories/calvo/news/bubble-trouble-tracking-changing-hydrothermal-features-long-valleys-hot.

[5] U.S. Geological Survey. Hot creek geologic site, long valley, california. USGS Volcanoes page, 2023. URL https://www.usgs.gov/volcanoes/long-valley-caldera/science/hot-creek-geologic-site-long-valley-california.

[6] June Lake Loop Community. Eastern sierra hot springs. Website, 2023. URL https://junelakeloop.com/eastern_sierra_hot_springs.

[7] C. W. Chesterman and F. J. Kleinhampl. Travertine hot springs, mono county, california. *California Geology*, 44(8), 1991. URL https://www.osti.gov/biblio/5783429.

[8] Bruce W. Fouke. Hot-spring systems geobiology: Abiotic and biotic influences on travertine formation at mammoth hot springs, yellowstone national park, usa. *Sedimentology*, 58:170–219, 2011. doi: 10.1111/j.1365-3091.2010.01209.x. URL https://www.igb.illinois.edu/sites/default/files/upload/Fouke2011_Sedimentology.pdf.

[9] T. J. Vick, E. L. Dodsworth, B. P. Swingley, J. Raymond, and B. P. Hedlund. Microbiology and geochemistry of little hot creek, a hot spring environment in the long valley caldera, california. *Geobiology*, 8(2):140–154, 2010. doi: 10.1111/j.1472-4669.2009.00228.x. URL https://oasis.library.unlv.edu/sls_fac_articles/94.

[10] D. R. Meyer-Dombard, T. J. Vick, C. A. Amend, B. P. Hedlund, B. S. Wade, C. S. Romanek, A. L. M. Mucci, and B. W. Fouke. Environmental and biological influences on carbonate precipitation in little hot creek, long valley caldera, california. *Frontiers in Microbiology*, 9:1464, 2018. doi: 10.3389/fmicb.2018.01464. URL https://www.frontiersin.org/articles/10.3389/fmicb.2018.01464/full.

[11] Steven W. Ruff and Jack D. Farmer. Silica deposits on mars with features resembling hot spring biosignatures at el tatio in chile. *Nature Communications*, 7:13554, 2016. doi: 10.1038/ncomms13554. URL https://www.nature.com/articles/ncomms13554.pdf.

[12] Hsiang-Wen Hsu, Frank Postberg, Yuh-Fang Chang, Rafael Sekine, Jürgen Moragas-Klostermeyer, Sascha Kempf, and Mihály Horányi. Ongoing hydrothermal activities within enceladus. *Nature*, 519(7542):207–210, 2015. doi: 10.1038/nature14262. URL https://www.nature.com/articles/nature14262.pdf.

Ruby Fulford
PTYS 590
Field Trip Report

# Rock Glaciers: Internal Structure and Climate Signals

Rock glaciers are lobate, tongue-shaped masses of ice and rock found at a wide range of elevations around the world. They most commonly occur in continental mountain ranges, like the Sierra Nevadas (Florentine et al., 2014). Like traditional alpine glaciers, rock glaciers flow due to the presence of internal ice. Unlike traditional glaciers, ice is rarely visible on the surface of rock glaciers.

Figure 1: A rock glacier flowing from Sourdough Peak in Alaska. Source: nps.gov

## Composition and Internal Structure

Internal structure can vary widely between individual rock glaciers. There are two commonly accepted endmembers:

1. Relatively pure glacial ice covered with a layer of debris
2. Rockier, heterogenous mix of rock and debris-filled ice

Many variations of rock glacier structure exist between these two endmembers. Different models of rock glacier formation suggest different ice origins, with some models presenting true glacial origins and others presenting periglacial origins in which ice seasonally freezes and refreezes (Petersen et al., 2020). There is evidence that both glacial and periglacial ice play a role in rock glacier formation, sometimes both occurring within the same glacier (Florentine et al., 2014).

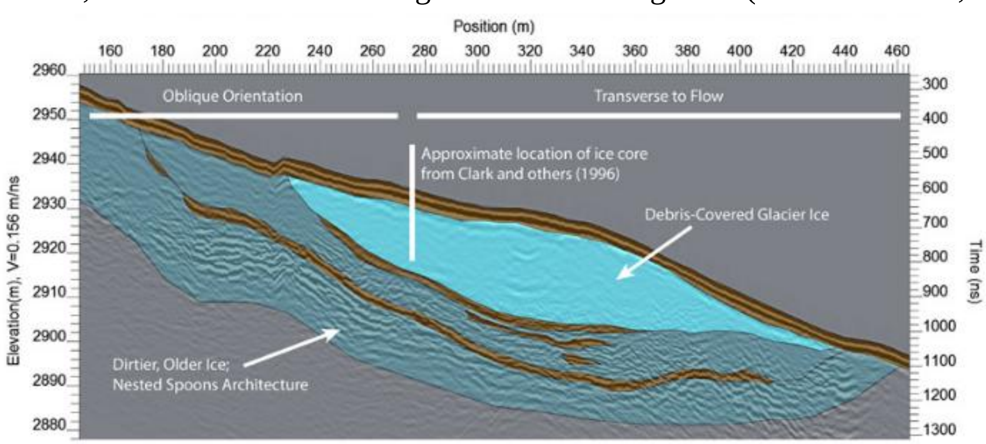


Figure 2: Proposed internal structure of Galena Creek Rock Glacier overlayed on GPR data. Taken from Petersen et al. (2020) Figure 8.

Radar observations, especially ground penetrating radar (GPR), are very useful for studying the internal structure of rock glaciers. GPR can identify subsurface interfaces between materials with different dielectric properties and can therefore reveal the nature of internal rock and ice layers within rock glaciers. Below, I outline a few examples of rock glacier structure from influential rock glacier studies.

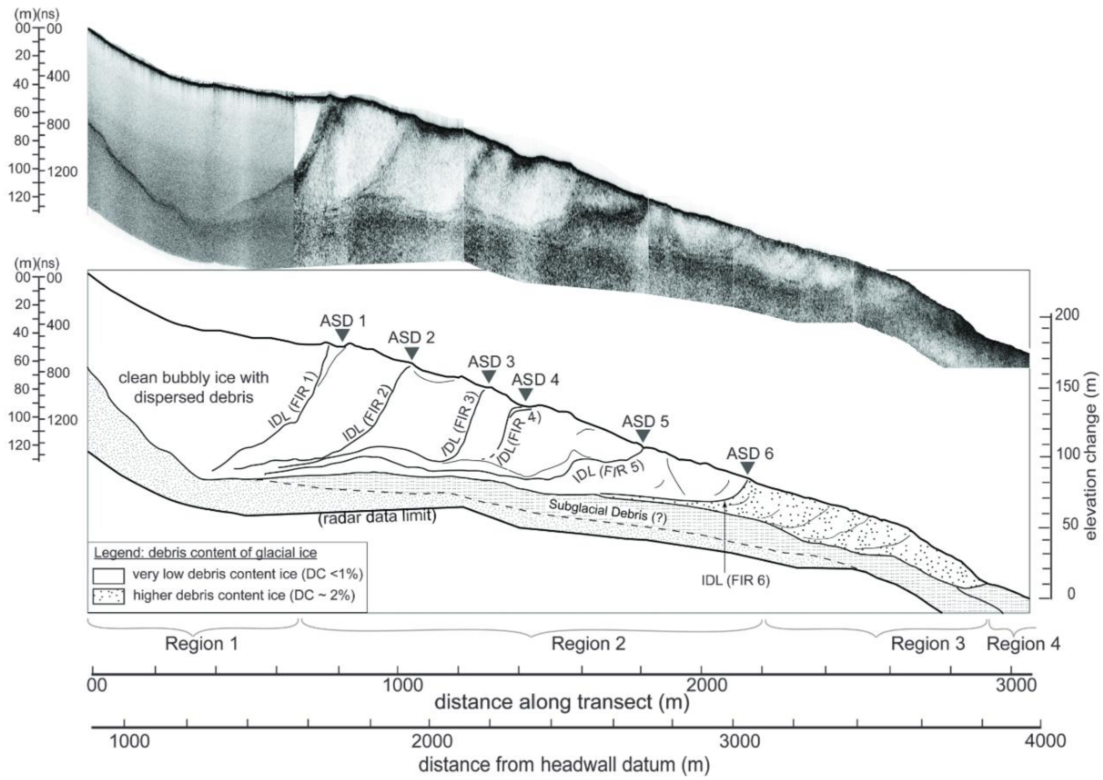


Figure 3: Longitudinal transect of Friedman Glacier, showing GPR observations of six inclined debris layers (IDLs). Taken from Mackay et al. (2014) Figure 8.

**Galena Creek Rock Glacier:** The Galena Creek Rock Glacier in Wyoming was the target of a 2020 study by Petersen et al. GPR data taken along this glacier is interpreted to represent a layer of debris covering a layer of pure ice, with a basal layer of older, dirtier ice (Fig. 2). The cleaner top layer of ice is thought to have formed from snowfall packed and preserved beneath falling debris

**Debris bands in Antarctic rock glaciers:** Mackay et al. (2014) conducted an extensive study of two glaciers in the same region of Antarctica: Mullins glacier and Friedman glacier. GPR data found six bands of concentrated debris separating layers of pure ice, nearly identical across both glaciers (Fig. 3). The bands, referred to as inclined debris layers (IDLs), form when rock falls onto a glacier's surface and is transported downslope by glacial flow.

**Upward dipping reflectors in rock glaciers:** Not all subsurface features are associated with layers of debris. Sometimes they indicate tectonic features. GPR data for several rock glaciers

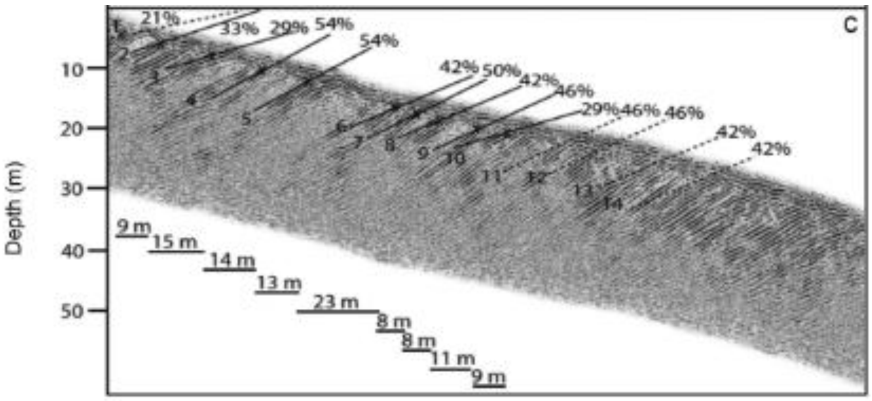


Figure 4: Upslope-dipping reflectors in Lone Peak Rock Glacier in Montana, USA. Taken from Florentine et al. (2014) Figure 5.

show upward-dipping reflectors in the shallow subsurface. In some cases, such reflectors indicate compressional stress (Monnier and Kinnard, 2015). In some cases, such as the Lone Peak Rock Glacier in Montana (Fig. 4), upslope dipping reflectors are spatially correlated with transverse ridges on the rock glacier's surface and likely represent thrust faults associated with changes in ice flow dynamics (Florentine et al., 2014).

## Climate Signals

The internal structure of rock glaciers can offer insight into past climate fluctuations. Periglacial rock glaciers may contain a fraction of liquid water, which can be a sign of permafrost melt caused by increasing temperatures (Monnier and Kinnard, 2015). Debris-rich layers like IDLs form during warmer periods with higher sublimation rates when ice ablation outpaces ice accumulation. Conversely, purer ice layers form during colder periods when ice accumulation is higher than ice ablation. Mackay et al. (2014) determined that rock glaciers containing discrete IDLs between pure ice layers are able to record long term, low-frequency climate fluctuations. The spacing of IDLs in the Mullins and Friedman glaciers, along with radiocarbon dating of ice cores taken from these glaciers, indicated a 41 ka periodicity in the mass balance for these glaciers, which corresponds to periodic changes in Earth's obliquity.

Rock glaciers could also record changes in specific conditions like precipitation and temperature, though the effect of these parameters on rock glacier structure is not yet well understood.

Figure 5: A rock glacier in Owens Valley, CA, USA. This is a study site for the PTYS 590 and PTYS 549 Fall 2025 field trip. Image taken from Google Earth.

## Owens Valley Rock Glacier

The rock glacier we are visiting in Owens Valley is shown in Figure 5. The landform's internal structure is unknown because no available data probes its subsurface. Transverse ridges similar to those observed in Montana by Florentine et al. (2014) cross the rock glacier's surface, which could indicate subsurface thrust faulting or shear zones. The radar class will be taking GPR data on multiple paths across the rock glacier, and we will interpret the data to explore the glacier's internal structure. Ideally, we will be able to determine which of the rock-glacier end members this landform more closely resembles. We may be able to connect ice and debris layers to past climate fluctuations in the Owens valley region.

## Martian Rock Glaciers

Mars is home to dozens of lobate debris aprons that resemble terrestrial rock glaciers, which might offer insight into Mars's climate evolution (Fig. 6). A study by Levy et al. presents observations of boulder bands on 45 Martian lobate debris aprons. The authors concluded that these boulder bands form when rocky debris is incorporated into ice accumulation zones and transported within the glacier to form a debris band (Levy et al., 2021), similar to IDLs in Antarctic rock glaciers (Mackay et al., 2014). Debris bands are buried by future ice deposits, and when ice sublimates the debris layers outcrop as boulder bands. If debris bands form during periods of negative ice balance like they do on Earth, then Martian rock glaciers consist of multiple ice deposition events (Levy et al., 2021). The spacing of the boulder bands provides a climate proxy that reflects history of orbit-paced climate change on Mars over the past 300-800 Myr, and implies large-scale obliquity change episodes in this time period. Radar observations of Martian rock glaciers could confirm the origins of the boulder bands and give more detailed insight into Martian climate history.

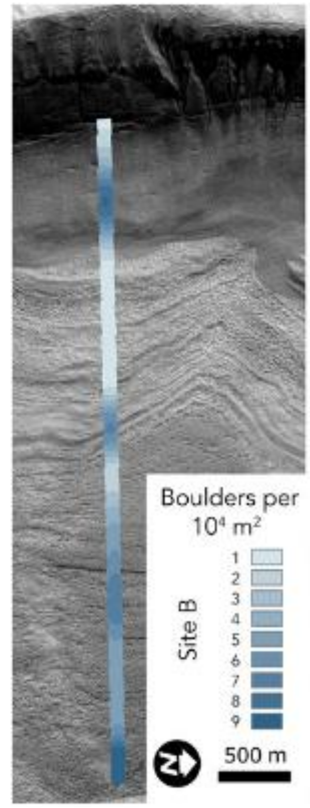


Figure 6: A lobate debris apron on Mars. Changing boulder density is shown along the feature. Taken from Levy et al. (2021) Figure 1.

## References

Florentine, C., Skidmore, M., Speece, M., Link, C., Shaw, C.A., 2014. Geophysical analysis of transverse ridges and internal structure at Lone Peak Rock Glacier, Big Sky, Montana, USA. J. Glaciol. 60, 453–462. https://doi.org/10.3189/2014JoG13J160

Levy, J.S., Fassett, C.I., Holt, J.W., Parsons, R., Cipolli, W., Goudge, T.A., Tebolt, M., Kuentz, L., Johnson, J., Ishraque, F., Cvijanovich, B., Armstrong, I., 2021. Surface boulder banding indicates Martian debris-covered glaciers formed over multiple glaciations. Proc. Natl. Acad. Sci. 118, e2015971118. https://doi.org/10.1073/pnas.2015971118

Mackay, S.L., Marchant, D.R., 2017. Obliquity-paced climate change recorded in Antarctic debris-covered glaciers. Nat. Commun. 8, 14194. https://doi.org/10.1038/ncomms14194

Mackay, S.L., Marchant, D.R., Lamp, J.L., Head, J.W., 2014. Cold-based debris-covered glaciers: Evaluating their potential as climate archives through studies of ground-penetrating radar and surface morphology. J. Geophys. Res. Earth Surf. 119, 2505–2540. https://doi.org/10.1002/2014JF003178

Monnier, S., Kinnard, C., 2015. Internal Structure and Composition of a Rock Glacier in the Dry Andes, Inferred from Ground-penetrating Radar Data and its Artefacts. Permafr. Periglac. Process. 26, 335–346. https://doi.org/10.1002/ppp.1846

Petersen, E.I., Levy, J.S., Holt, J.W., Stuurman, C.M., 2020. New insights into ice accumulation at Galena Creek Rock Glacier from radar imaging of its internal structure. J. Glaciol. 66, 1–10. https://doi.org/10.1017/jog.2019.67

Elana Alevy

**Owens Valley Meteorite Provenance:** The Owens Valley meteorite ("Owens Valley") was recovered in 1913 after it was reportedly discovered by a sheepherder in Inyo County. In total, the main mass of collected sample measures at 192.8 kg. Nearly ten years passed before the sample was obtained by Lincoln Ellsworth and subsequently donated in full to the U.S. National Museum. There, an end cut was created, which exposed a fresh surface to be etched and photographed for chemical characterization and classification of the meteorite. Additional pieces of the main mass were sectioned off and can be traced to meteorite collections in New York, Tempe, AZ, London, and Paris [1].

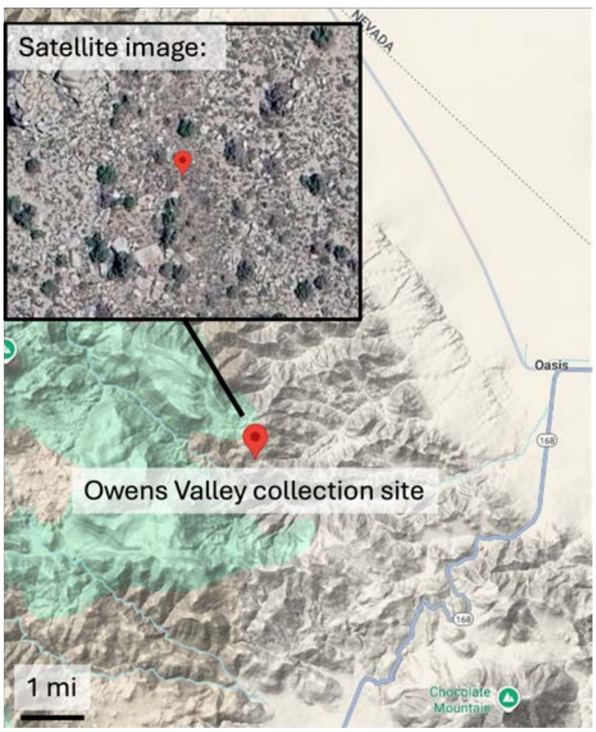


Figure 1. Google Maps data with the approximate Owens Valley collection site coordinates marked in red. Inset shows satellite imagery of the site. Scale bar is 1 mile.

*Recovery Setting*: The Meteoritical Bulletin database reports recovery coordinates of approximately 37º28'N, 118º0'W level (Figure 1) [1]. This location lies near the California/Nevada border in the eastern margin of the White Mountains, the range just northeast of Bishop, CA. (Figure 1). Satellite imagery of the recovery coordinates reveal that the collection area contains sparse vegetation and a predominantly gravelly terrain with several large, meter-scale rocks (Figure 1). The light-colored ground and lack of extensive vegetation are favorable conditions for spotting and recovering meteoritic material.

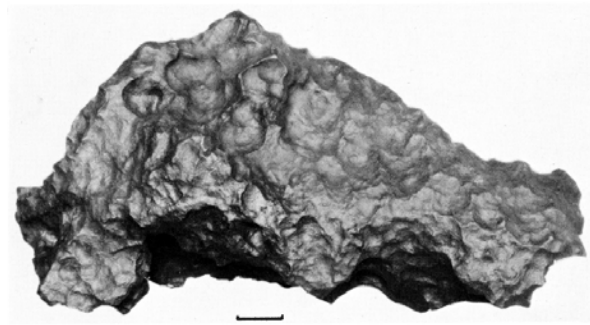

Figure 2. Photograph of Owens Valley in the U.S.N.M collection. The surface exhibits regmaglypts, a characteristic useful in identifying meteorites. Scale bar is ~5 cm.

Bedrock geology of the recovery site is predominantly Beer Creek monzonite, a medium- to coarse-grained porphyritic rock, which commonly contains diorite inclusions. K-Ar dates constrain an age for this unit between 151 and 163 Myr. Downslope from the sample collection site runs the Cottonwood Creek, which is characterized by Quaternary alluvium of stream gravel, sand, and sediment from old fans [2]. At high elevations, Quaternary glacial deposits in the form of till and moraine material also exist, which could account for the poorly sorted material visible in satellite imagery of the sampling site [3].

**Owens Valley Classification and Characterization:** An early catalogued classification of Owens Valley is simply "coarse octahedrite," a structural class of iron meteorites. The updated and most current, recommended classification for Owens Valley is an iron type IIIAB. The IIIAB group is the largest of the iron meteorite groups with well-constrained chemical compositions [4].

*Sample description:* Owens Valley was not an observed "fall," meaning it reached Earth and subsequently experienced extensive exposure to terrestrial weathering before it was discovered and collected after an unknown duration of time. The result of this terrestrial exposure is visible on Owens Valley as extensive corrosion and modification of the regmaglypts, the bowl-shaped depressions across the main mass that formed during atmospheric entry (Figure 2) [1]. Records of corrosion are also highly localized, specifically along cracks and fissures in the metal (Figure 3). Additionally, the sample exhibits 12-17 mm-wide pits that suggest troilite (FeS) grains in contact

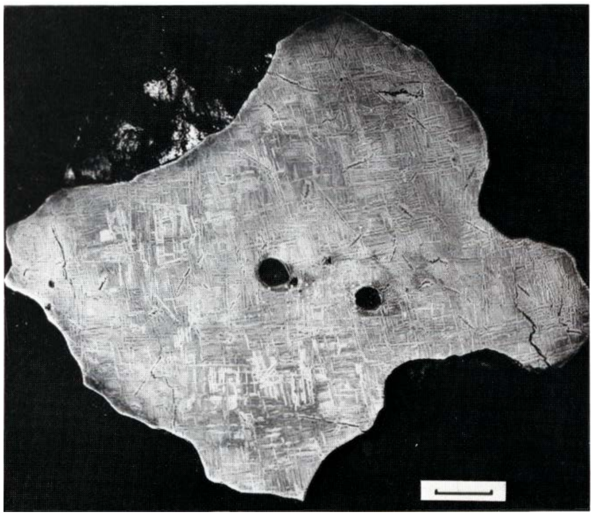

Figure 3. Interior of Owens Valley from Buchwald (1975). Lamellae of Fe, Ni-rich minerals and two rounded troilite nodules are pictured. Scale bar is ~3 cm.

with the surface had been weathered out and ablated away from the sample [1].

Etching of a cut face reveals a Widmanstätten pattern, which is the preserved structure of iron-nickel alloy crystallization from parent body melting. Owens Valley also contains Fe,Ni-rich minerals including kamacite, taenite, and schreibersite ($(Fe, Ni)_3P$) in elongated crystal forms, and troilite in nodule form (Figure 3).

*Parent Body Implications*: Iron meteorites include both magmatic and non-magmatic subgroups, which are distinguished based on their chemical composition trends [5]. They represent material excavated from the cores of differentiated planetesimals that fractionally crystallized [e.g., 6].

Shearing and brecciation of schreibersite in Owens Valley suggests that plastic deformation on the parent body contributed to the meteorite's early textural evolution. Subsequently, the sulfides crystallized within interstitial voids before the metallic matrix finally cooled with additional phosphides [1] to form the texture observed in the cut sample.

**Meteorite Occurrences on Mars:** The Owens Valley meteorite is one of 363 IIIAB iron meteorites identified and collected on Earth. To date, over 75,000 meteorites on Earth's surface have been approved in the Meteoritical Bulletin [7]. For comparison, only a handful of meteorites have been located on Mars using rover data.

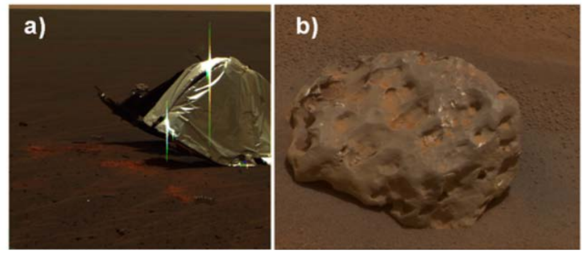


Figure 4. Opportunity's view of Heat Shield Rock, the 31 cm rock exhibiting a spectral signature consistent with iron meteorites from [8].

Curiosity identified meteorites Aeolis Palus 002 ("Lebanon") and Aeolis Palus 001 ("Littleton") in Gale Crater using the NavCam instrument [9]. The Opportunity rover identified "Heat Shield Rock," a 31 cm-large rock identified close to Opportunity's heat shield (Figure 4) [8 and references therein]. Similar to Owens Valley, the surface of Heat Shield Rock exhibits regmaglypts, often observed on iron meteorites. Heat Shield Rock's spectral emissivity of ~0.3 is consistent with metal in iron meteorites, and APXS bulk compositional data enabled classification of "Heat Shield Rock" as an IAB iron meteorite named Meridiani Planum [10].

Additional samples on Mars identified with the exploration rovers include Barberton, Santa Catarina, and other adjacent cobble-sized rocks. Their compositions, obtained through rover instrumentation, are most consistent with the mesosiderite group, a type of stony-iron meteorite. This suite of samples forms a potential strewn field near Endurance crater, suggesting an impact dispersed multiple stones from a single mesosiderite impactor [8].

Thus, meteorites on planetary surfaces are compelling subject of study. They have the potential to inform research on atmospheric conditions, weathering processes, and aeolian processing on planetary surfaces like Mars [11]. Further modeling of meteorite flux on other planetary bodies as well as observation with rovers and orbital methods would help to better constrain the meteoritic abundances on other planetary surfaces.

**References**: [1] Buchwald, Vagn F. (1975) Handbook of Iron Meteorites. University of California Press, pp. 1418. [2] McKee, E. H. and Nelson, C. A. (1967). Geologic map of the Soldier Pass quadrangle, California and Nevada. U.S. Geological Survey, Geologic Quadrangle Map GQ-654. [3] Horton, J. D., San Juan, C. A., and Stoeser, D. B. (2017). The State Geologic Map Compilation 9SGMC) geodatabase of the conterminous United States: U.S. Geological Survey Data Series 1052, doi: 10.3133/ds1052. [4] Goldstein, J. I., Scott, E. R. D., & Chabot, N. L. (2009). Iron meteorites: Crystallization, thermal history, parent bodies, and origin. Geochemistry, 69(4), 293-325. [5] Mittlefehldt, D. W. (2008). Meteorites–A brief tutorial. Reviews in Mineralogy and Geochemistry, 68(1), 571-590. [6] Scott, E. D. (1972). Chemical fractionation in iron meteorites and its interpretation. Geochimica et Cosmochimica Acta, 36(11), 1205-1236. [7] The Meteoritical Bulletin. [8] Schröder, C., et al. (2008), Meteorites on Mars observed with the Mars Exploration Rovers, J. Geophys. Res., 113, E06S22, doi:10.1029/2007JE002990. [9] Rudin, M. C., Wiens, R. C., & Horgan, B. (2025). Searching for meteorites on the martian surface from orbit. 56th LPSC, Abstract #1265. [10] Connolly, H. C., Jr., et al. (2006), The meteoritical bulletin, no. 90, 2006, September, Meteorit. Planet. Sci., 41(9), 1383 – 1418. [11] Bland, P. A., & Smith, T. B. (2000). Meteorite accumulations on Mars. Icarus, 144(1), 21-26.

# Geological Report: Mantle Xenoliths at Papoose Canyon, Owen's Valley, CA

## 1. Introduction

Xenoliths are fragments of rock carried from depth to the surface by ascending magma, providing direct samples from otherwise inaccessible parts of the Earth's interior. At Papoose Canyon in the Big Pine Volcanic Field (BPVF) of Owen's Valley, xenoliths brought up by Quaternary basalts provide a unique opportunity to study lithospheric mantle evolution in a tectonically active region adjacent to the Sierra Nevada batholith and Basin and Range province.

This report describes the setting of Papoose Canyon, the field occurrence of mantle xenoliths (peridotites and pyroxenites), and the implications for lithospheric structure and geodynamics (Ducea & Saleeby, 1996; Blondes et al., 2008; Mordick & Glazner, 2006; Ormerod et al., 1991).

## 2. Regional Geological Setting

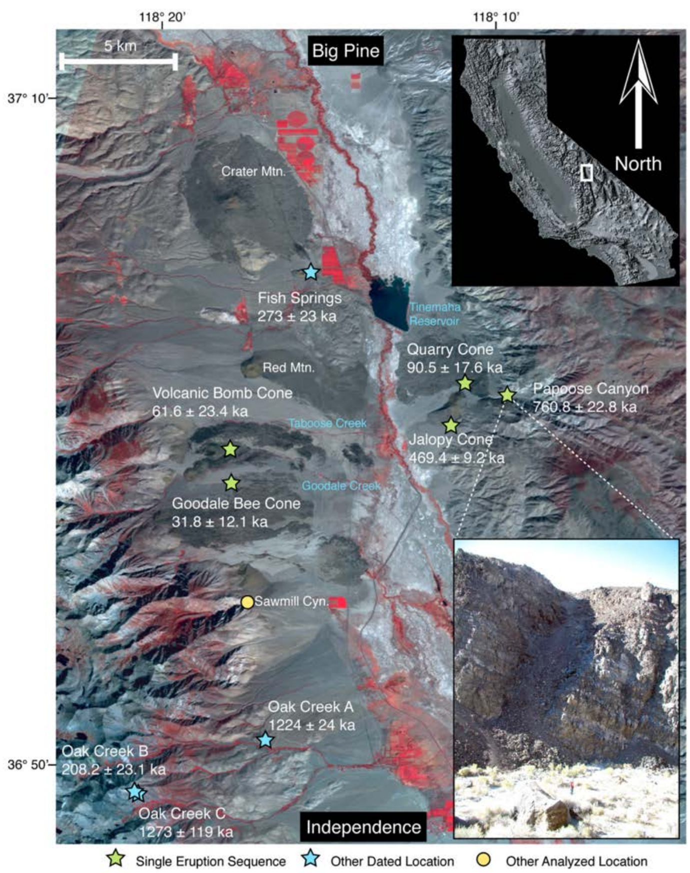


*Fig 1. Satellite map with major volcanic eruptions and their ages in Big Pine Volcanic Field (Blondes et al., 2008).*

The Big Pine Volcanic Field (BPVF) lies along the eastern flank of the Sierra Nevada, within Owen's Valley (Fig. 1). Basaltic volcanism occurred between ~1.2 Ma and 32 ka, producing ~0.5 km$^3$ of lava from ~40 vents aligned along Quaternary normal faults (Blondes et al., 2008). Owen's Valley is part of the Eastern California Shear Zone, accommodating strain transfer between the Basin and Range and the San Andreas system.

The Sierra Nevada batholith on the western flank of Owen's valley forms the shallow crust while the xenoliths within the basaltic lava flows reveal the nature of the lower crust and upper mantle beneath. Importantly, BPVF lavas are among the most primitive basalts in the Basin and Range province, with high Mg# and abundant xenolith cargo, indicating rapid ascent (Wang et al., 2002; Mordick & Glazner, 2006).

## 3. Xenolith Types and Occurrences

At Papoose Canyon, basaltic cones and flows erupted primitive, Mg-rich basalts that entrained abundant ultramafic and mafic xenoliths. These xenoliths are especially visible in blocky bombs and in flow bases. The Papoose Canyon cone (760 ka) preserves a stacked sequence of flows with systematic chemical changes in lava chemistry, making it an excellent natural laboratory for xenolith–magma interactions (Blondes et al., 2008).

The BPVF xenolith suites have been classified as:

- Mantle Peridotites: Spinel lherzolites, harzburgites, and dunites dominate. These ultramafic rocks consist mainly of olivine + orthopyroxene ± clinopyroxene ± spinel. (Blondes et al, 2008).

- Mantle Pyroxenites: Orthopyroxenites, clinopyroxenites, and websterites are common, some likely representing cumulates or veins frozen into the lithospheric mantle likely produced during earlier mantle tapping (Ducea & Saleeby, 1996).

- Lower crustal xenoliths: Some rarer xenolith occurrences of gabbros, diorites, and granitoids indicate incorporation of lower crustal fragments (Ducea & Saleeby, 1996). The notable absence of garnet, unlike deeper xenolith suites in the central Sierra Nevada, is consistent with shallow (35-45 km) origins (Ducea & Saleeby, 1996).

The primitive BPVF basalts, are rich in MgO (~10 wt%) and carry isotopic signals that reveal mantle source heterogeneity (Blondes et al., 2008). Isotopic evidence suggest contributions from both lithospheric and asthenospheric mantle reservoirs. Papoose Canyon flows (760 ka) show systematic decreases in incompatible element concentrations through time while maintaining constant MgO (Blondes et al., 2008), indicating melt–rock interaction or mixing of isotopically distinct mantle sources.

## 4. Thermobarometry and Depth of Origin

Geo-thermo-barometry studies on the mantle xenoliths constrain their equilibration conditions:

- Temperatures: ~1180–1350 °C (Ducea & Saleeby, 1996; Mordick & Glazner, 2006)

- Pressures/Depths: ~1.2–1.5 GPa, corresponding to ~35–45 km depth (Ducea & Saleeby, 1996; Mordick & Glazner, 2006)

- Rapid ascent with minimal crustal storage (Mordick & Glazner, 2006)

The combination of shallow depth of origin and high temperatures of the xenoliths genesis imply their equilibration occurred at or just below the Moho. The shallow yet hot geotherm implies the asthenosphere extends upward to the base of the crust, consistent with geophysical evidence for high electrical conductivity beneath Owen’s Valley (Park & Ducea, 2003).

## 5. Broader Tectonic Implications

Xenoliths from Papoose Canyon are ideal for reconstruction of the lithospheric processes beneath the Sierra Nevadas. The 35–45 km equilibration depths and high temperatures suggest that the lithospheric mantle is thin and asthenosphere rises to near-Moho depths implying shallow but hot lithospheric conditions (Ducea & Saleeby,1996).

Compared to the central Sierra Nevada, which retains their dense granulitic/eclogitic lower crust underneath. The Owen's Valley mantle section is lighter peridotite, consistent with loss of dense lower crust during late Cenozoic extension (Ducea & Saleeby, 1996) which suggests local delamination or descent of the eclogite base.

The rapid ascent of primitive basalts without crustal storage explains the absence of rhyolitic volcanism in the BPVF (contrast with Coso Volcanic Field to the south, where basalts stalled and generated rhyolites; Mordick & Glazner, 2006). Thus, the BPVF xenoliths record a lithosphere that has been tectonically thinned, thermally rejuvenated, and tapped repeatedly by primitive basaltic magmatism.

## 6. Conclusion

The xenoliths at Papoose Canyon provide a snapshot of the lithosphere–asthenosphere boundary beneath Owen's Valley. Their petrography and thermobarometry show derivation from shallow, hot mantle just beneath the Moho (~35–45 km, up to ~1350 °C). Their major element compositions reflect sampling from both depleted and enriched mantle domains, which became entrained in the rapidly ascending magma.

These observations tie into the broader tectonic narrative. The Sierra Nevada has undergone lithospheric thinning and with localized lower crustal removal, producing a buoyant, hot mantle lid – ideal conditions for magma genesis (Fig. 2). These rapidly ascending magmas entrained the xenoliths, parcels of the upper mantle and lower crust. And these xenoliths act as a window into a dynamic mantle that continues to shape the eastern Sierra–Basin and Range margin even today.

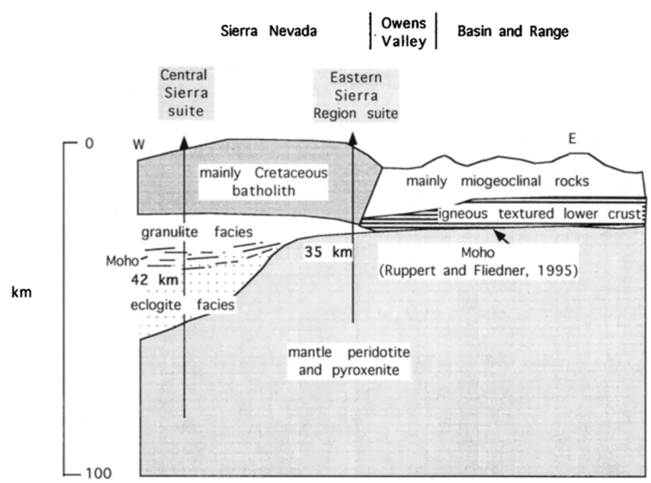


*Fig 2. Schematic cross-section of recent Sierra Nevada composition and structure (Ducea & Saleeby, 1996)*

## 7. Planetary Science Analog

Mantle xenoliths from the Big Pine Volcanic Field (BPVF)act as useful analogs for planetary interiors. On Mars and the Moon, we cannot sample the mantle directly, but mission samples returned and meteorites have been known to bear mantle material (e.g., Fig. 3; NWA 11421 Treiman et al, 2023) which carry chemical signatures of deep sources. Martian meteorites like shergottites and nakhlites show evidence of heterogeneous mantle sources, while lunar basalts erupted with little crustal interaction—both comparable to the primitive, xenolith-bearing basalts at Papoose Canyon. Studying these terrestrial xenoliths helps planetary scientists interpret mantle composition and melting on other rocky planets.

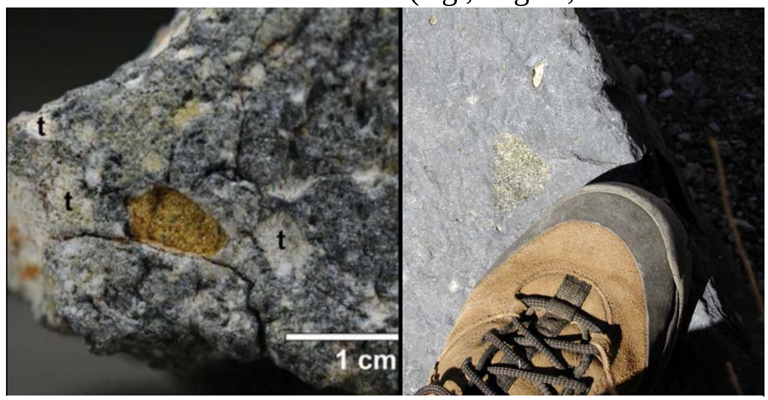


*Fig 3. Left: Lunar mantle fragment (greenish brown clast) in meteorite NWA11421 (Treiman et al, 2023); Right: Ultramafic xenolith (mantle fragment) in Papoose Canyon, Owen's Valley, CA*

## 8. References

Blondes, M. S., Reiners, P. W., Ducea, M. N., Singer, B. S., & Chesley, J. (2008). Temporal–compositional trends over short and long time-scales in basalts of the Big Pine Volcanic Field, California. Earth and Planetary Science Letters, 269(1–2), 140–154.

Ducea, M. N., & Saleeby, J. B. (1996). Buoyancy sources for a large, unrooted mountain range, the Sierra Nevada, California: Evidence from xenolith thermobarometry. Journal of Geophysical Research: Solid Earth, 101(B4), 8229–8244.

Mordick, B. E., & Glazner, A. F. (2006). Clinopyroxene thermobarometry of basalts from the Coso and Big Pine volcanic fields, California. Contributions to Mineralogy and Petrology, 152(1), 111–124.

Ormerod, D. S., Rogers, N. W., Hawkesworth, C. J., Leeman, W. P., & Menzies, M. A. (1991). Tectonic and magmatic transitions in the Western Great Basin, USA. Journal of Petrology, 32(3), 581–618.

Park, S. K., & Ducea, M. N. (2003). Can in situ measurements of mantle electrical conductivity constrain the water content of the upper mantle? Geophysical Research Letters, 30(4), 1218.

Treiman, A. H., & Semprich, J. (2023). A dunite fragment in meteorite Northwest Africa (NWA) 11421: A piece of the Moon's mantle. American Mineralogist, 108(12), 2182–2192.

Wang, K., Plank, T., Walker, J. D., & Smith, E. I. (2002). A mantle melting profile across the Basin and Range, SW USA. Journal of Geophysical Research: Solid Earth, 107(B1).

# Los Angeles County Water & Land Grab in Owens Valley

## I. History

The Los Angeles County aqueduct was constructed in 1913 with the purpose of supplying water to the residents of drought-prone Los Angeles. But despite its name, the aqueduct was built about 250 miles away from the city, in the rural Owens Valley. The Los Angeles Times deemed the project a “Titanic Project to Give City a River” (*Butler* [2022]). Los Angeles city officials had spent the last couple decades posing as farmers, determining who owned property with water in Owens Valley, and purchasing the properties under the guise of agricultural practices (*Sahagun* [2017]).

By the 1920s, the population increase in LA (boosted by the supply of water from Owens Valley), had cut the flow of the aqueduct in half, influencing the city to purchase even more land to supply 300 million gallons of water each day. This devastated Owens Valley’s farms, and thus, its economy. To make matters worse, in 1924 the city began suing local farmers, claiming that they were stealing the water that had become the city’s property in order to support their farms. In return, about 40 Owens Valley locals attacked a portion of the aqueduct with 500 pounds of dynamite (*Butler* [2022]).

LA continued to purchase land in Owens Valley to support the aqueduct, and the Owens Valley locals continued to respond with attacks to the aqueduct. According to *Butler* [2022], a local newspaper recorded 11 attacks on the aqueduct between 1924 and 1931. despite the city having purchased 90% of the valley by 1926.

Figure 1: LA County aqueduct, 1913 (*Butler* [2022])

## II. Hydrogeology

The USGS report on Owens Valley (*California Water Science Center* [2018]) characterized it as having three hydrologic system components: “(1) an unsaturated zone affected by precipitation and evapotranspiration [the combination of evaporation and plant transpiration]; (2) a surface-water system composed of the Owens River, the Los Angeles Aqueduct, tributary streams, canals, ditches, and ponds; and (3) a saturated ground-water system contained in the valley fill.”


Figure 2: Map of land ownership in Owens Valley (*Licari* [2024])

According to their report, this hydrologic system was drastically changed by an increase of water export beginning in 1970. The water table (the point below the surface at which groundwater is first found) has decreased in altitude as this export has continued, and in 1984 they found that the extraction of water would need to decrease at least 75,000 acre-ft/year to keep the water table at the same level it was at that time.

**III. Modern Day**

An investigation by *The Guardian* reveals how the history of this land grab has impacted the residents of Owens Valley, as well as how the situation continues to worsen even today (*Licari* [2024]). As of today, the Los Angeles Department of Water and Power (DWP) owns 90% of privately available land in Owens Valley, and aqueducts from the region supply about 73% of the LA's water. Residents of Owens Valley live on land owned by the LA DWP, and have recently had their leases modified to make transferring the land to new owners difficult. Due to a rule in the 1924 LA city charter that outlaws the sale or lease of city property, the DWP began only allowing its leases in Owens Valley to be transferred once, meaning new tenants moving to the valley would not be able to pass on their leases, and would instead have to surrender them to the city. This has driven people away from moving to Owens Valley, leaving those who currently live there to either continue paying rent or surrender their lease to DWP. Since these changes were made in 2016, "at least 13% of leases in Inyo county [where Owens Valley lies] have reverted back to DWP control".

Increasing temperatures due to climate change will only worsen the issue, as increasingly hot and dry cities like LA will require even more water from northern areas of the state. According to *The Guardian*'s investigation, LA expects to require 30% of its water supply to come from Owens Valley by 2045. The situation in Owens Valley is unlikely to improve in the coming years unless greater efforts are made to diversify the city's water supply and rely more heavily on conservation efforts, and, of course, to combat the effects of climate change.

# References

Butler, K., When California's water wars turned violent, PBS, Public Broadcasting Service. Available at: https://www.pbs.org/wgbh/americanexperience/features/flood-desert-california-water-wars-violent/, 2022.

California Water Science Center, Owens Valley hydrogeology, available at: https://www.usgs.gov/centers/california-water-science-center/science/owens-valley-hydrogeology, 2018.

Licari, K., Revealed: The rural Californians who can't sell their businesses – because LA is their landlord, the Guardian, Guardian News and Media. Available at: https://www.theguardian.com/us-news/article/2024/may/29/la-dwp-owens-valley-land-ownership, 2024.

Sahagun, L., L.A. took their water and land a century ago. now the Owens Valley is fighting back, Los Angeles Times. Available at: https://www.latimes.com/local/california/la-me-owens-valley-eminent-domain-20170712-story.html, 2017.

**STRATIGRAPHY OF THE WHITE-INYO MOUNTAINS.** Chaucer Langbert[1]. [1]Lunar and Planetary Laboratory, The University of Arizona, Tucson, AZ 85721, USA

**Introduction:** The White-Inyo mountains (Fig. 1) are located in the westernmost range of the Basin and Range structural province in California [1]. Along the California-Nevada border north of Death Valley, these mountains preserve some of the most important and best-known Late Proterozoic to Cambrian sections in the United States [2]. They extend for 110 miles from Montgomery Pass in a south-southeastward direction to Malpais Mesa, opposite Owens Lake.

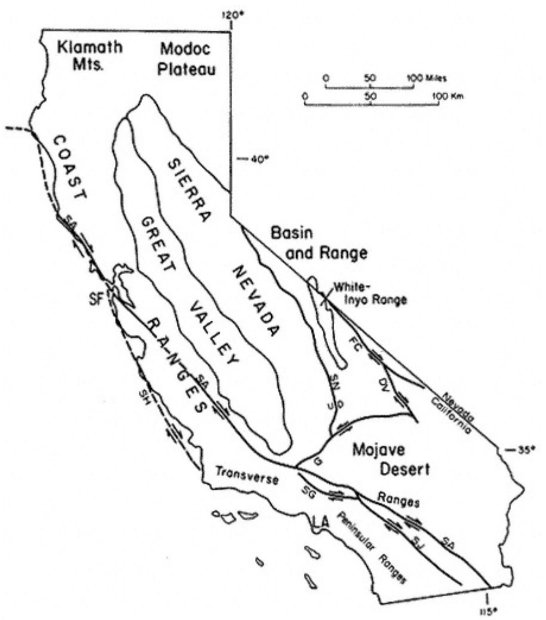


Figure 1: White-Inyo Range in relation to other physiographic and structural features in California. Arrows show relative horizontal slipping along faults. From [1].

The White Mountain range is the highest range that is completely within the Great Basin of North America, and its southern edge expands to about 20 miles wide before it meets its counterpart, the Inyo Mountains. Together the White and Inyo ranges form a continuous block separated by a narrow gap crossed by State Route 186.

**History of Mountain-Building Events:** Rocks in the White-Inyo Range span from the late Precambrian (700 Ma) to the Holocene (last 10,000 years). Figure 2 outlines the major time intervals during which mountain-building episodes (orogenies) shaped the region.

From the late Precambrian through the Devonian (700–345 Ma), the range accumulated thick sedimentary sequences—sand, shale, dolomite, and limestone—deposited along the western margin of North America in a marine basin. By the Mississippian (345 Ma), plate collisions began to influence the area. The first, the Antler orogeny, uplifted nearby regions and changed sedimentation patterns. After a quieter Pennsylvanian and Permian interval (320–225 Ma), the Sonoma orogeny (230–220 Ma) brought volcanism and new sedimentary deposits.

| Era | Period | Ma | Orogeny |
|---|---|---|---|
| Cenozoic | Quaternary | 1.8 | |
| | Tertiary | 65.0 | |
| Mesozoic | Cretaceous | 136.0 | |
| | Jurassic | 195.0 | }NEVADAN |
| | Triassic | 225.0 | }SONOMA |
| Paleozoic | Permian | 280.0 | |
| | Pennsylvanian | 320.0 | |
| | Mississippian | 345.0 | }ANTLER |
| | Devonian | 395.0 | |
| | Silurian | 435.0 | |
| | Ordovician | 500.0 | |
| | Cambrian | 570.0 | |
| Precambrian | | | |

Figure 2: Geologic timescale showing the approximate time span of mountain-building events (orogenies) in the White-Inyo Range. From [1].

The most intense deformation came with the Nevadan orogeny (starting 155 Ma), marked by compressional folding, metamorphism, and widespread intrusion of plutons. Later, during the Cenozoic, large-scale uplift and erosion removed much of the sedimentary record. Beginning $\sim$10 Ma, volcanism resumed with tuff and basalt flows, while Basin and Range extension created new valleys and uplifted the present-day White-Inyo block.

**White-Inyo Stratigraphy and Structure:** The stratigraphy of the White-Inyo Range records a nearly continuous sequence from the Late Precambrian through the Cambrian, making it one of the most complete and accessible sections in North America. The lower part of the section includes thick units of quartzite, shale, and dolomite (e.g., Reed Dolomite and Deep Spring Formation), overlain by the Cambrian Campito, Poleta, and Harkless formations. These units preserve critical evidence of the transition from Precambrian to Cambrian faunas, including the earliest trilobites and archaeocyathid reefs. Chemostratigraphic work [3] shows that stable isotope variations through these units are regionally reproducible, helping correlate the boundary globally. Younger Paleozoic carbonates and clastics were deposited atop this sequence, though much of the record has since been removed by erosion and deformation (Fig. 3).

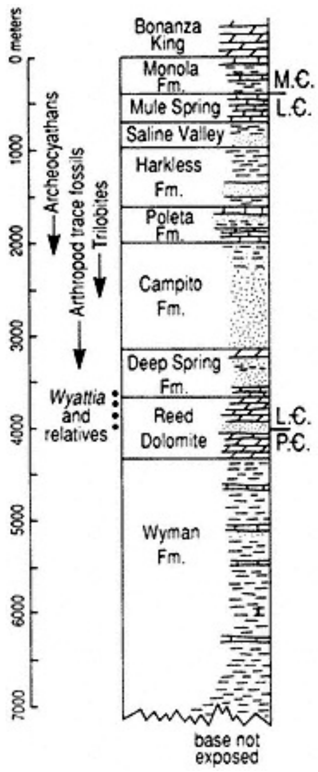


Figure 3: White-Inyo Range latest Precambrian to Middle Cambrian stratigraphic section showing distribution of key faunal elements of the Precambrian-Cambrian transition. From [1].

Structurally, the White-Inyo block is dominated by large folds (anticlines and synclines) and thrust faults that pushed older Precambrian and Paleozoic rocks over younger strata, exposing ancient formations in structural cores. During the Jurassic and Cretaceous, plutons intruded the sedimentary pile, heating and deforming the surrounding crust. Some intrusions domed and displaced host layers, while others cut across them or rose buoyantly, leaving broad metamorphic aureoles (Fig. 4). Erosion later stripped away the cover, exposing these granitic cores at the surface.

In the Cenozoic, Basin and Range extension further reshaped the landscape. Normal faulting tilted and uplifted the White-Inyo block while dropping adjacent valleys, which were subsequently filled with sediments and volcanic ash. The result is a landscape that records successive pulses of deformation, magmatism, and erosion.

**Summary:** The White-Inyo Range preserves a uniquely complete record of tectonic, magmatic, and biologic processes spanning more than 700 million years.

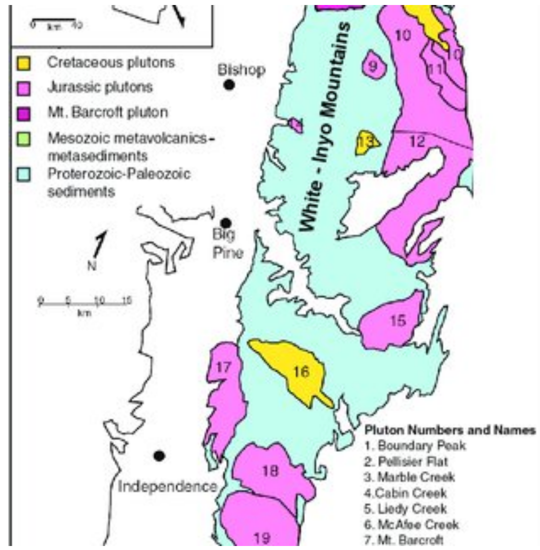


Figure 4: Simplified geologic map of the central White-Inyo Range showing Jurassic (J) and Cretaceous (K) plutons and their structural positions, cropped to save space. From [4].

Thick Precambrian to Cambrian sequences in the White-Inyo Range provide one of the world's best exposures of this critical transition, linking the sedimentary history of the continental margin with the explosive diversification of early life. Successive orogenies folded, faulted, and metamorphosed these rocks, while Jurassic–Cretaceous plutons intruded and altered the crust. Cenozoic uplift, volcanism, and Basin and Range extension sculpted the modern landscape, allowing us to study stratigraphy, structure, and evolution of Earth's crust in the western United States.

**References:** **[1]** Jr. Hall Clarence A., ed. *Natural History of the White-Inyo Range, Eastern California*. UC Press E-Books Collection, 1982–2004. Berkeley: University of California Press, 1991. URL: http://ark.cdlib.org/ark:/13030/ft3t1nb2pn/. **[2]** University of California Museum of Paleontology. *The White-Inyo Mountains*. https://ucmp.berkeley.edu/cambrian/whites.html. Accessed: 2025-09-19. unknown. **[3]** Frank A. Corsetti and Alan J. Kaufman. "Chemostratigraphy of Neoproterozoic–Cambrian units, White-Inyo region, eastern California and western Nevada". In: *PALAIOS* 9.2 (1994), pp. 211–219. DOI: 10.2307/3515065. URL: https://doi.org/10.2307/3515065. **[4]** K. Michelsen et al. "Origin of the variations in magnetic susceptibility with depth in the Barcroft granodiorite pluton, White Mountains, California". In: *AGU Fall Meeting Abstracts* (Dec. 2008).

# Big Pine Volcanic Field

## 1 Introduction

The Big Pine Volcanic Field (BPVF) in California's Owens Valley contains more than 20 volcanic vents across a ∼500 km$^2$ region, representing a well-preserved Quaternary volcanic field (Vazquez and Woolford). This basaltic system serves as an important analog for understanding volcanic processes on other planetary bodies.

The BPVF sits within the Eastern California Shear Zone, part of the broader Basin and Range Province, a region of active crustal stretching that accommodates roughly 25% of Pacific-North America plate motion (Savage et al.). This extensional environment creates the conditions necessary for magma to reach the surface. Volcanic activity is closely linked to major fault systems including the Owens Valley fault, Sierra Nevada fault, and White Mountains fault (Vazquez and Woolford). The alignment of volcanic vents along these faults demonstrates how crustal fractures provide pathways for ascending magma.

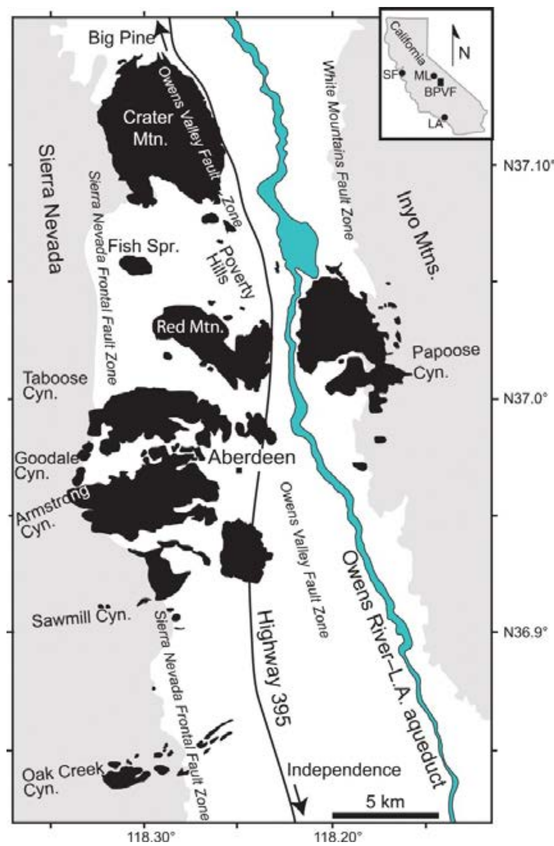


**Figure 1:** Map of the BPVF showing Quaternary volcanic rocks (black). The blue line shows the LA Aqueduct. Inset shows BPVF location relative to San Francisco (SF), Los Angeles (LA), and Mammoth Lakes (ML). Figure reproduced from Vazquez and Woolford.

## 2 Architecture and Characteristics

The BPVF features scoria cones (small volcanic hills built from ejected lava fragments) that mark individual vents, with nearly conical forms on the valley floor and irregular accumulations along mountain fronts (Vazquez and Woolford). This architecture is characteristic of monogenetic volcanic fields, where individual eruptions typically produce single volcanic edifices rather than long-lived composite volcanoes.

The field has erupted predominantly basaltic rocks with one silicic unit. The magmas show compositional changes over time that indicate multiple mantle sources, providing insights into magma generation processes in continental extensional settings (Blondes et al.; Gazel et al.).

## 3 Temporal Evolution

Previous dating indicates ∼1.2 million years of volcanic activity, with recent cosmogenic $^{36}$Cl dating providing improved age constraints (Vazquez and Woolford). This new dating reveals that volcanic activity was episodic throughout the Quaternary period, with the youngest eruptions occurring approximately 17,000 years ago (during the late Pleistocene) and covering approximately 35 km$^2$. The cosmogenic dating demonstrates that multiple volcanic centers were active during overlapping time periods, with some cones showing evidence of renewed activity separated by thousands of years.

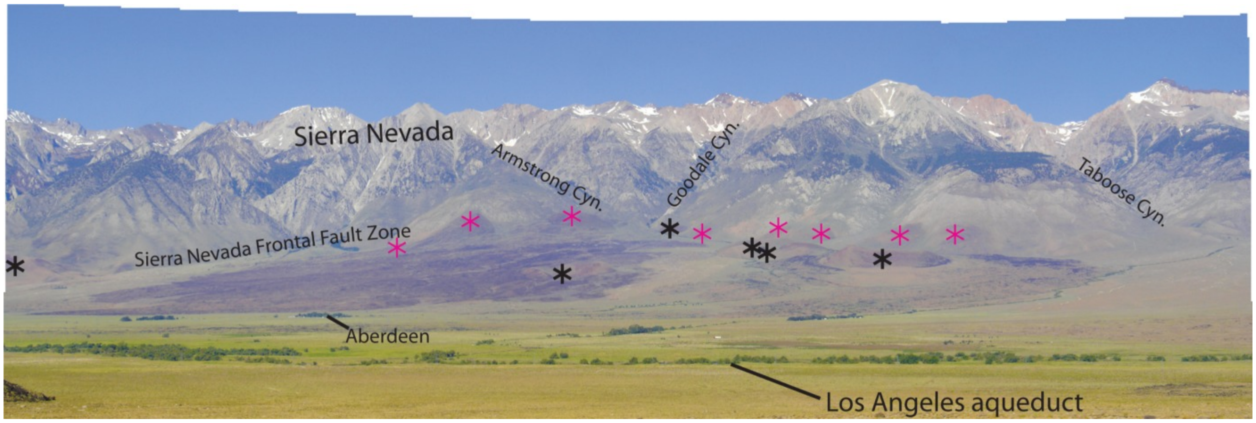


Figure 2: BPVF scoria cones and lava flows in Owens Valley, CA. Red asterisks show ∼17 ka vents along the Sierra Nevada Frontal Fault Zone and black asterisks show 27–62 ka vents. Trees mark the Los Angeles Aqueduct. Figure reproduced from Vazquez and Woolford.

## 4 Fault-Cutting Relationships

Post-volcanic tectonic deformation has significantly affected the volcanic products of the BPVF, demonstrating ongoing fault activity in the region. Many BPVF scoria cones and lavas have been displaced by faulting, with measured vertical displacement rates of 0.25 mm/yr along major fault systems (Beanland and Clark). The youngest lava flows, erupted 17,000 years ago, were emplaced along fault zones and have subsequently been offset by continued fault movement (Vazquez and Woolford).

These observations confirm that the fault systems remain tectonically active. This has implications for volcanic hazard assessment, as future volcanic activity could occur along these same active fault pathways.

## 5 Planetary Science Applications

Monogenetic volcanic fields like the BPVF provide insights into Martian volcanism. Morphometric studies use similar terrestrial examples to identify potential volcanic features on Mars (Brož and Hauber). The arid preservation conditions also demonstrate how similar volcanic landforms might survive in Mars' dry environment.

## Works Cited

Beanland, Sarah, and Malcolm M Clark. *The Owens Valley fault zone, eastern California, and surface faulting associated with the 1872 earthquake*. U.S. Department of the Interior, USGS, 1994.

Blondes, Madalyn S., et al. "Temporal–compositional trends over short and long time-scales in basalts of the Big Pine Volcanic Field, California". *Earth and Planetary Science Letters*, 2008. doi.org/10.1016/j.epsl.2008.02.012.

Brož, P., and E. Hauber. "A unique volcanic field in Tharsis, Mars: Pyroclastic cones as evidence for explosive eruptions". *Icarus (New York, N.Y. 1962)*, 2012. doi.org/10.1016/j.icarus.2011.11.030.

Gazel, Esteban, et al. "Lithosphere versus asthenosphere mantle sources at the Big Pine Volcanic Field, California". *Geochemistry, geophysics, geosystems : G3*, 2012. doi.org/10.1029/2012GC004060.

Savage, J. C., et al. "An apparent shear zone trending north-northwest across the Mojave Desert into Owens Valley, eastern California". *Geophysical Research Letters*, 1990. doi.org/10.1029/GL017i012p02113.

Vazquez, J. A., and J. M. Woolford. "Late Pleistocene ages for the most recent volcanism and glacial-pluvial deposits at Big Pine volcanic field, California, USA, from cosmogenic 36Cl dating". *Geochemistry, geophysics, geosystems : G3*, 2015. doi.org/10.1002/2015GC005889.

Scan for Geologic Resources!

THE GEOLOGICAL SOCIETY OF AMERICA®

# GEOLOGIC TIME SCALE v. 6.0

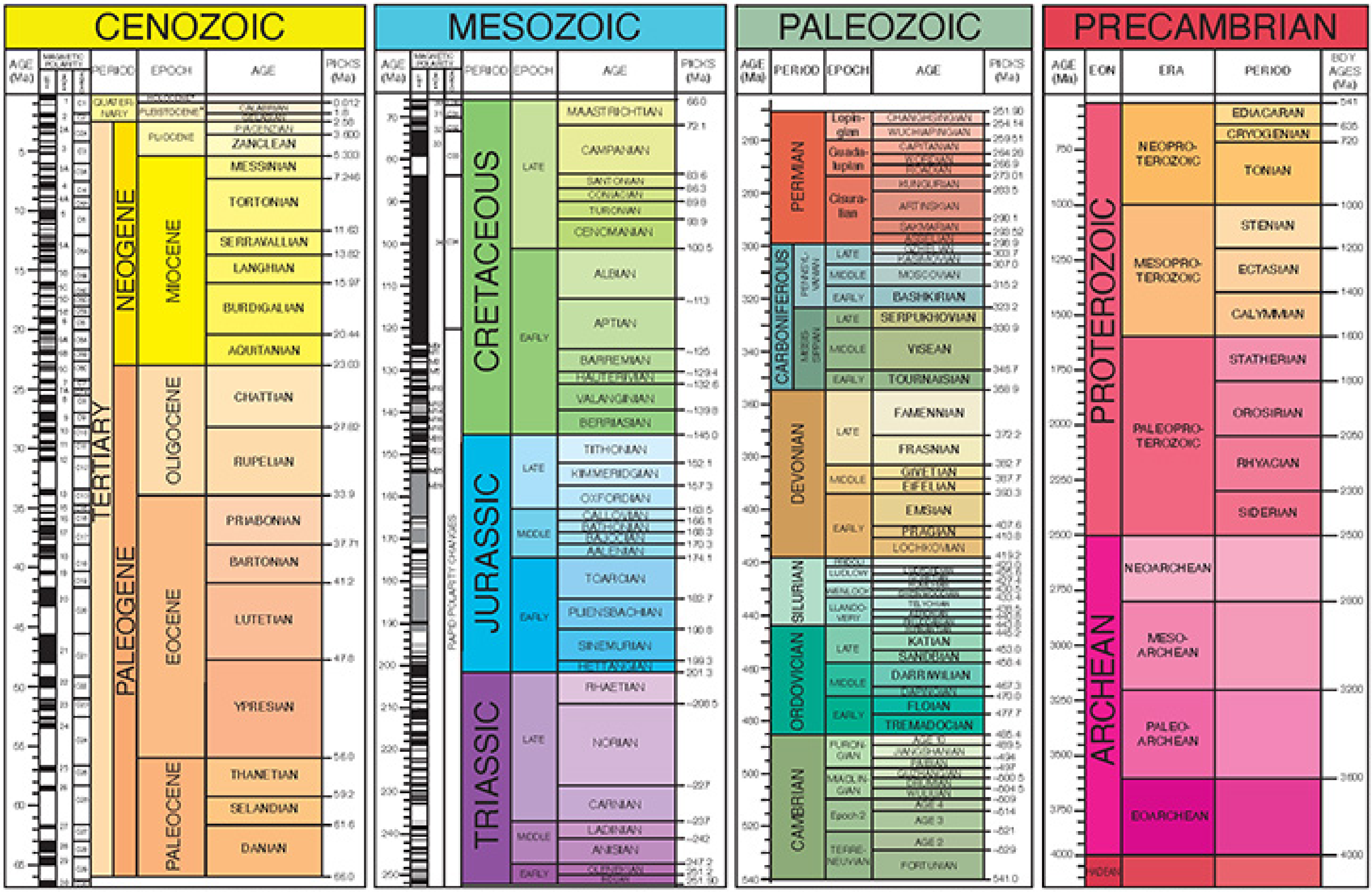


*The Pleistocene is divided into four ages, but only two are shown here. What is shown as Calabrian is actually three ages: Calabrian from 1.8 to 0.774 Ma, Chibanian from 0.774 to 0.129 Ma, and Late from 0.129 to 0.0117 Ma. The Holocene is divided into three ages: Greenlandian from 0.0117 to 0.0082 Ma, Northgrippian from 0.0082 to 0.0042 Ma, and Meghalayan from 0.0042 to present. The geologic community broadly recognizes the Anthropocene as a proposed new time interval of Earth history, partly coincident with the Holocene. Currently, the Anthropocene has an informal designation, with a proposed age span extending from the present to a beginning point between ca. 15,000 yr B.P. and as recent as 1950 CE.

The Cenozoic, Mesozoic, and Paleozoic are the Eras of the Phanerozoic Eon. Names of units and age boundaries usually follow the Gradstein et al. (2012), Cohen et al. (2012), and Cohen et al. (2013, updated) compilations. Numerical age estimates and picks of boundaries usually follow the Cohen et al. (2013, updated) compilation. The numbered epochs and ages of the Cambrian are provisional. A "~" before a numerical age estimate typically indicates an associated error of ±0.4 to more than 1.6 Ma.

Walker, J.D., and Geissman, J.W., compilers, 2022, Geologic Time Scale v. 6.0: Geological Society of America, https://doi.org/10.1130/2022.CTS006C. (Walker—University of Kansas; Geissman—University of Texas–Dallas, University of New Mexico.)

REFERENCES CITED
Cohen, K.M., Finney, S., and Gibbard, P.L., 2012, International Chronostratigraphic Chart: International Commission on Stratigraphy, https://stratigraphy.org/ICSchart/ChronostratChart2012.pdf (accessed Sept. 2022).
Cohen, K.M., Finney, S.C., Gibbard, P.L., and Fan, J.-X., 2013 (updated), The ICS International Chronostratigraphic Chart: Episodes, v. 36, p. 199–204, http://www.stratigraphy.org/ICSchart/ChronostratChart2021-10.pdf (accessed Sept. 2022).
Gradstein, F.M., Ogg, J.G., Schmitz, M.D., et al., 2012, The Geologic Time Scale 2012: Boston, USA, Elsevier, https://doi.org/10.1016/B978-0-444-59425-9.00004-4.

©2022 The Geological Society of America | www.geosociety.org

**GRAIN PROPERTIES OF MARS ANALOG METER-SCALE AEOLIAN BEDFORMS NEAR FOSSIL FALLS, CALIFORNIA, USA, AND IMPLICATIONS FOR SEDIMENT TRANSPORT.** Sarah L. Preston[1] and Mackenzie D. Day[1], [1]University of California Los Angeles Department of Earth, Planetary, and Space Sciences, Los Angeles, California, USA (slp7@ucla.edu)

**Introduction:** Meter-scale aeolian bedforms are common on Mars, but rare on Earth, where centimeter-scale impact ripples and decameter-scale dunes dominate. These large aeolian bedforms are an enticing object of study. Understanding the grain-scale properties of these bedforms is crucial to unraveling the mystery of their formation; however, they pose a trafficability hazard to Mars rovers and thus are risky to study in situ [1]. Therefore, analog field work is necessary.

Here, we analyze the grain-scale properties of a field of Mars-analog meter scale aeolian bedforms near Fossil Falls, California, USA (Fig. 1) and explore the role of grain-scale properties in large ripple formation, migration, and evolution.

***Figure 1.*** Meter-scale ripples in the Bagnold dunes, Gale crater, Mars (top, mcam05320) and at the Fossil Falls field site (bottom).

**Geologic Context:** The bedforms investigated in this work are located on the eastern flank of Red Hill, a 62 +/- 3 ka cinder cone volcano in the Coso Volcanic Range in southeastern California, USA [2]. The bedforms are composed of basaltic scoria cinder from Red Hill's most recent eruption. The cinder is typically porphyritic, vesicular, and coarser-grained than is expected for aeolian sediment.

The bedforms have a mean wavelength of approximately 2.5 meters and a mean height of 8 centimeters. Trenching reveals coarse grained (>2000 μm) surfaces armoring fine-grained (<1000 μm) interiors with low-angle cross stratification.

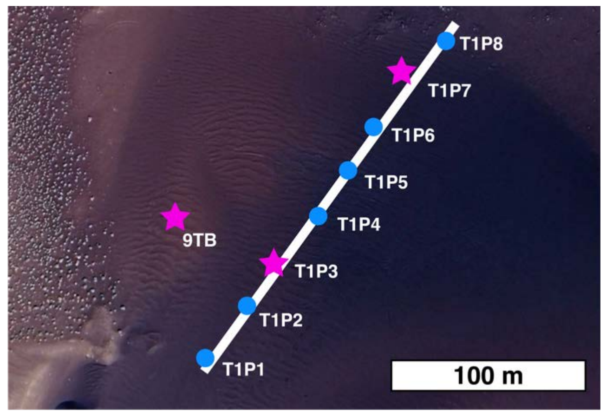


***Figure 2.*** Locations of samples collected 5/2024 for grain size analysis (pink stars and blue circles) and thin section preparation (pink stars).

**Methods:** We collected samples in February and May 2024 at one bedform interior and on the stoss, crest, and lee surfaces of eight bedforms along a transect (Fig. 2). We prepared thin sections from the stoss, crest, and lee of bedform T1P3; the crest of bedform T1P7; and the interior of bedform 9TB. We photographed each thin section and used ImageJ to manually trace each grain [3].

*Grain size.* We sieved each sample to determine grain size. Additionally, we used the Measure feature in ImageJ to determine the diameter of each grain in the thin sections.

*Grain shape.* We used the Measure feature in ImageJ to determine the roundedness and circularity of each grain in the thin sections.

*Grain composition.* We performed transmitted light microscopy to determine the proportion basalt, minerals, and pore space in each grain. We additionally identify the minerals in each grain and note distinctive textures.

**Results:** Grain size decreases moving downwind (Fig. 3), with finer grains in bedform interiors than on bedform surfaces. This is consistent with aeolian transport, wherein finer grains are far easier to transport.

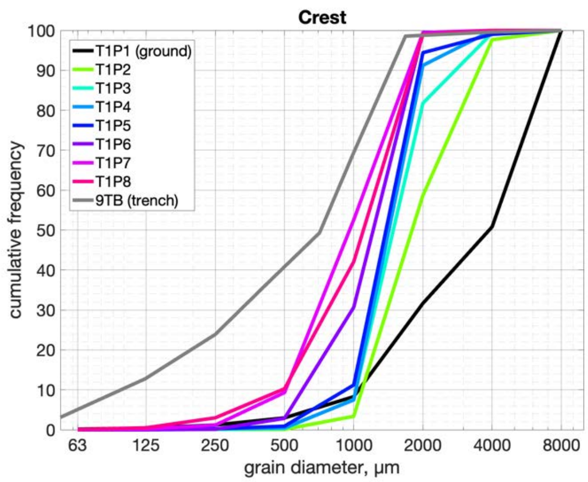


***Figure 3***. Cumulative grain size distributions of the crest surface samples.

Preliminary results indicate little difference in grain roundedness or sphericity with increasing transport distance; this is not expected, as the high-energy collisions between grains during aeolian transport quickly round grains.

Petrography reveals that there are two end-member grain compositions: vesicular basalt grains and mineral grains (Fig. 4). The mineral grains are most commonly plagioclase, pyroxene, olivine, and iddingsite. Though mineral grains do not comprise the majority of any of the five thin sections, they are most common in the downwind crest sample. This may suggest that the vesicular basalt grains are too friable to survive aeolian transport. We present an analysis of the relationship between grain size, shape, and composition to determine how grain-scale erosive processes shape bedform-scale morphology by selecting for grain size and density.

**Discussion:** Other meter-scale aeolian bedforms on Earth (i.e., [4][5][6]) have coarse-grained armoring at the bedform surfaces, fine-grained interiors, and two modal grain densities; however, the bedforms studied in this work lack the extreme density sorting between lithics at bedform crests and pumice on bedform stoss and lee surfaces observed in Iceland and Argentina. Therefore, these bedforms are likely more analogous to the meter-scale bedforms seen on Mars and provide a unique opportunity to study the role of sediment density distribution in determining bedform morphology and migration. We will address how the interplay of terrestrial gravity and atmospheric properties with grain-scale boundary conditions generates Mars-analog morphologies at the bedform scale.

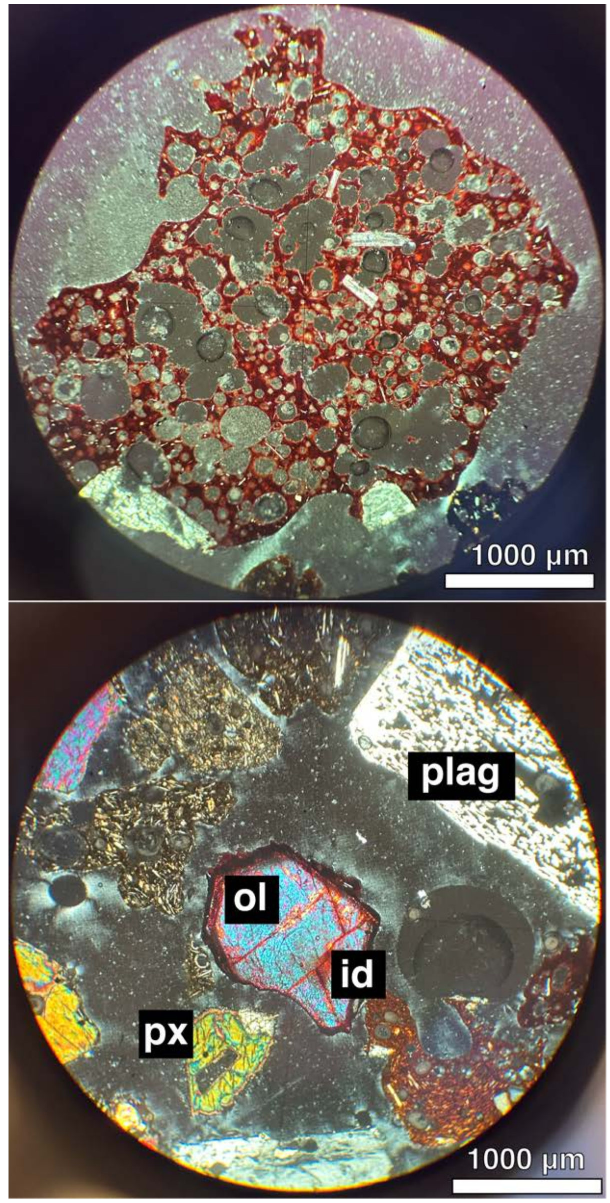


***Figure 4.*** Thin sections prepared from sediment samples showing the end-member vesicular basalt (top) and mineral grain (bottom) morphologies.

**Acknowledgments:** The authors thank A. Archbold, .J. Castillo, S. Chung, T. Horvath, E. Jhoti, and D. Paige for assistance with field work.

**References:** [1] Arvidson, R. E. et al., (2017). *Jounal of Field Robotics*, 34(3), 495–518. [2] Duffield, W. A., and Smith, G. I. (1978) *Journal of Research of the U.S. Geological Survey*, 6(3), 395–408. [3] Rasband, W. S. (2018, 1997). *ImageJ*. [4] Gillies, G. A, et al. (2012) *JGRES*, 117(F4). [5] de Silva, S. L., et al. (2013) *GSA Bulletin*, 125(11–12), 1912–1929. [6] Banham, S. G., et al. (2023), *54th Lunar and Planetary Science Conference,* Abst. no. 2806.

**PETROGRAPHY AND MORPHOLOGY OF MARS-ANALOG AEOLIAN BEDFORMS NEAR FOSSIL FALLS, CA.** Sarah L. Preston and Mackenzie Day, University of California Los Angeles, Department of Earth, Planetary, and Space Sciences (slp7@ucla.edu).

**Introduction:** Aeolian (wind-blown) bedforms are found on several bodies in the solar system, including Earth, Mars, Venus, Titan, Pluto, and 67P/Churyumov-Gerasimenko. On Earth, decameter-scale dunes and centimeter-scale ripples dominate. Although meter-scale aeolian bedforms, including coarse-grained ripples [1] and transverse aeolian ridges (TARs) [2], are common on Mars, they are relatively rare on Earth. The meter-scale large ripples that form from basaltic sands in active Martian dunes have few terrestrial analogs [3]. Coarse-grained meter-scale aeolian bedforms on Earth have been observed in the Puna desert in northwestern Argentina [4] and near the Askja Caldera in northeastern Iceland [5], although their inaccessibility limits their usefulness as Mars-analog study areas.

Here, we describe the petrography and morphology of a small field of actively migrating meter-scale aeolian bedforms near Fossil Falls, CA (Fig. 1) to investigate its suitability as a Mars analog.

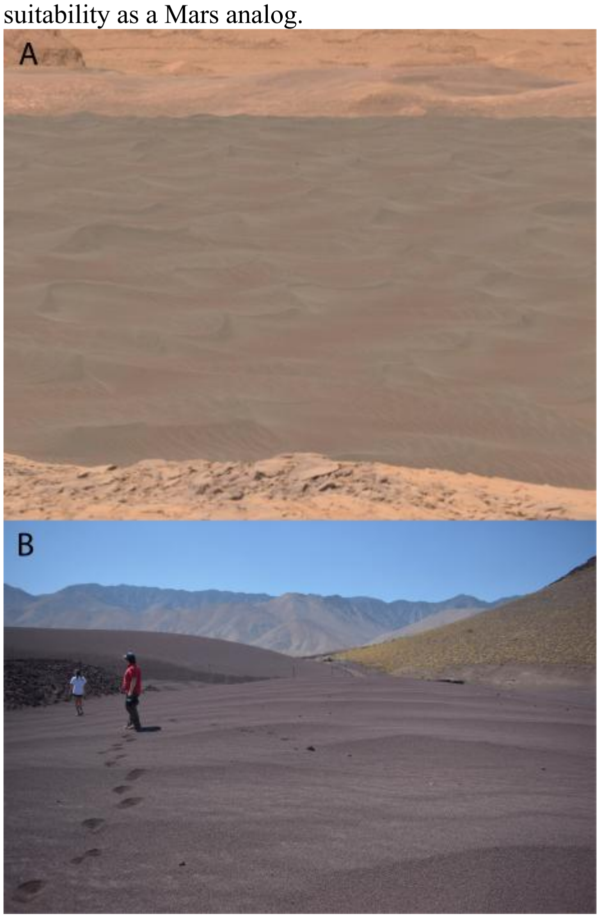


***Figure 1.*** Meter-scale aeolian bedforms A) in the Bagnold dune field, Gale crater, Mars (mcam05311, Sol 1173) and B) near Fossil Falls, CA.

**Geologic Context and Previous Work:** The bedform field investigated in this work is immediately east-southeast of Red Hill, a 62 +/- 3 ka cinder cone volcano at 35.986ºN, 117.912ºW [6]. The bedforms are composed of basaltic scoria; the sediment is typically vesicular and porphyritic, with phenocrysts of olivine, plagioclase, and pyroxene.

As previously reported [7], the grains are coarser than expected for aeolian transport; the median grain size of samples collected from bedform crest surfaces exceeds 2000 µm, although grain size decreases slightly with transport distance. When trenched, the bedforms display 1-5 cm of coarse armoring on their surfaces, with the thickest layer of coarse grains (>2000 µm) at the crests; fine-grained (typically <1000 µm) material in their interiors; and low-angle cross bedding. The bedforms are typically straight-crested, 10-30 cm tall, and 1-6 m in wavelength. Analysis of satellite images via Google Earth, coupled with the cross bedding visible in trenched bedforms, indicates that the bedforms are migrating.

**Methods:** Field work was conducted in February, May, and September 2024. Samples were collected in February and May 2024 and elevation data was collected in September 2024.

*Petrology*: Thin sections (Fig. 2) were prepared from samples collected from the stoss, crest, and lee surfaces of one ripple on a transect; from the crest of another ripple approximately 120 meters down the transect; and from the interior (~25 cm below the surface) of a ripple not on the transect. We perform point counts of each thin section with a petrographic microscope to determine the mineralogy and porosity of the sediment samples.

*Morphology:* A high-resolution LiDAR point cloud of the bedform field was collected via drone flight in September 2024 and processed to generate a 10 cm/px digital elevation model (DEM). Elevation profiles from the DEM are plotted in MATLAB. From these elevation profiles, we manually identify bedforms and extract the geometric parameters shown in Figure 3. We calculate ripple index and ripple similarity index, two well-established bedform morphology indices, to enable comparison to previous work.

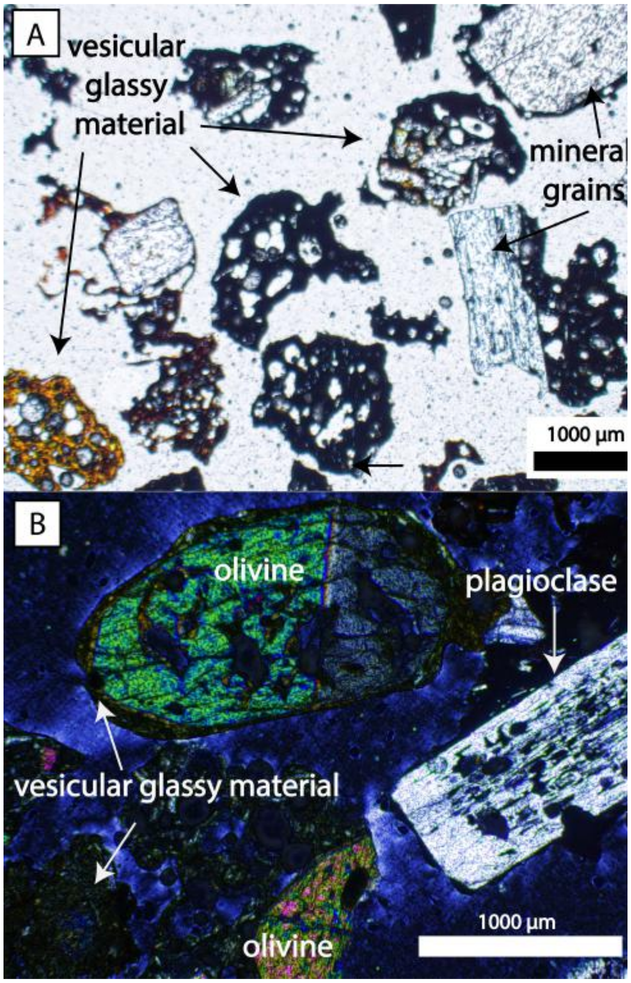


***Figure 2.*** Thin sections prepared from sediment samples. A) PPL image (25x magnification) of sediment collected from the bottom of a trench showing vesicular glassy material and mineral grains. B) XPL image (50x magnification) of sediment collected from a bedform crest showing individual grains of olivine and plagioclase; note the rim of vesicular glassy material on the olivine in the top left.

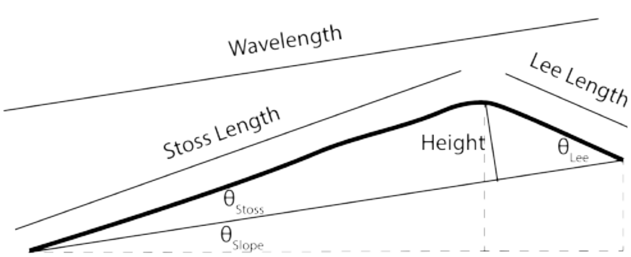


***Figure 3.*** Geometric parameters measured from bedform elevation profiles.

**Results, Discussion, and Future Work:**

Initial observations show two end-member grain morphologies: highly vesicular grains and individual mineral grains (Fig. 2). The downwind sample has a much higher proportion of individual mineral grains than the upwind sample, suggesting that the highly vesicular grains are extremely susceptible to physical weathering. Although this bedform field appears homogeneous in composition, the end member grain morphologies seen in the thin sections indicate the possibility of density sorting between the ripple crests and flanks in addition to the obvious size sorting between the ripple surfaces and interiors. This appears to be the case for the meter-scale bedforms in Iceland and Argentina, where the crests are composed primarily of lithics and scoria and the stoss and lee sides are composed primarily of pumice [4] [5].

Preliminary analysis of the DEM indicates asymmetrical bedforms with well-defined, consistent stoss and lee directions. Some larger bedforms appear to have short slip faces. The bedforms decrease in wavelength and decrease in height with increasing transport distance.

We present a comparison of the morphology and petrology of this bedform field to the morphology and petrology of other meter-scale aeolian bedforms on Earth and Mars. We assess the specific sediment transport processes that lead to the formation of these meter-scale bedforms and speculate on the applicability, quality, and limitations of this bedform field as a Mars analog.

Next steps include placing a weather station at or near the site to collect localized, accurate wind speed data; performing wind tunnel experiments to evaluate the role of grain size and density sorting in meter-scale ripple formation; and acquiring DEMs at repeat intervals to track migration rates. This field site may be an excellent location to assess rover trafficability hazards, test rover-analogous methodologies, and study Mars-analogous aeolian processes.

**Acknowledgments:** The authors thank Tyler Horvath and David Paige for collecting and processing the elevation data.

**References:** [1] Jerolmack et al. (2006) *JGR Planets, 111, E12.* [2] Balme et al. (2008) *Geomorphology*, 101(4),703-720. [3] Lapotre et al. (2016) *Science, 353, 6294, 55-58.* [4] de Silva et al. (2013) *GSA Bull., 125(11-12), 1912-1929.* [5] Banham et al. (2023) *LPSC LIV*, Abstract #2246. [6] Amos et al. (2013) *GSA Bull., 125(7-8), 1187-1202.* [7] Preston S. L. and Day M. D. (2024) *Tenth International Conference on Mars,* Abstract #3500.

# CALIFORNIA CAMPFIRE PERMIT

**Permit Expires December 31 of the year in which it was issued**

JOSEPH SCHOOLS

**Permit Holder's Name**

is authorized to build a campfire on federal public lands managed by the Bureau of Land Management or the USDA Forest Service subject to restrictions in place at the time. National and State Parks require special campfire permits.

## Using a Campfire Safely

Go to www.PreventWildfireCA.org for more campfire information.

"Campfire" means a fire which is used for cooking, personal warmth, lighting, ceremonial, or aesthetic purposes, including fires contained within outdoor fireplaces and enclosed stoves with flues or chimneys, stoves using jellied, liquid, solid, or gaseous fuels, portable barbeque pits, and space heating devices, which are used outside any structure.

- Know and comply with all current fire restrictions for the area where you plan to use a campfire.
- Clear all flammable materials from the ground for 5 feet in all directions from the edge of the fire. Keep a shovel and water nearby.
- Keep the fire small – Think of the fire in a cube 2 feet x 2 feet x 2 feet.
- Always personally supervise the campfire until it is completely extinguished, or ensure that another knowledgeable and responsible adult supervises the fire.
- Always personally make sure the fire is dead out and completely cold before you leave it unsupervised. Extinguish the fire with water and a shovel using the "drown, stir, and feel" method.

You are legally responsible and may be liable for fire suppression costs if your fire escapes.

> Prevent the spread of invasive species. Get your firewood near where you burn it. Don't bring firewood from home and don't take it home with you. Learn more at www.firewood.ca.gov

JOSEPH SCHOOLS — jschools@arizona.edu

Permit Holder's Signature — Email Address

[redacted]

Street Address

Tucson Arizona 85743

City, State, ZIP

California Wildland Fire Coordinating Group (CWCG) — 09/26/2025

Issued By — Date Issued

THIS PERMIT IS NOT TRANSFERABLE

# EXTINGUISHING YOUR FIRE

Prepared by

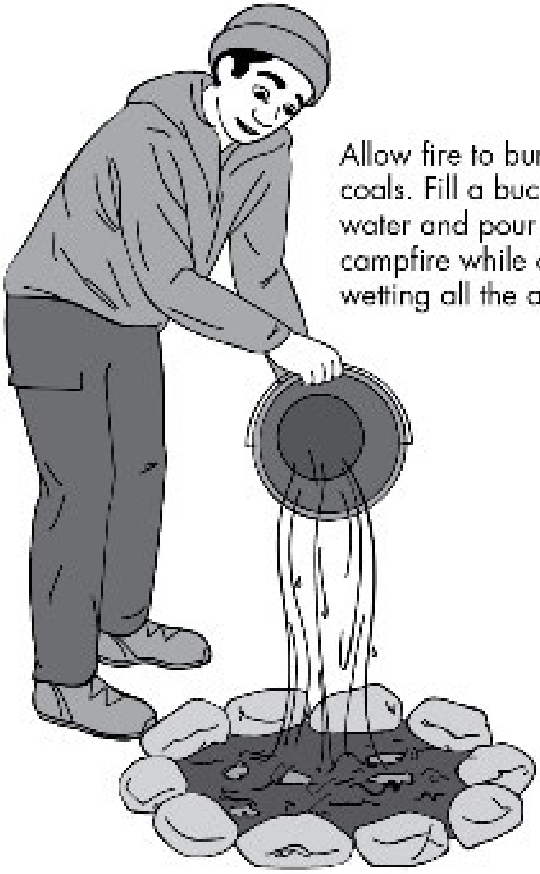

Allow fire to burn down to coals. Fill a bucket with water and pour it on the campfire while completely wetting all the ashes.

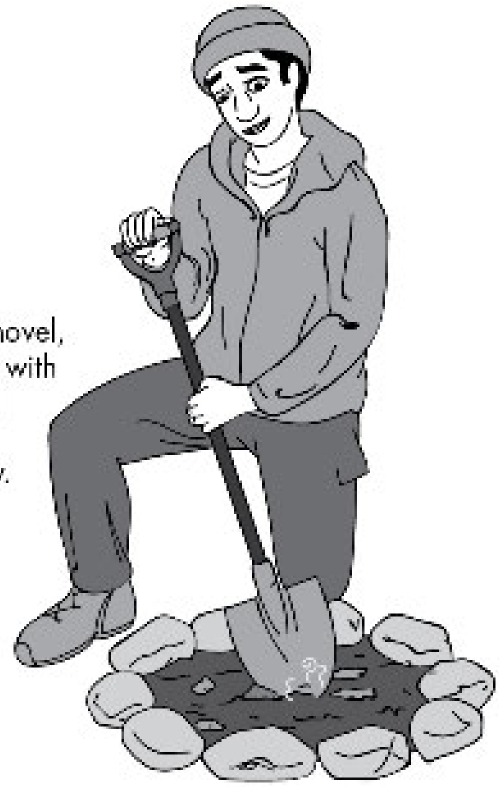

Using a shovel, mix water with ashes and embers thoroughly.

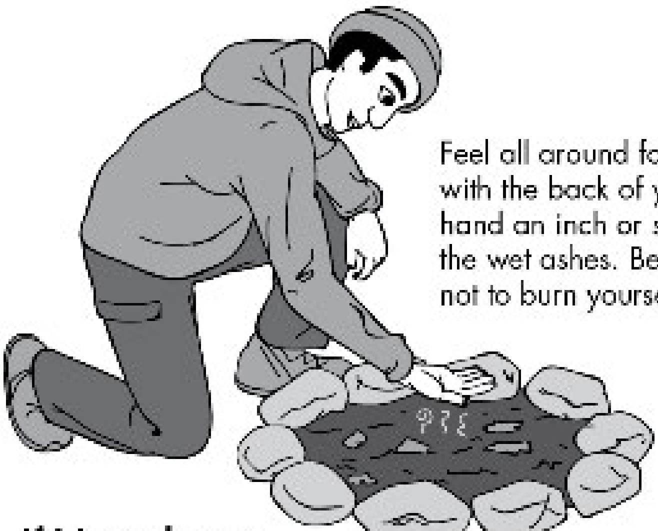

Feel all around for heat with the back of your hand an inch or so above the wet ashes. Be careful not to burn yourself.

**If it's too hot to touch, it's too hot to leave.**

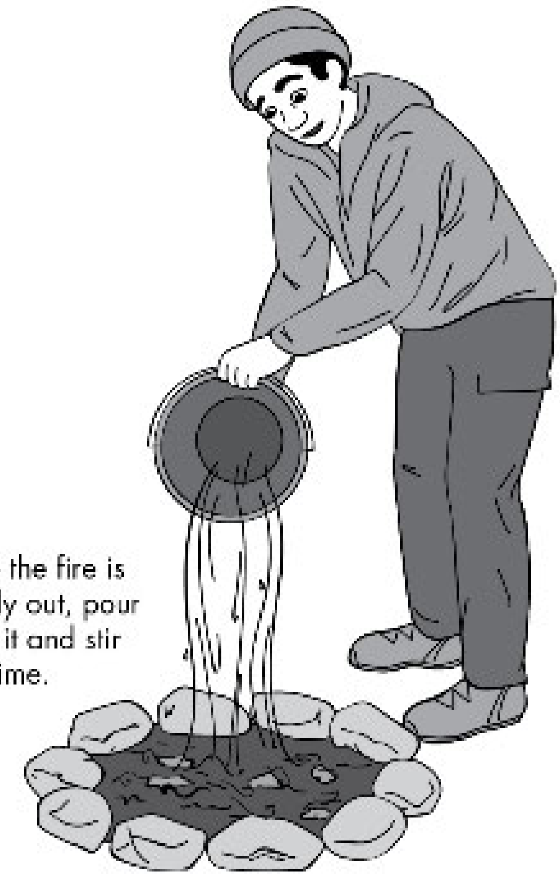

To ensure the fire is completely out, pour water on it and stir one last time.

# Battleship

Another fun activity from:

www.funorama.com

Defensive Grid

| | 1 | 2 | 3 | 4 | 5 | 6 | 7 | 8 | 9 | 10 |
|---|---|---|---|---|---|---|---|---|---|---|
| A | | | | | | | | | | |
| B | | | | | | | | | | |
| C | | | | | | | | | | |
| D | | | | | | | | | | |
| E | | | | | | | | | | |
| F | | | | | | | | | | |
| G | | | | | | | | | | |
| H | | | | | | | | | | |
| I | | | | | | | | | | |
| J | | | | | | | | | | |

Put the following ships on your defensive grid by placing the appropriate letters -- horizontally, vertically or diagonally.

1 - Aircraft Carrier

A A A A A

1 - Battleship

B B B B

1 - Cruiser

C C C

2 - Destroyers

D D    D D

Offensive Grid

| | 1 | 2 | 3 | 4 | 5 | 6 | 7 | 8 | 9 | 10 |
|---|---|---|---|---|---|---|---|---|---|---|
| A | | | | | | | | | | |
| B | | | | | | | | | | |
| C | | | | | | | | | | |
| D | | | | | | | | | | |
| E | | | | | | | | | | |
| F | | | | | | | | | | |
| G | | | | | | | | | | |
| H | | | | | | | | | | |
| I | | | | | | | | | | |
| J | | | | | | | | | | |

Instructions (2 Players Required):

Both players place their ships on the defensive grid according to the chart above. Whoever goes first calls out a position (i.e. G-6). The other player says either “Hit” or “Miss” depending upon whether one of his ships is in the position called out. The person calling out should mark a hit or a miss on the “offensive grid” to keep track of the shots. The other person should mark the shot on the “defensive grid”. If the shot is a “Hit”, the player goes again--otherwise the other player takes a turn. Once the opposing player has scored a hit on all of the spaces for a particular ship, you must call out “Hit...you sunk my Cruiser“ (or whatever type of ship it was). Once a player has sunk all the opponents ships, he is declared the winner.

battleship image copyright © www.arttoday.com

# SUPER TIC TAC TOE

Like the normal version, but more. The board is made up of 9 sub-games within the larger supergame. Player one begins by placing an X inside one of the sub-games. The square chosen within that sub-game determines the next sub-game for player two to make their move, and so on. For example, if player one chooses the middle square in the upper-right sub-game, player two must place their move within the middle sub-game. If you win a sub-game, you win that space in the uber-game. Connect three squares in a row in the super game to win. This game can be broken. There might not be a winner. Maybe you'll have fun. You'll probably get mad at your opponent.

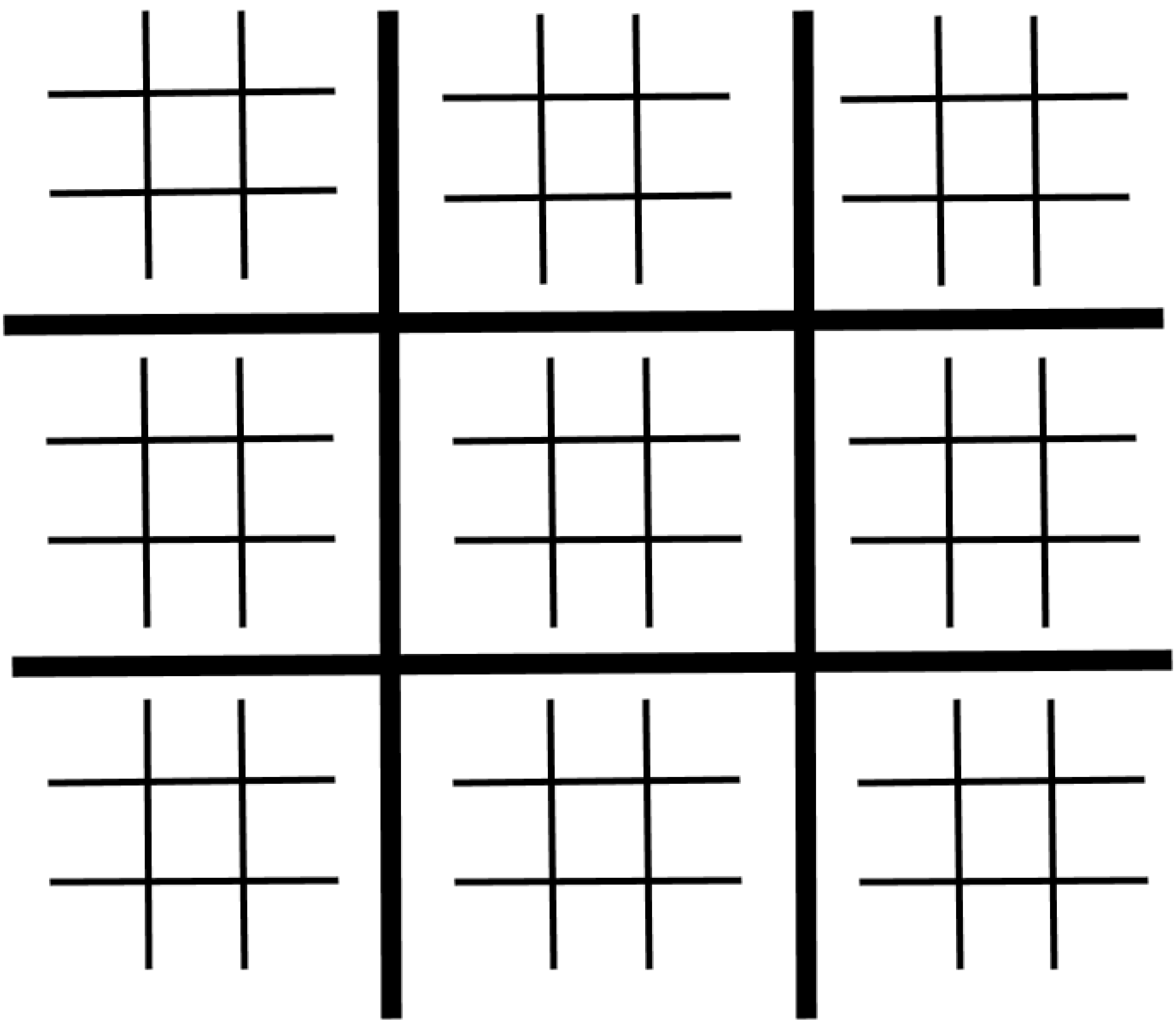

1

| | | | | | | | | |
|---|---|---|---|---|---|---|---|---|
| | | 5 | | | 7 | | | |
| | | | | | | 9 | | 2 |
| 7 | | 1 | 2 | | 9 | 6 | | |
| 9 | 5 | | | 8 | | 3 | | |
| | 2 | | | 3 | 6 | | | |
| | | 7 | | | 5 | | 1 | |
| | | | 6 | | | | 5 | 9 |
| 5 | 3 | | | 9 | | | | |
| | | | 1 | 5 | | 2 | 6 | |

2

| | | | | | | | | |
|---|---|---|---|---|---|---|---|---|
| | | 2 | | 8 | | | | |
| | 1 | | | | 3 | 4 | 9 | |
| | | 9 | | 7 | | | | 5 |
| 6 | 4 | | | | | 3 | | |
| | | | | | 4 | 8 | | 9 |
| | | 5 | | 2 | 7 | | | 4 |
| | 9 | | | | | | 1 | |
| | | | 8 | 9 | 2 | | | |
| | | 7 | 1 | 4 | | | 2 | |

3

| | | | | | | | | |
|---|---|---|---|---|---|---|---|---|
| | | | 6 | 5 | | | | |
| 7 | | | | 4 | | 9 | 5 | 2 |
| 3 | | 5 | 1 | | | | | 4 |
| | | 3 | | | | | 4 | 5 |
| 2 | | 7 | | | | | 9 | |
| 4 | | | 5 | 2 | 6 | | 7 | |
| | 7 | | | | 8 | 5 | | |
| | | 4 | | | | 7 | 2 | |
| | 9 | | | | 5 | | 6 | |

4

| | | | | | | | | |
|---|---|---|---|---|---|---|---|---|
| | 4 | | 3 | | | | | 9 |
| | | 7 | 6 | | 5 | | | |
| | | 2 | 4 | | | 5 | | 1 |
| 1 | | 3 | | | | | | 2 |
| 8 | | | | | 4 | | | |
| 2 | | | | | 6 | 9 | 8 | |
| | 3 | 1 | 7 | | | | | |
| | 9 | | | 2 | | | | 5 |
| | 2 | | | | | 1 | 9 | 4 |

5

| | | | | | | | | |
|---|---|---|---|---|---|---|---|---|
| | | | | | 1 | | 8 | 2 |
| | | | 5 | 6 | | 1 | | 7 |
| 6 | 3 | | | 7 | 2 | | | |
| | | | 7 | | | 9 | 1 | |
| | | 3 | 4 | | 6 | 7 | | |
| | | 2 | | | | | 4 | |
| | 1 | | | | 3 | | 7 | |
| | 2 | 5 | | 1 | | | | |
| | | 6 | | 5 | | 3 | | |

6

| | | | | | | | | |
|---|---|---|---|---|---|---|---|---|
| | | | 4 | | | 8 | | 2 |
| 3 | | 7 | | | 5 | | | |
| | | 2 | | | | 9 | | |
| 9 | | 3 | | | | 1 | | |
| | | 1 | | | 7 | 4 | 9 | 8 |
| | | | 6 | | 1 | | | 7 |
| | 3 | | 8 | 6 | | 2 | 4 | |
| | 4 | | 3 | 5 | | | | |
| 2 | 9 | | | | | | 3 | |

7

| | | | | | | | | |
|---|---|---|---|---|---|---|---|---|
| | 3 | | 2 | | 4 | 5 | | 8 |
| | | 4 | 6 | | 7 | | | 2 |
| | | 5 | | | 3 | | | 4 |
| | 2 | 1 | | | | | 4 | |
| | 5 | | 9 | 3 | 2 | | | |
| | 6 | | | | | 3 | | |
| 5 | | | 4 | 7 | | | | |
| 6 | | | 3 | 1 | | 7 | 5 | |
| 7 | | | | | | | 1 | 6 |

8

| | | | | | | | | |
|---|---|---|---|---|---|---|---|---|
| 2 | 5 | | | 7 | | | | |
| | | | 5 | 9 | | 1 | 3 | |
| | | | | 2 | 3 | | 6 | 7 |
| | | | | | | | 9 | 6 |
| 8 | 1 | 4 | | | | | | |
| | | | 7 | | 5 | | | |
| 4 | | 2 | 1 | | | 6 | | |
| | | 8 | | | 6 | 3 | 1 | |
| | | 1 | | 3 | | 8 | | 9 |

9

| | | | | | | | | |
|---|---|---|---|---|---|---|---|---|
| | | 8 | 2 | | | | 1 | 5 |
| 2 | | | 3 | 6 | | | | |
| 9 | 5 | 6 | | | | | 2 | |
| | | | | | | | | 4 |
| 7 | | 5 | | 3 | 2 | | | |
| | | | 6 | 5 | 7 | | 8 | |
| | 6 | 1 | | | | 4 | | |
| | | | 1 | 4 | 3 | 5 | | |
| | 2 | | | | | 8 | 7 | |

10

| | | | | | | | | |
|---|---|---|---|---|---|---|---|---|
| 1 | | | 7 | 8 | 4 | | | |
| 8 | 2 | | | | | 9 | 3 | |
| | 6 | | | | 2 | | | |
| | | | 3 | 2 | | | | 7 |
| | | 5 | | 9 | | | 8 | 2 |
| 6 | 1 | | | | | | | |
| | | | | | 8 | 5 | 9 | |
| 9 | | 6 | | 5 | | | | |
| 7 | | | | | | 8 | 2 | 3 |

11

| | | | | | | | | |
|---|---|---|---|---|---|---|---|---|
| | 5 | 9 | | 8 | | | | |
| | | | | | | 2 | | 7 |
| | | 7 | 6 | 1 | | | | |
| | 1 | 6 | 5 | 9 | | | 8 | |
| | | | 7 | | | | | 1 |
| | 9 | 8 | | | | 6 | 2 | |
| 8 | | | | | 9 | | 4 | |
| 2 | | | | | | | 1 | 8 |
| 9 | 6 | | | | 5 | | | 2 |

12

| | | | | | | | | |
|---|---|---|---|---|---|---|---|---|
| | | | | | 5 | 4 | | 6 |
| | 6 | 2 | | | 9 | 1 | | |
| 9 | | | | 8 | 4 | | | |
| | 9 | | | | | 6 | | 5 |
| 3 | | 8 | | 2 | | | | |
| | | 5 | | | 8 | 2 | 1 | |
| 8 | | | 7 | 6 | | | 2 | |
| | | | | | | | 4 | 7 |
| 1 | | 7 | 4 | | | | | |

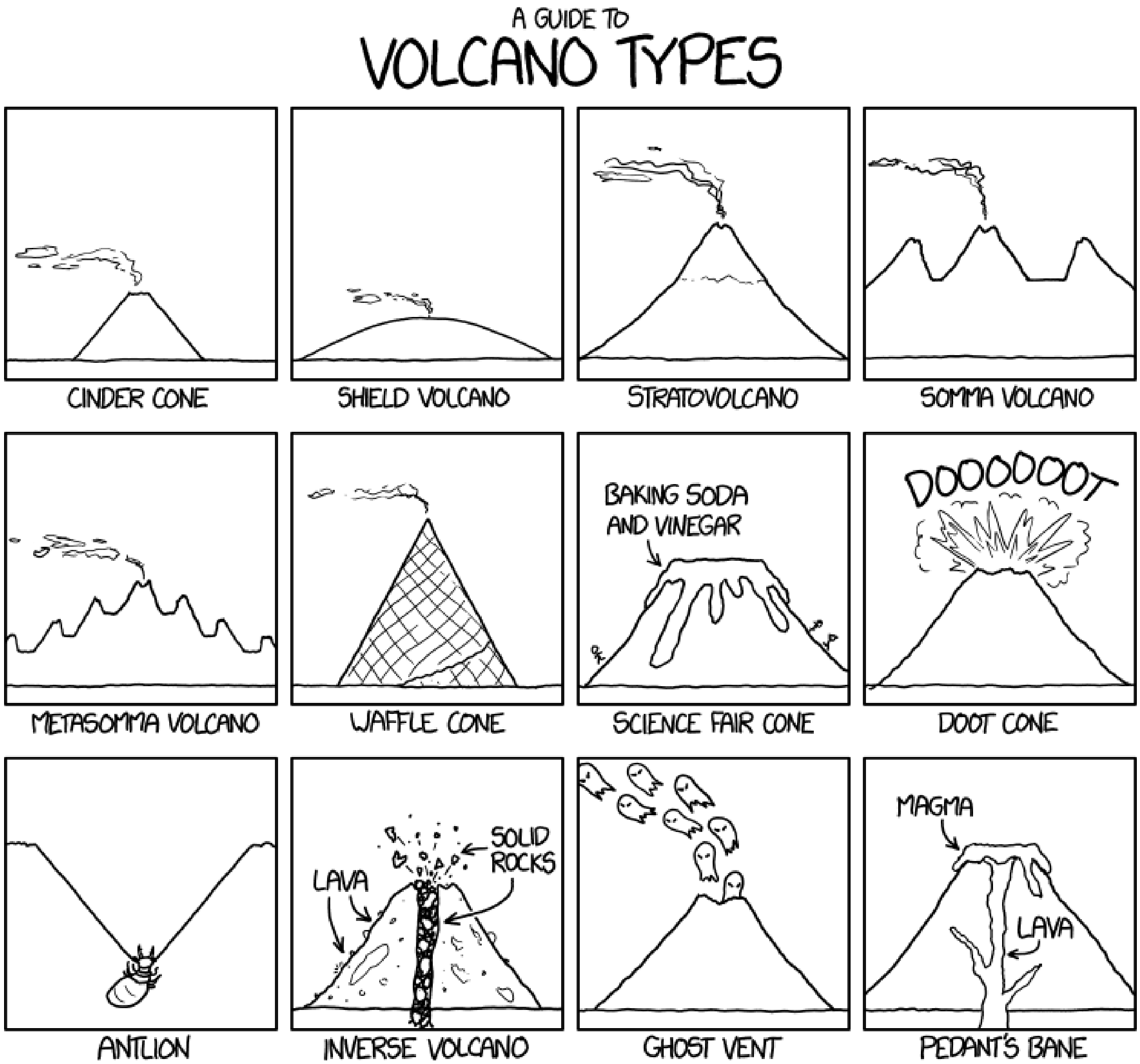
A GUIDE TO
VOLCANO TYPES
CINDER CONE
SHIELD VOLCANO
STRATOVOLCANO
SOMMA VOLCANO
METASOMMA VOLCANO
WAFFLE CONE
BAKING SODA AND VINEGAR
SCIENCE FAIR CONE
DOOOOOOT
DOOT CONE
ANTLION
SOLID ROCKS
LAVA
INVERSE VOLCANO
GHOST VENT
MAGMA
LAVA
PEDANT'S BANE

John Gemperline

2 hrs ·

Me for the next week on the grad geology field trip: